Supplementary Materials for

Architecture of the nuclear pore inner ring complex

Tobias Stuwe, Christopher J. Bley, Karsten Thierbach, Stefan Petrovic, Sandra Schilbach, Daniel J. Mayo, Thibaud Perriches, Emily J. Rundlet, Young E. Jeon, Leslie N. Collins, Ferdinand M. Huber, Daniel H. Lin, Marcin Paduch, Akiko Koide, Vincent Lu, Jessica Fischer, Ed Hurt, Shohei Koide, Anthony A. Kossiakoff, André Hoelz*

*correspondence to: hoelz@caltech.edu

This PDF file includes:

Other Supplementary Materials for this manuscript include the following:

Materials and Methods

Bacterial expression constructs

DNA fragments were amplified by PCR using *C. thermophilum* and *H. sapiens* cDNA. SUMO (small ubiquitin-like modifier) tagged proteins were cloned into a modified pET28a vector or a modified pET-MCN vector containing an N-terminal hexahistidine tag followed by a SUMO tag using BamHI and NotI restriction sites (*42, 43*). Hexahistidine tagged proteins were cloned into a modified pET28a vector containing a N-terminal hexahistidine tag followed by a PreScission protease cleavage site using NdeI and NotI restriction sites (*44*). GST tagged proteins were cloned into pGEX-6P1 using the BamHI and NotI restriction sites. Additionally, DNA coding for Nsp1 (residues 467-674) and Nup57 (residues 77-319) or Nup57 (residues 146-319) were cloned sequentially into pETDuet1 (Novagen) for expression of untagged protein. Nsp1 was cloned into the first multiple cloning site using NcoI and NotI restriction sites while Nup57 was cloned into the second multiple cloning site using NdeI and XhoI restriction sites. The selected synthetic antibody (sAB) fragments of sAB-158 and sAB-160 were cloned into the pSFV4 vector (Peter Loppnau, Structural Genomics Consortium, University of Toronto) using the restriction sites NcoI and SalI, and subsequently digested using SalI and BsaI and re-ligated to obtain the C-terminal hexahistidine tag. Mutants were generated by QuikChange mutagenesis and confirmed by DNA sequencing. Details of expression constructs are shown in Table S5.

Protein expression and purification

Proteins were expressed in *E. coli* BL21-CodonPlus(DE3)-RIL cells (Stratagene) in Luria-Bertani media and induced at an OD 600 of 0.8 with 0.5 mM IPTG. For details of the expression times and temperatures see Table S5. Seleno-L-methionine (SeMet) labeled proteins were expressed by a methionine pathway inhibition protocol, as previously described (*45*). Cells were harvested by centrifugation and re-suspended in a buffer containing 20 mM TRIS (pH 8.0), 500 mM NaCl, 5 mM 2-mercaptoethanol (β-ME), supplemented with complete EDTA-free protease inhibitor cocktail (Roche). For purification, the cell suspensions of all proteins and protein complexes were supplemented with 1 mg DNase I (Roche) and lysed using a cell disruptor (Avestin). Cell lysates were cleared by centrifugation at 30,000 x *g* for 1 hour. The supernatants were filtered through a 0.45-μm filter (Millipore) and purified using standard chromatography methods; for details see Table S6. Proteins were concentrated to ~10-20 mg/ml for biochemical interaction experiments, complex reconstitution, and crystallization.

Purification of Nup192•Nic96$^{R2\text{-}SOL}$. Nup192 and GST tagged Nic96$^{R2\text{-}SOL}$ were expressed individually. After harvesting cells, were re-suspended in 50 mM TRIS (pH 8.0), 500 mM NaCl, 5 mM β-ME, 10 % (v/v) glycerol supplemented with complete EDTA-free protease inhibitor cocktail (Roche), 2 μM bovine lung aprotinin (Sigma) and 1 mM phenylmethanesulfonyl fluoride (PMSF; Sigma). Prior to lysis, cell suspensions of GST-Nic96$^{R2\text{-}SOL}$ and Nup192 were mixed in a 1:2 ratio. Clarified lysate was loaded onto a Ni-NTA column equilibrated in a buffer containing 25 mM TRIS (pH 8.0), 500 mM NaCl, 5 mM β-ME, 20 mM imidazole, and 5 % (v/v) glycerol and eluted with an imidazole gradient. Peak fractions were pooled and loaded onto a Glutathione Sepharose 4 Fast Flow (GE Healthcare) column and eluted using a glutathione gradient. Peak fractions were pooled and dialyzed overnight against a buffer containing 20 mM TRIS (pH 8.0), 150 mM NaCl, 5 mM DTT, and 5 % (v/v) glycerol in the presence of PreScission protease. The protein was concentrated and further purified over a HiLoad Superdex 200 16/60 PG column equilibrated in a buffer containing 20 mM TRIS (pH 8.0), 150 mM NaCl, and 5 mM DTT. Peak fractions were pooled and concentrated to ~20 mg/ml for biochemical interaction experiments.

Purification of CNT•Nic96. Cells containing CNT and Nic96 were grown individually and re-suspended in 50 mM TRIS (pH 8.0), 500 mM NaCl, 4 mM β-ME, 10 % (v/v) glycerol supplemented with complete EDTA-free protease inhibitor cocktail (Roche), 2 μM bovine lung aprotinin (Sigma) and 1 mM phenylmethanesulfonyl fluoride (PMSF; Sigma). Prior to lysis, cell suspension containing CNT and Nic96 were mixed in a 3:1 ratio. Clarified lysate was loaded onto a Ni-NTA column equilibrated in a buffer containing 25 mM TRIS (pH 8.0), 500 mM NaCl, 5 mM β-ME, 20 mM imidazole, and 5 % (v/v) glycerol and eluted with an imidazole gradient. Peak fractions were pooled and desalted using a HiPrep

26/20 Desalting (GE Healthcare) column equilibrated in a buffer containing 20 mM TRIS (pH 8.0), 150 mM NaCl, 5 mM DTT, and 5 % (v/v) glycerol in the presence of ULP1 protease. After SUMO cleavage, the protein was loaded onto a MonoQ 5/50 GL (GE Healthcare) column equilibrated in 20 mM TRIS (pH 8.0), 150 mM NaCl, 5 mM DTT, and 5 % (v/v) glycerol and eluted with a sodium chloride gradient. Protein-containing fractions were pooled and concentrated to ~5 mg/ml for biochemical interaction experiments.

Purification of sABs. The expression of sABs was induced at an OD 600 of 0.9 with 0.25 mM IPTG and grown at 37 °C for 3 hours. The lysate was incubated at 65 °C for 30 minutes and then cooled on ice for 15 minutes before centrifugation at 30,000 x *g* for 1 hour. The supernatant was filtered through a 0.45-μm filter (Millipore) and loaded onto a Ni-NTA column equilibrated in 20 mM TRIS (pH 8.0), 500 mM NaCl, and 20 mM imidazole. Protein was eluted with a linear gradient of 20 mM TRIS (pH 8.0), 500 mM NaCl, and 500 mM imidazole. Protein-containing fractions from the Ni-NTA affinity purification were pooled and loaded onto a 5 ml HiTrap MabSelect SuRe (GE Healthcare) column equilibrated in a buffer containing 20 mM TRIS (pH 8.0) and 500 mM NaCl and eluted using a linear gradient of an elution buffer containing 0.1 M acetic acid. The eluted fractions were dialyzed against a buffer containing 20 mM TRIS (pH 8.0) and 100 mM NaCl and concentrated to ~50 mg/ml for biochemical interaction experiments, complex reconstitution, and crystallization.

Purification of CNT•Nic96^{R1}. Purified CNT was mixed with 2-fold molar excess of purified SUMO-Nic96^{R1} and incubated on ice for 30 minutes. The mixture was then loaded onto a HiLoad Superdex 200 16/60 PG column equilibrated in buffer containing 20 mM TRIS (pH 8.0), 100 mM NaCl, and 5 mM DTT. To obtain untagged CNT•SUMO-Nic96^{R1}, the proteins were mixed in the presence of ULP1 protease. Fractions containing either CNT•SUMO-Nic96^{R1} or untagged CNT•Nic96^{R1} were pooled and concentrated to ~30 mg/ml for biochemical studies.

Purification of CNT•Nic96^{R1}•sAB-158. Purified CNT was mixed with 2-fold molar excess of purified SUMO-Nic96^{R1}, 2-fold molar excess of purified sAB-158, and ULP1 protease, followed by incubation on ice for 30 minutes. The mixture was then loaded onto a Superdex 200 10/300 GL column equilibrated in buffer containing 20 mM TRIS (pH 8.0), 100 mM NaCl, and 5 mM DTT. Fractions containing *CNT•Nic96^{R1}•sAB-158* were pooled and concentrated to ~50 mg/ml for biochemical studies and crystallization.

Purification of Nup82^{NTD}•Nup159^{T}•Nup145N^{APD}. Purified Nup82^{NTD}•Nup159^{T} was mixed with a 1.2-fold molar excess of Nup145N^{APD} and incubated on ice for 30 minutes. The mixture was then loaded onto a Superdex 200 16/60 PG column equilibrated in buffer containing 20 mM TRIS (pH 8.0), 100 mM NaCl, and 5 mM DTT. Peak fractions containing a stoichiometric Nup82^{NTD}•Nup159^{T}•Nup145N^{APD} hetero-trimer were pooled and concentrated to ~30 mg/ml for biochemical studies and crystallization.

Reconstitution of hsNup49^{CCS2+3}•hsNup57^{CCS3}* complexes.* Purified *hs*Nup49^{CCS2+3}* was mixed with an equimolar amount of *hs*Nup57^{CCS3}* and incubated on ice for 30 minutes. The mixture was then loaded onto a HiLoad Superdex 200 16/60 PG column equilibrated in buffer containing 20 mM TRIS (pH 8.0), 100 mM NaCl, and 5 mM DTT. Peak fractions containing a stoichiometric *hs*Nup49^{CCS2+3}*•*hs*Nup57^{CCS3}* complex were pooled and concentrated to ~20 mg/ml for crystallization.

Reconstitution of CNT•Nic96•Nup192•Nup53. The hetero-nonameric IRC protomer including the CFC proteins Nup82^{NTD} and Nup159^{T} was reconstituted as follows. A Nup192•Nup53 complex was formed by mixing purified Nup192 and Nup53 with a 1.2 fold molar excess of Nup53, incubated on ice for 30 minutes and purified over a HiLoad Superdex 200 16/60 PG column equilibrated in a buffer containing 20 mM TRIS (pH 8.0), 100 mM NaCl and 5 mM DTT. The Nup192•Nup53 dimer was subsequently mixed with a 1.2-fold molar excess of CNT•Nic96, incubated for 30 minutes on ice and further purified over a HiLoad Superdex 200 16/60 PG gel filtration column equilibrated in 20 mM TRIS (pH 8.0), 100 mM NaCl and 5 mM DTT. Complex-containing fractions were pooled and concentrated to ~8 mg/ml for biochemical studies.

Reconstitution of CNT•Nic96•Nup192•Nup53•Nup145N•Nup82^{NTD}•Nup159^{T}. To reconstitute CNT•Nic96•Nup192•Nup53•Nup145N•Nup82•Nup159, 1 mg of purified CNT•Nic96•Nup192•Nup53 was mixed with 0.8 mg of purified Nup82^{NTD}•Nup159^{T}•Nup145N, incubated for 30 minutes on ice, and

purified over a Superose 6 10/300 GL column equilibrated in 20 mM TRIS (pH 8.0), 100 mM NaCl and 5 mM DTT.

Generation of synthetic antibodies and monobodies

The selection of synthetic binders was performed using avi-tagged CNT, CNT•Nic96^{R1}, and CNT•Nic96$^{139-201}$, containing Nup49 with an N-terminal avi-tag. Biotinylation was carried out using 40 μM protein in a buffer containing 50 mM BICINE (pH 8.3), 100 mM biotin, 10 mM ATP, 10 mM magnesium acetate, and 30 μg biotin ligase (BirA) at 30 °C for 2 hours in a total volume of 2 ml. After labeling, protein was buffer exchanged using a 5 ml HiTrap Desalting (GE Healthcare) column equilibrated with a buffer containing 20 mM TRIS (pH 8.0), 100 mM NaCl, and 5 mM DTT and purified again using a HiLoad Superdex 200 16/60 PG column equilibrated in the same buffer. The extent of biotinylation and efficiency of capture were tested by incubating 10 μg protein with 50 μl of Streptavidin MagneSphere Paramagnetic Particles (Promega), followed by a single washing step with 50 μl buffer, containing 20 mM TRIS (pH 8.0), 100 mM NaCl, and 5 mM DTT, and resolving the bound proteins by SDS-PAGE and visualizing by Coomassie Brilliant Blue staining.

For sAB identification, four rounds of competitive selection were performed using 100 nM (round 1), 50 nM (round 2), 10 nM (round 3), and 10 nM (round 4) biotinylated CNT, CNT•Nic96^{R1}, or CNT•Nic96$^{139-201}$ and a phage display library according to previously published protocols (*46, 47*). After successful selection, the specificity of candidate sABs was tested against the biotinylated CNT, CNT•Nic96^{R1}, and CNT•Nic96$^{139-201}$ using a single point competitive ELISA assay (*46*). Only sequence-unique sABs with the desired binding properties were chosen for further biochemical characterization. Monobody libraries were screened with a similar protocol and affinities determined by yeast display, as previously described (*48, 49*).

To evaluate the binding affinity and specificity of the selected sABs and MBs, 1.5-fold molar excess of sAB or MB was incubated with CNT, CNT•Nic96^{R1}, or CNT•Nic96$^{139-201}$ and loaded onto a MonoQ 5/50 GL column equilibrated in a buffer containing 20 mM TRIS (pH 8.0), 100 mM NaCl, and 5 mM DTT and eluted using a NaCl gradient. Interacting sABs or MBs eluted with the CNT, CNT•Nic96^{R1}, or CNT•Nic96$^{139-201}$, whereas non-interacting sABs or MBs eluted prior to the gradient step. The screened sABs or MBs formed stable complexes with CNT, CNT•Nic96^{R1}, and CNT•Nic96$^{139-201}$, but failed to differentiate between them.

Multi-angle light scattering coupled to analytical size-exclusion chromatography

Purified proteins and complex formation were characterized by inline multi-angle light scattering following separation on Superdex 200 10/300 GL or Superose 6 10/300 GL columns (*50*). All proteins and complexes were analyzed in a buffer containing 20 mM TRIS (pH 8.0), 100 mM NaCl and 5 mM DTT, except those involving Nup192^{TAIL}, which were carried out in a buffer containing 20 mM TRIS (pH 8.0), 200 mM NaCl and 5 mM DTT. The chromatography system was connected in series with an 18-angle light scattering detector (DAWN HELEOS II, Wyatt Technology), a dynamic light scattering detector (DynaPro Nanostar, Wyatt Technology), and a refractive index detector (Optilab t-rEX, Wyatt Technology). Data were collected every 1 second at a flow rate of 0.5 ml/min at 25 ºC and analyzed using ASTRA 6 software, yielding molar mass and mass distribution (polydispersity) of the samples. For interaction studies, proteins were mixed and incubated on ice for 30 minutes prior to being applied to the gel filtration column. Protein containing fractions were analyzed by SDS-PAGE followed by Coomassie brilliant blue staining.

Thermal stability assay

Purified CNT (10 μg) was incubated in a total volume of 50 μl for 30 minutes at 40-61 ºC, increased in 3.5 ºC increments. Soluble and pellet fractions were separated by centrifugation at 30,000 x *g* for 35 minutes at 4 ºC, resolved by SDS-PAGE, and visualized by Coomassie brilliant blue staining.

GST pull-down protein-protein interaction analysis

Bait protein (5 μg, purified GST-Nic96^{R1} or GST) was incubated for 30 minutes with an equimolar amount of target proteins in a buffer containing 20 mM TRIS (pH 8.0), 100 mM NaCl, 4 mM DTT. The

mixtures were then incubated for 30 minutes with 20 µl pre-washed Glutathione Sepharose 4B resin (GE Healthcare). The beads were collected by centrifugation at 500 x *g* for 2 minutes and washed five times with 200 µl binding buffer. Bound proteins were released from the resin by addition of 0.5 µg PreScission protease and incubation for 20 minutes at room temperature. Samples from the load, PreScission eluted supernatant, and post-elution beads were analyzed by SDS-PAGE and visualized by Coomassie brilliant blue staining. Because Nup49 and Nup57 were poorly behaved when expressed individually, they were not tested in isolation.

Yeast strains, media and miscellaneous genetic methods

Preparation of all media (yeast peptone dextrose, YPD; synthetic dextrose complete, SDC), LiAc-mediated yeast transformation and genetic manipulation was carried out according to standard protocols. For details of the yeast expression constructs and haploid *S. cerevisiae* strains see Tables S7 and S8. To generate the listed shuffle strains the respective essential genes were replaced with either the *HIS3* or the *natNT2* cassette by homologous recombination, as previously described (*51, 52*). Due to the lethality of the deletions, the indicated parental strain was complemented with a pRS416 construct carrying the respective full-length *S. cerevisiae* gene with an N-terminal mCherry tag under the control of the P_{NOP1} promoter prior to chromosomal integration. Subsequently, pRS415-eGFP or pRS415-mCherry constructs carrying the various Nup variants were introduced. The transformants were selected twice on SDC-leucine (Leu) plates followed by plating twice on SDC+5-fluoroorotic acid (5-FOA) to ensure the loss of the pRS416-mCherry construct prior to analysis. The *NUP192* shuffle constructs and the *nup49-313* mutant (EVPIP) were described previously (*53, 54*).

Yeast cell growth analyses and fluorescence microscopic assays

For viability and growth analysis, *S. cerevisiae* strains carrying eGFP-tagged variants of the respective *scNUP* were grown at 30 °C. Ten-fold dilution series were generated, of which 20 µl were spotted on SDC-Leu and SDC+5-FOA plates and grown at 23 °C for 5 days. For growth analysis of the shuffled strains, 7.5 µl of the dilution series were spotted on YPD plates and grown at 23 °C, 30 °C, and 37 °C for 2-4 days. For *sc*Nup57 co-localization analysis, cells with a genomic, C-terminal GFP-tagged *scNUP57* and pRS415-mCherry constructs carrying the various *NUP* variants in the respective knockout background were grown at 30 °C to mid log phase and afterwards shifted for 6 hours to 37 °C. The large ribosomal subunit *sc*Rpl25 reporter assay was performed as described previously (*55*). The pRS411 (for *scNUP192* and *scNIC96* mutant analysis) or the pRS413 (for *scNUP49* mutant analysis) vectors carrying mCherry-tagged *scRPL25* were co-transformed with the respective pRS415-eGFP variant plasmids (see above) into the indicated shuffle strain. The transformants were selected twice on SDC-LEU-MET or SDC-LEU-HIS plates followed by plating twice on SDC-MET+5-FOA or SDC-HIS+5-FOA to ensure the loss of the pRS416-mCherry construct. For analysis, cells were grown in selective SDC-MET or SDC-HIS medium at 30 °C to mid-log phase. For fluorescence microscopy, live cells were washed once with water, re-suspended and analyzed using a Carl Zeiss Observer Z.1 equipped with a Hamamatsu camera C10600 Orca-R2. The statistical analysis was carried out using three sets of independent images with at least 500 cells each for every analyzed sample. Error bars represent standard deviation.

FISH mRNA Export Assay

Liquid cultures of deletion yeast strains were grown at 30 °C (23 °C for the *nic96Δ/Nup57-GFP* strain) in YPD media to an OD 600 of 0.4 and subsequently shifted to 37 °C for 4 hours prior to fixation in formaldehyde. These cells were then analyzed by FISH using an Alexa647-labeled 50-mer oligo(dT) probe as previously described (*56, 57*). The statistical analysis was carried out using three sets of independent images with at least 500 cells each for every analyzed sample. Error bars represent standard deviation.

Crystallization and structure determination

Crystals of $Nup192^{TAIL}$, $Nup188^{TAIL}$, $hsNup49^{CCS3*}$, $hsNup57^{CCS3*}$, $Nup57^{CCS3*}$, $hsNup49^{CCS2+3*}$•$hsNup57^{CCS3*}$ with 2:4 and 2:2 stoichiometry, $Nup82^{NTD}$•Nup159T•$Nup145N^{APD}$, and

CNT•Nic96^{R1}•sAB-158 were grown at 21 °C in hanging drops containing 1 μl of protein and 1 μl of a reservoir solution. SeMet-labeled crystals were grown under similar conditions. For CNT•Nic96^{R1}•sAB-158, native crystals were derivatized with *p*-chloromercuribenzoic acid (PCMB), ethyl mercury thiosalicylate (EMTS), potassium hexachloroosmate (K_2OsCl_6), and potassium osmate (K_2OsO_4). Crystals were cryoprotected by supplementing the drop with cryo protectant and flash-frozen in liquid nitrogen. For details of the crystallization and cryo protection see Table S9. X-ray diffraction data were collected at 100 K at beamline 8.2.2 at the Advanced Light Source (ALS), Lawrence Berkley National Laboratory (LBNL), beamline BL12-2 at the Stanford Synchrotron Radiation Source (SSRL), and beamline GM/CA-CAT 23ID-D at the Advanced Photon Source (APS). The X-ray diffraction data were processed using the HKL2000 and XDS (*58, 59*).

Initial phases for all structures were calculated in PHASER using single anomalous dispersion (SAD) X-ray diffraction data obtained from SeMet derivatives (*60*). Solvent flattening and NCS averaging were performed in RESOLVE, yielding improved phases and experimental maps of excellent quality. In the case of CNT•Nic96^{R1}•sAB-158, the best experimental map was obtained using SAD X-ray diffraction data obtained from the K_2OsCl_6 derivative. Iterative rounds of model building and refinement were performed with COOT and PHENIX (*61, 62*). The unambiguous assignment of the CNT•Nic96^{R1}•sAB-158 sequence register was aided by anomalous difference Fourier map calculations using the derivatives. Subsequently, the assigned sequence register was verified by methionine mutants yielding 22 additional selenium sites (Nup49: I263M, H276M, L31M, A307M, L332M, E438M; Nup57: I82M, H109M, L113M, E127M, I138M, L198M, I233M, L253M, V304M; Nsp1: L527M, L548M, A628M; and Nic96^{R1}: L140M, L158M, L161M, L178M). In total 78 heavy atom sites were identified in anomalous difference Fourier maps (fig. S29).

For all structures, the final models possess excellent R_{work} and R_{free} values and the assessment of their stereochemical qualities with MolProbity revealed no Ramachandran outliers (*63*). For details of the data collection and refinement statistics see Tables S2 to S4.

Illustrations and figures

Gel filtration profiles and MALS graphs were generated in IGOR (WaveMetrics) and assembled in Adobe Illustrator. Sequence alignments were generated using ClustalX (*64*) and colored with ALSCRIPT (*65*). Electrostatic potentials were calculated with APBS (Adaptive Poisson-Blotzmann Solver) software (*66*). Structure figures were generated with PyMOL (www.pymol.org).

Coordinates and Structure Factors

The coordinates and structure factors have been deposited with the Protein Data Bank with accession codes 5CWV (Nup192^{TAIL}), 5CWU (Nup188^{TAIL}), 4JQ5 (*hs*Nup49$^{CCS2+3*}$), 4JNV and 4JNU (*hs*Nup57^{CCS3*}), 5CWT (Nup57^{CCS3*}), 4JO7 (*hs*Nup49$^{CCS2+3*}$•*hs*Nup57^{CCS3*}, 2:2 stoichiometry), 4JO9 (*hs*Nup49$^{CCS2+3*}$•*hs*Nup57^{CCS3*}, 2:4 stoichiometry), 5CWW (Nup82^{NTD}•Nup159^{T}•Nup145N^{ΔPD}) and 5CWS (CNT•Nic96^{R1}•sAB-158).

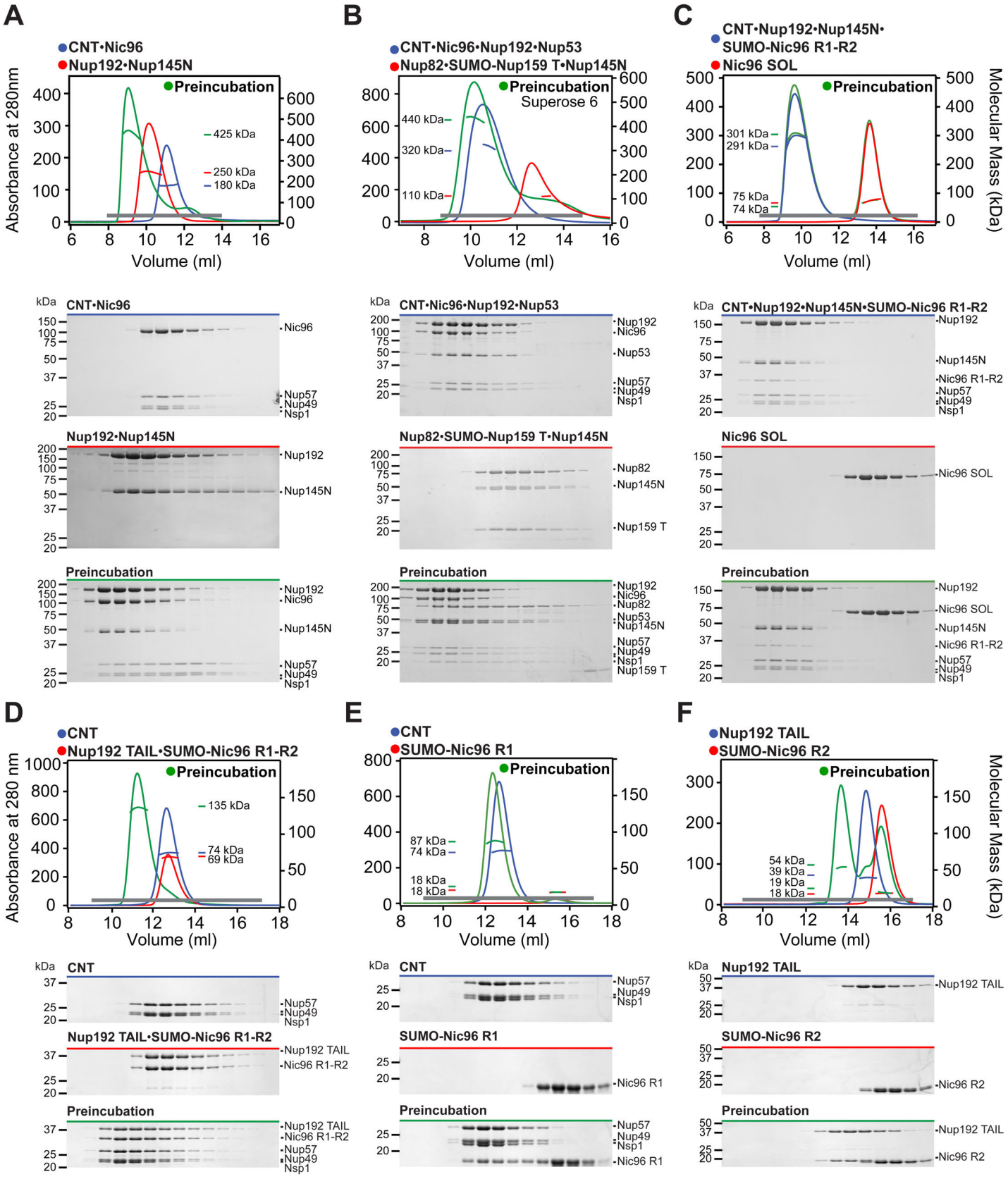
A
CNT•Nic96
Nup192•Nup145N
Preincubation
425 kDa
250 kDa
180 kDa
Absorbance at 280nm
Volume (ml)
CNT•Nic96
Nic96
Nup57
Nup49
Nsp1
Nup192•Nup145N
Nup192
Nup145N
Preincubation
Nup192
Nic96
Nup145N
Nup57
Nup49
Nsp1
B
CNT•Nic96•Nup192•Nup53
Nup82•SUMO-Nup159 T•Nup145N
Preincubation
Superose 6
440 kDa
320 kDa
110 kDa
Volume (ml)
CNT•Nic96•Nup192•Nup53
Nup192
Nic96
Nup53
Nup57
Nup49
Nsp1
Nup82•SUMO-Nup159 T•Nup145N
Nup82
Nup145N
Nup159 T
Preincubation
Nup192
Nic96
Nup82
Nup53
Nup145N
Nup57
Nup49
Nsp1
Nup159 T
C
CNT•Nup192•Nup145N•
SUMO-Nic96 R1-R2
Nic96 SOL
Preincubation
301 kDa
291 kDa
75 kDa
74 kDa
Molecular Mass (kDa)
Volume (ml)
CNT•Nup192•Nup145N•SUMO-Nic96 R1-R2
Nup192
Nup145N
Nic96 R1-R2
Nup57
Nup49
Nsp1
Nic96 SOL
Nic96 SOL
Preincubation
Nup192
Nic96 SOL
Nup145N
Nic96 R1-R2
Nup57
Nup49
Nsp1
D
CNT
Nup192 TAIL•SUMO-Nic96 R1-R2
Preincubation
135 kDa
74 kDa
69 kDa
Absorbance at 280 nm
Volume (ml)
CNT
Nup57
Nup49
Nsp1
Nup192 TAIL•SUMO-Nic96 R1-R2
Nup192 TAIL
Nic96 R1-R2
Preincubation
Nup192 TAIL
Nic96 R1-R2
Nup57
Nup49
Nsp1
E
CNT
SUMO-Nic96 R1
Preincubation
87 kDa
74 kDa
18 kDa
18 kDa
Volume (ml)
CNT
Nup57
Nup49
Nsp1
SUMO-Nic96 R1
Nic96 R1
Preincubation
Nup57
Nup49
Nsp1
Nic96 R1
F
Nup192 TAIL
SUMO-Nic96 R2
Preincubation
54 kDa
39 kDa
19 kDa
18 kDa
Molecular Mass (kDa)
Volume (ml)
Nup192 TAIL
Nup192 TAIL
SUMO-Nic96 R2
Nic96 R2
Preincubation
Nup192 TAIL
Nic96 R2

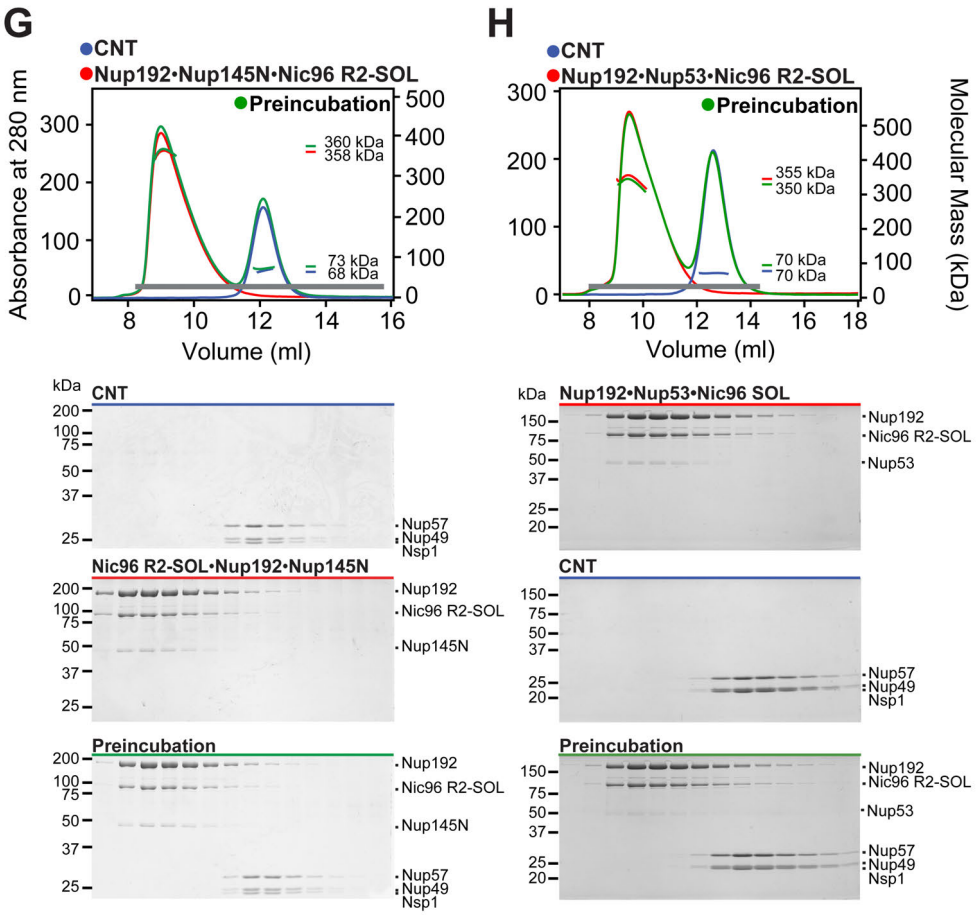
G
CNT
Nup192•Nup145N•Nic96 R2-SOL
Preincubation
360 kDa
358 kDa
73 kDa
68 kDa
Absorbance at 280 nm
Volume (ml)
H
CNT
Nup192•Nup53•Nic96 R2-SOL
Preincubation
355 kDa
350 kDa
70 kDa
70 kDa
Molecular Mass (kDa)
Volume (ml)
kDa
CNT
Nup57
Nup49
Nsp1
Nic96 R2-SOL•Nup192•Nup145N
Nup192
Nic96 R2-SOL
Nup145N
Preincubation
Nup192•Nup53•Nic96 SOL
Nup53

Fig. S1.
Reconstitution and dissection of the IRC. (**A** to **H**) SEC-MALS and SDS-PAGE analysis corresponding to Figure 1. SEC-MALS profiles of nucleoporins or nup complexes are shown individually (red and blue) and after their preincubation (green). Measured molecular masses are indicated for the peak fractions. Gray bars indicate fractions that were resolved on SDS-PAGE gels and visualized by Coomassie staining.

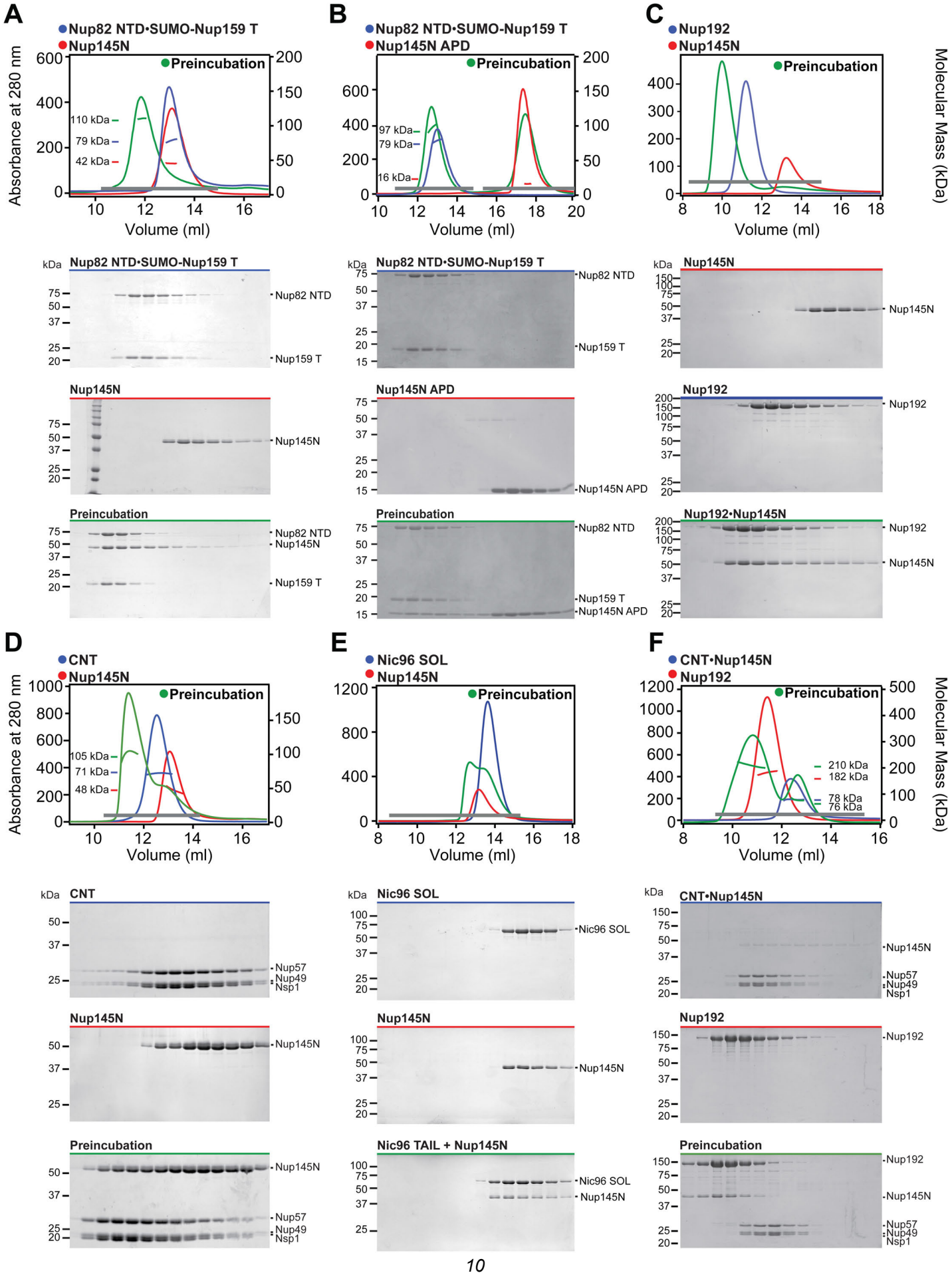
A
Nup82 NTD•SUMO-Nup159 T
Nup145N
Preincubation
110 kDa
79 kDa
42 kDa
Absorbance at 280 nm
Volume (ml)
Molecular Mass (kDa)
B
Nup82 NTD•SUMO-Nup159 T
Nup145N APD
Preincubation
97 kDa
79 kDa
16 kDa
Volume (ml)
C
Nup192
Nup145N
Preincubation
Volume (ml)
kDa
Nup82 NTD•SUMO-Nup159 T
Nup82 NTD
Nup159 T
Nup145N
Nup145N APD
Nup192
Nup192•Nup145N
Preincubation
D
CNT
Nup145N
Preincubation
105 kDa
71 kDa
48 kDa
Volume (ml)
E
Nic96 SOL
Nup145N
Preincubation
Volume (ml)
F
CNT•Nup145N
Nup192
Preincubation
210 kDa
182 kDa
78 kDa
76 kDa
Volume (ml)
CNT
Nup57
Nup49
Nsp1
Nic96 SOL
Nic96 TAIL + Nup145N

Fig. S2.
Reconstitution and dissection of the IRC (continued). (**A** to **F**) SEC-MALS and SDS-PAGE analysis corresponding to Figure 1. SEC-MALS profiles of nucleoporins or nup complexes are shown individually (red and blue) and after their preincubation (green). Measured molecular masses are indicated for the peak fractions. Gray bars indicate fractions that were resolved on SDS-PAGE gels and visualized by Coomassie staining.

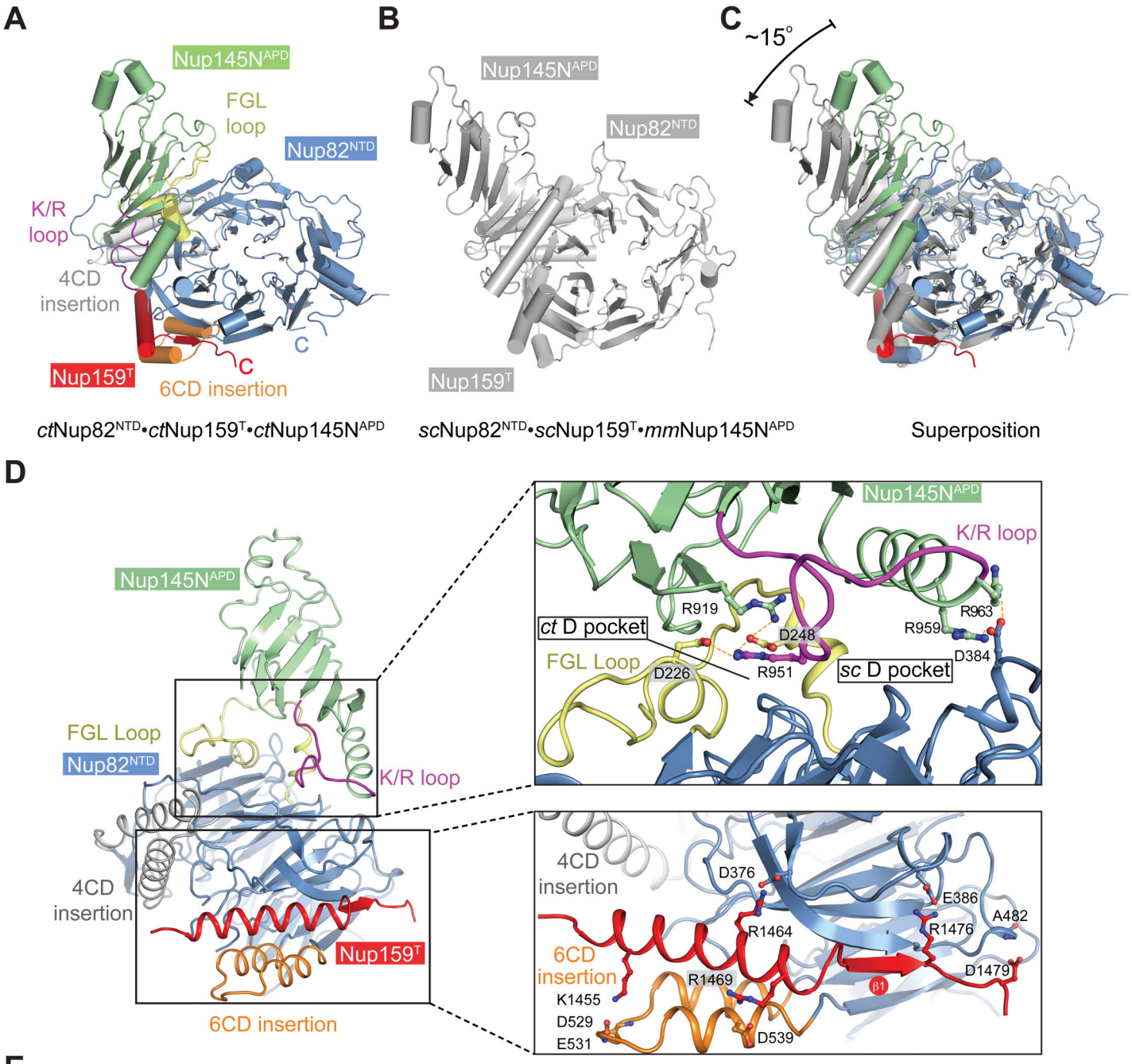
A
Nup145N^APD
FGL loop
Nup82^NTD
K/R loop
4CD insertion
C
C
Nup159^T
6CD insertion
ctNup82^NTD•ctNup159^T•ctNup145N^APD
B
Nup145N^APD
Nup82^NTD
Nup159^T
scNup82^NTD•scNup159^T•mmNup145N^APD
C
~15°
Superposition
D
Nup145N^APD
FGL Loop
Nup82^NTD
K/R loop
4CD insertion
Nup159^T
6CD insertion
Nup145N^APD
K/R loop
R919
ct D pocket
D248
R959
R963
FGL Loop
D226
R951
sc D pocket
D384
4CD insertion
D376
E386
A482
R1464
R1476
6CD insertion
R1469
D1479
β1
K1455
D529
E531
D539
E
Nup159
αA
β1
ctNup159 T
scNup159 T
. . . . . L R A R E A K R K A T L R M L R E S L A R V G P N V V R L R D D D
F K V V E V G L A M N T K K Q I G D F F K N L N M A K . . . . . .
1449
1460
1470
1481
Nup82
αE'
αF'
ctNup82 FGL loop
scNup82 FGL loop
D L K K L A D A T Y L D Q D F G V S T S A T N K G F S P D A F D M E V
. . . . . N K P . . N N S F G L D A R V N D . . . . . .
220
230
240
250
254
Nup145N
ctNup145N K/R loop
mmNup98 K/R loop
. H S W P R G G P T . . . I K G . .
D G V W P T D K T S R C L I K S P D
947
958

Fig. S3.
Structure of the minimal CFC in complex with Nup145N^{APD}. (**A**) Structure of the Nup82^{NTD}•Nup159^{T}•Nup145N^{APD} hetero-trimer shown in cartoon representation. Nup145N^{APD} (green), Nup159^{T} (red), and Nup82^{NTD} (blue), the Nup82^{NTD} helical 4CD (grey) and 6CD (orange) insertions and FGL loop (yellow), and the conserved Nup145N^{APD} K loop (purple) are illustrated. (**B**) Structure of the previously determined *sc*Nup82^{NTD}•*sc*Nup159^{T}•*mm*Nup145N^{APD} hetero-trimer (PDB ID: 3TKN) shown in cartoon representation (*67*). (**C**) Superposition of the two hetero-trimers in cartoon representation, revealing the evolutionary conservation of their architectures, and differing mainly by an angular displacement of Nup145^{APD}. (**D**) The *Inset* marks the location of the two close-up views, depicting the molecular details of the Nup145N^{APD}-Nup82^{NTD} interaction (top) and the Nup159^{T}-Nup82^{NTD} interaction (bottom). The D pocket that binds the K loop is indicated. (**E**) Sequence alignments of the conserved *S. cerevisiae* and *C. thermophilum* Nup159^{T}, the Nup82^{NTD} FGL loop, and the Nup145N K/R loop. Sequence similarity is shaded from white (less than 60 % similarity), to yellow (60 % similarity), to red (100 % identity) using the BLOSUM62 matrix. Numbering below alignment is according to the *C. thermophilum* proteins. Secondary structure is shown above the alignment.

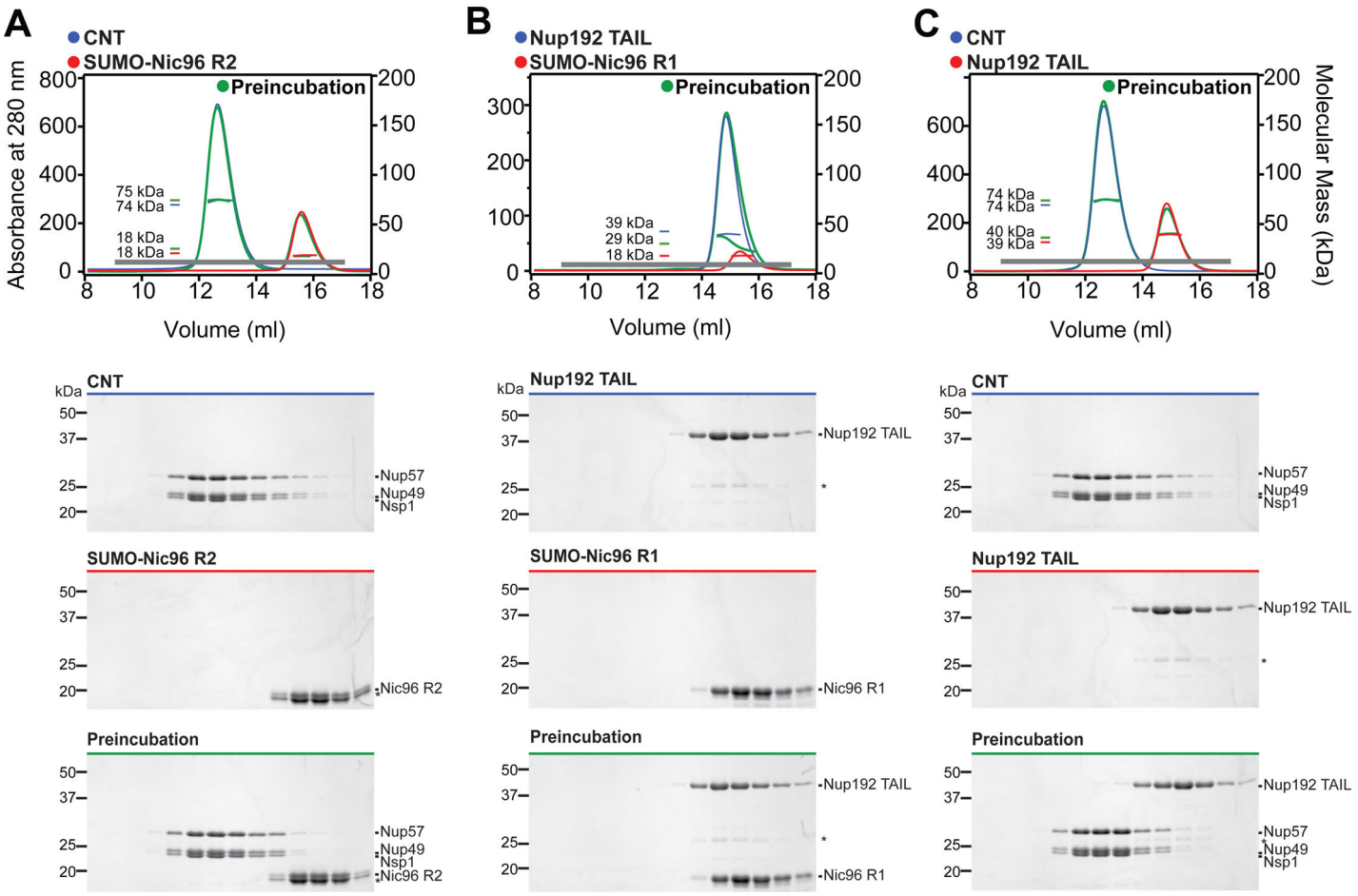
A
CNT
SUMO-Nic96 R2
Preincubation
Absorbance at 280 nm
75 kDa
74 kDa
18 kDa
18 kDa
Volume (ml)
B
Nup192 TAIL
SUMO-Nic96 R1
Preincubation
39 kDa
29 kDa
18 kDa
Volume (ml)
C
CNT
Nup192 TAIL
Preincubation
74 kDa
74 kDa
40 kDa
39 kDa
Volume (ml)
Molecular Mass (kDa)
kDa
CNT
Nup57
Nup49
Nsp1
SUMO-Nic96 R2
Nic96 R2
Preincubation
Nup192 TAIL
SUMO-Nic96 R1
Nic96 R1
*

Fig. S4.
The CNT does not interact with Nic96^{R2} or Nup192^{TAIL}, nor does Nic96^{R1} bind Nup192^{TAIL}. (**A** to **C**) SEC-MALS profiles of nucleoporins or nup complexes are shown individually (red and blue) and after their preincubation (green). Measured molecular masses are indicated for the peak fractions. Gray bars indicate fractions that were resolved on SDS-PAGE gels and visualized by Coomassie staining. Asterisks indicate degradation products or contamination.

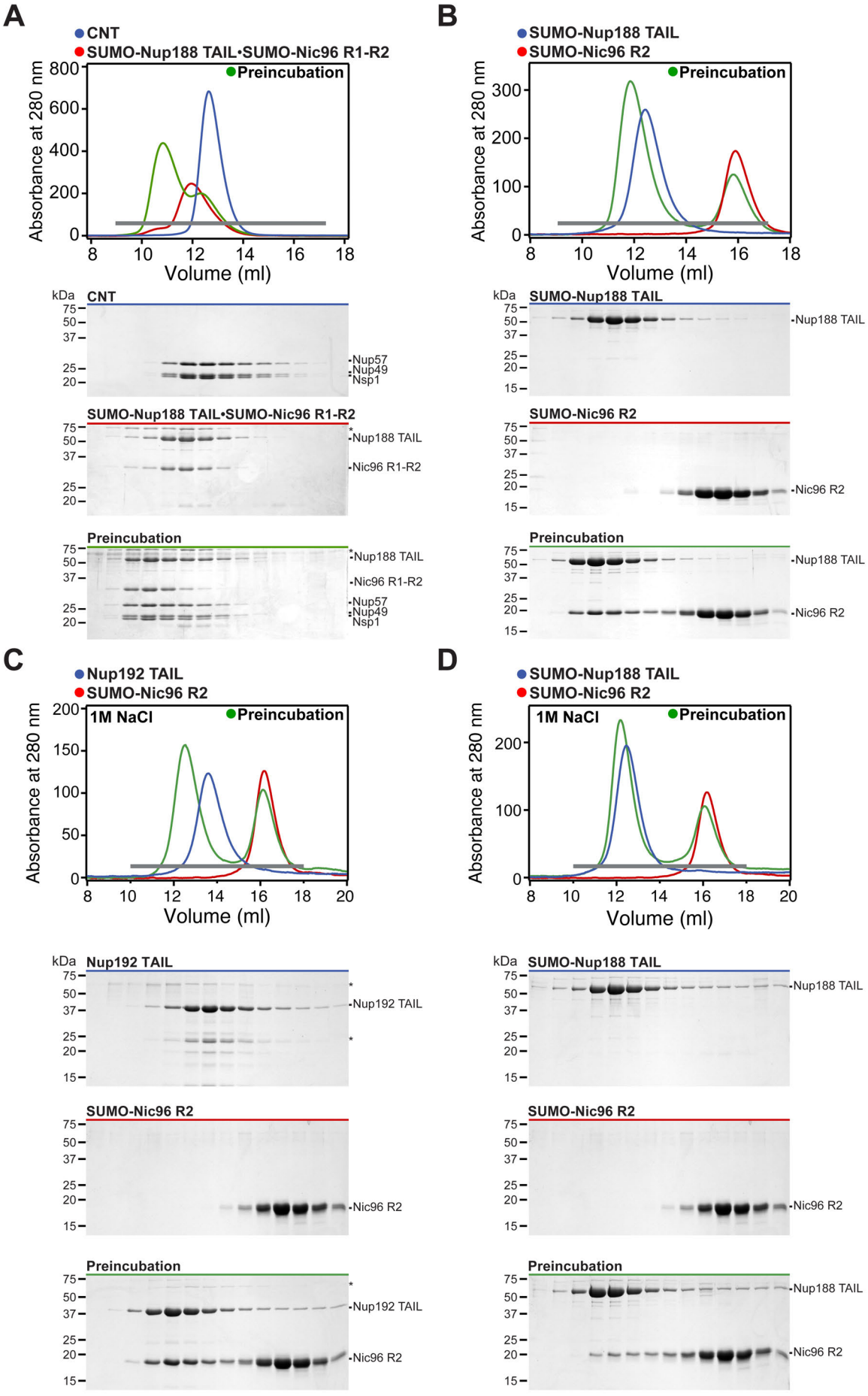
A
CNT
SUMO-Nup188 TAIL•SUMO-Nic96 R1-R2
Preincubation
Absorbance at 280 nm
Volume (ml)
kDa
CNT
Nup57
Nup49
Nsp1
SUMO-Nup188 TAIL•SUMO-Nic96 R1-R2
Nup188 TAIL
Nic96 R1-R2
Preincubation
B
SUMO-Nup188 TAIL
SUMO-Nic96 R2
Preincubation
Absorbance at 280 nm
Volume (ml)
kDa
SUMO-Nup188 TAIL
Nup188 TAIL
SUMO-Nic96 R2
Nic96 R2
Preincubation
C
Nup192 TAIL
SUMO-Nic96 R2
1M NaCl
Preincubation
Absorbance at 280 nm
Volume (ml)
kDa
Nup192 TAIL
SUMO-Nic96 R2
Nic96 R2
Preincubation
D
SUMO-Nup188 TAIL
SUMO-Nic96 R2
1M NaCl
Preincubation
Absorbance at 280 nm
Volume (ml)
kDa
SUMO-Nup188 TAIL
Nup188 TAIL
SUMO-Nic96 R2
Nic96 R2
Preincubation

Fig. S5.
Nup188^{TAIL} forms an alternative complex with the CNT. (**A**) Reconstitution of SUMO-Nup188^{TAIL}•SUMO-Nic96^{R1-R2}•CNT. (**B**) Reconstitution of SUMO-Nup188^{TAIL}•SUMO-Nic96^{R2}. (**C, D**) SEC analysis of Nup192^{TAIL}•SUMO-Nic96^{R2} and SUMO-Nup188^{TAIL}•SUMO-Nic96^{R2} carried out in a 1 M NaCl buffer. SEC profiles of nucleoporins or nup complexes are shown individually (red and blue) and after their preincubation (green). Gray bars indicate fractions that were resolved on SDS-PAGE gels and visualized by Coomassie staining. Asterisks indicate degradation products or contamination.

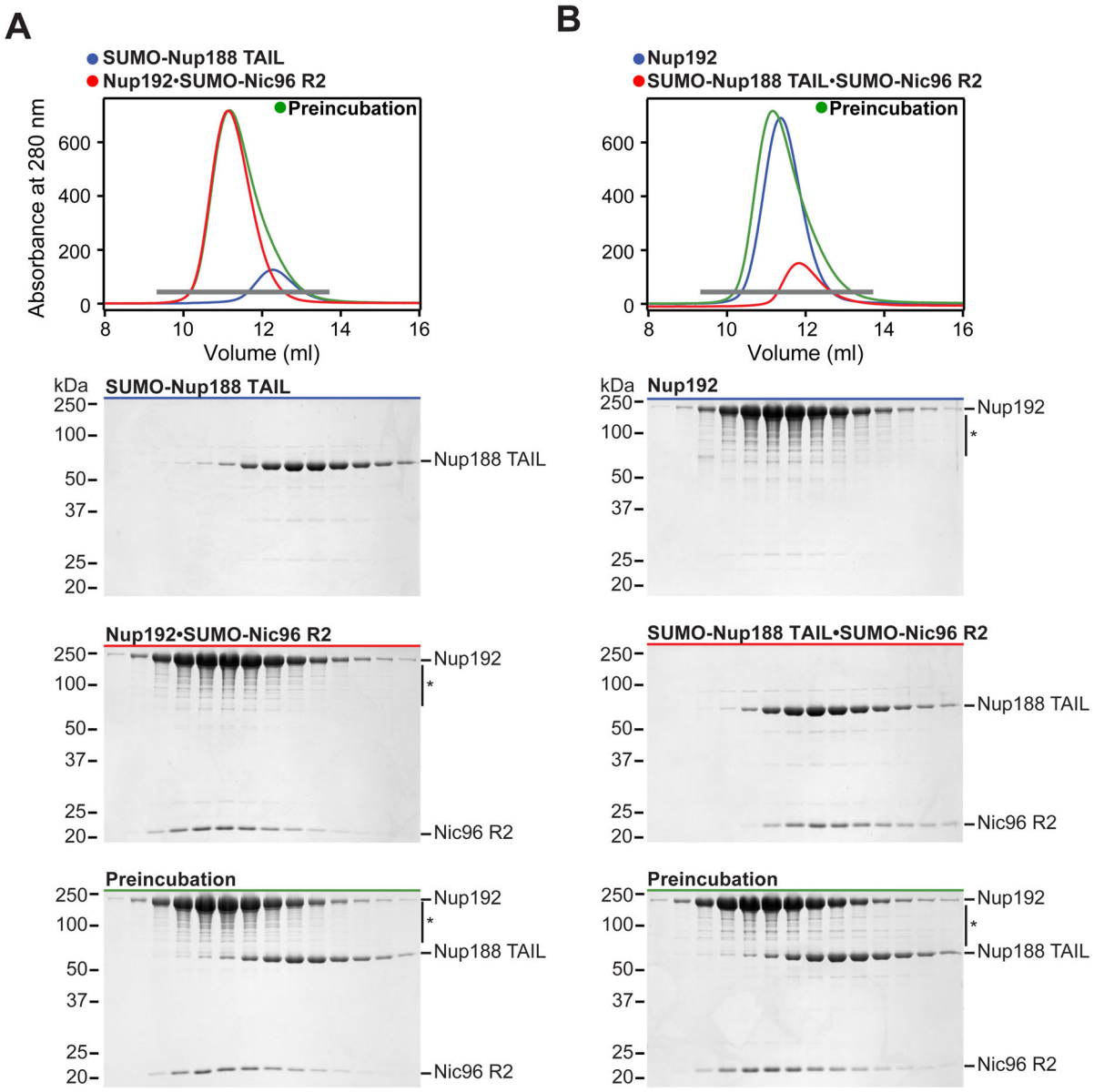
A
SUMO-Nup188 TAIL
Nup192•SUMO-Nic96 R2
Preincubation
Absorbance at 280 nm
Volume (ml)
kDa
SUMO-Nup188 TAIL
Nup188 TAIL
Nup192•SUMO-Nic96 R2
Nup192
Nic96 R2
Preincubation
B
Nup192
SUMO-Nup188 TAIL•SUMO-Nic96 R2
Preincubation
Volume (ml)
kDa
Nup192
SUMO-Nup188 TAIL•SUMO-Nic96 R2
Nup188 TAIL
Nic96 R2
Preincubation

Fig. S6.
Binding of Nup192 and Nup188 to Nic96 is mutually exclusive. (**A**) SEC interaction analysis of SUMO-Nup188^{TAIL} challenging a preformed Nup192•SUMO-Nic96^{R2} complex. (**B**) SEC interaction analysis of Nup192 challenging a preformed SUMO-Nup188^{TAIL}•SUMO-Nic96^{R2} complex. SEC profiles of nucleoporins or nup complexes are shown individually (red and blue) and after their preincubation (green). Proteins were mixed at equimolar ratios. Gray bars indicate fractions that were resolved on SDS-PAGE gels and visualized by Coomassie staining. Asterisks indicate degradation products or contamination.

Nup192 TAIL

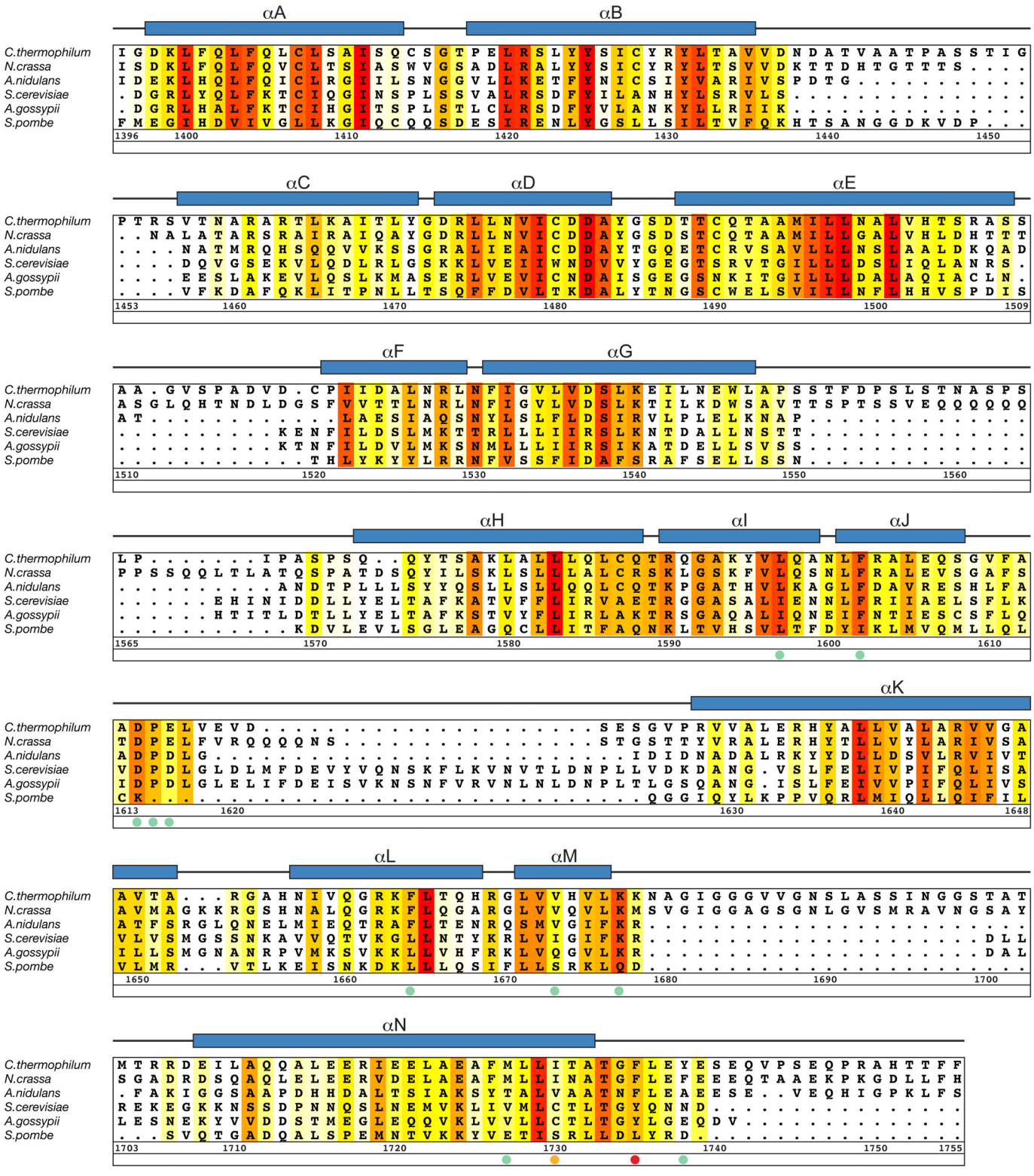
αA
αB
αC
αD
αE
αF
αG
αH
αI
αJ
αK
αL
αM
αN
C.thermophilum
N.crassa
A.nidulans
S.cerevisiae
A.gossypii
S.pombe

Fig. S7.
Multispecies sequence alignment of Nup192^{TAIL}. Sequences from six diverse fungal species were aligned and colored by sequence similarity according to the BLOSUM62 matrix from white (less than 40 % similarity), to yellow (40 % similarity), to red (100 % identity). Numbering below alignment is relative to *C. thermophilum*. Secondary structure observed in the Nup192^{TAIL} structure is shown above the alignment; α-helices (blue bars) and black lines (unstructured regions). Residues tested for their ability to interact with Nic96 in a mutational analysis (Figures 2 and S12) are indicated with dots below the alignment and colored according to the measured effect; no effect (green), mild effect (orange), abolished binding (red).

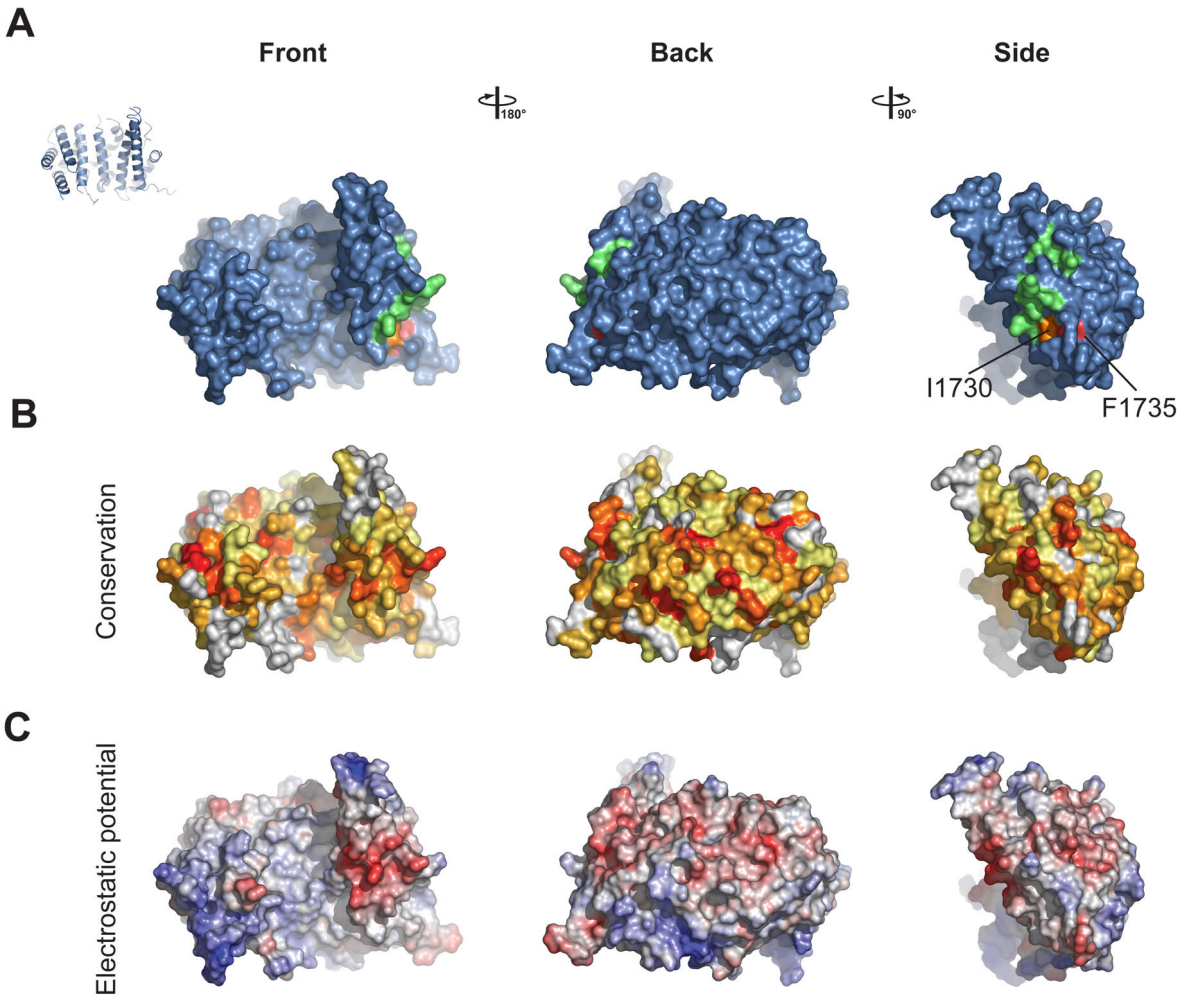
A
Front
Back
Side
180°
90°
I1730
F1735
B
Conservation
C
Electrostatic potential

Fig. S8.
Surface properties of Nup192^{TAIL}. Surface representation of Nup192^{TAIL} is shown in three different orientations, front, back and side. The degree of rotation around the vertical axis is indicated between the respective views. (**A**) Mutated Nup192^{TAIL} residues are colored according to their effect on SUMO-Nic96^{R2} binding; no effect (green), mild effect (orange), abolished binding (red). (**B**) Surface representation colored according to sequence identity based on the alignment in Figure S7. (**C**) Surface representation colored according to electrostatic potential from -10 k_BT/e (red) to +10 k_BT/e (blue).

Nup188 TAIL

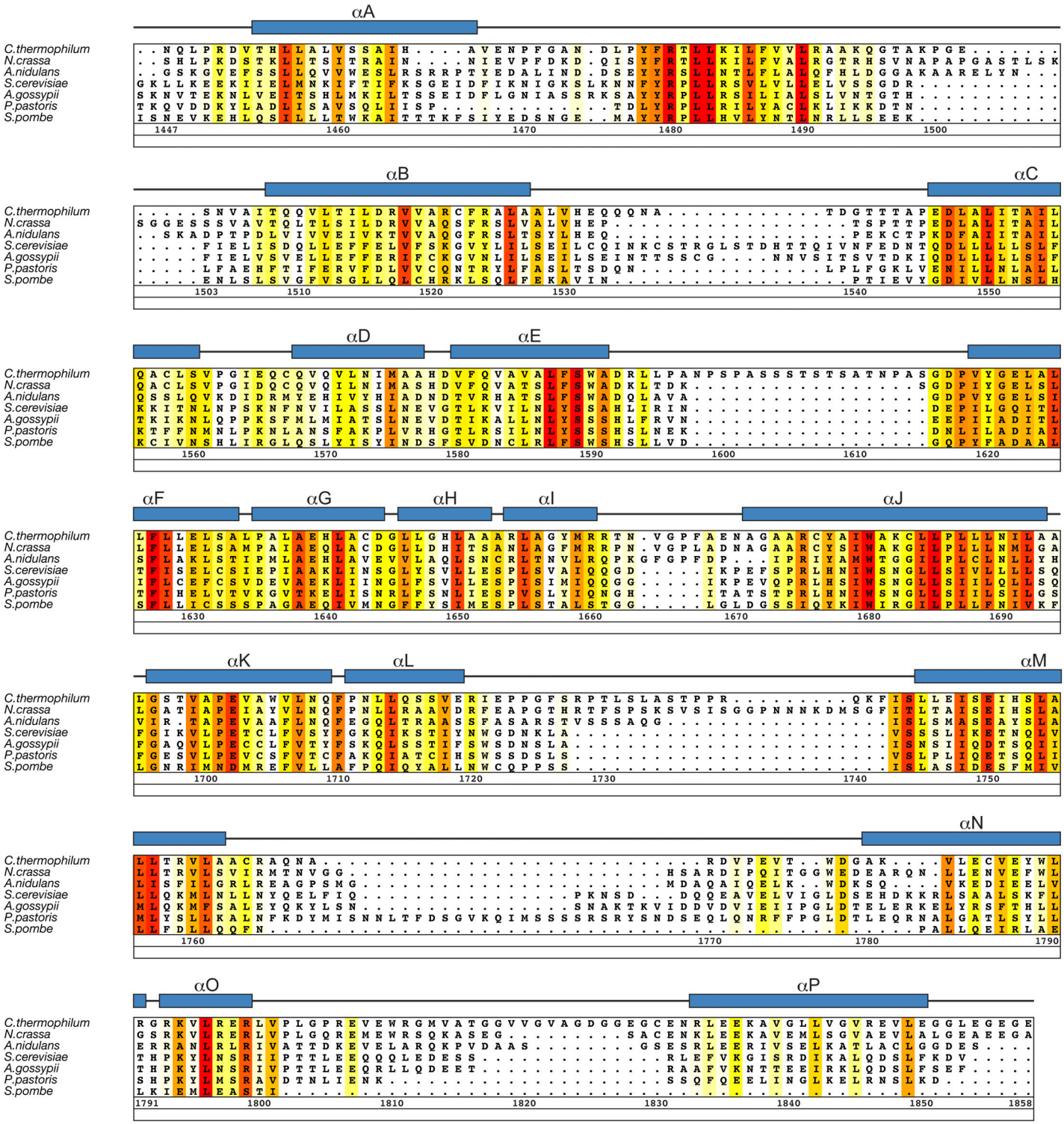
αA
αB
αC
αD
αE
αF
αG
αH
αI
αJ
αK
αL
αM
αN
αO
αP
C.thermophilum
N.crassa
A.nidulans
S.cerevisiae
A.gossypii
P.pastoris
S.pombe

Fig. S9.
Multispecies sequence alignment of Nup188^{TAIL}. Sequences from seven diverse fungal species were aligned and colored by sequence similarity according to the BLOSUM62 matrix from white (less than 40 % similarity), to yellow (40 % similarity), to red (100 % identity). Numbering below alignment is relative to *C. thermophilum*. Secondary structure observed in the Nup188^{TAIL} structure is shown above the alignment; α-helices (blue bars) and black lines (unstructured regions).

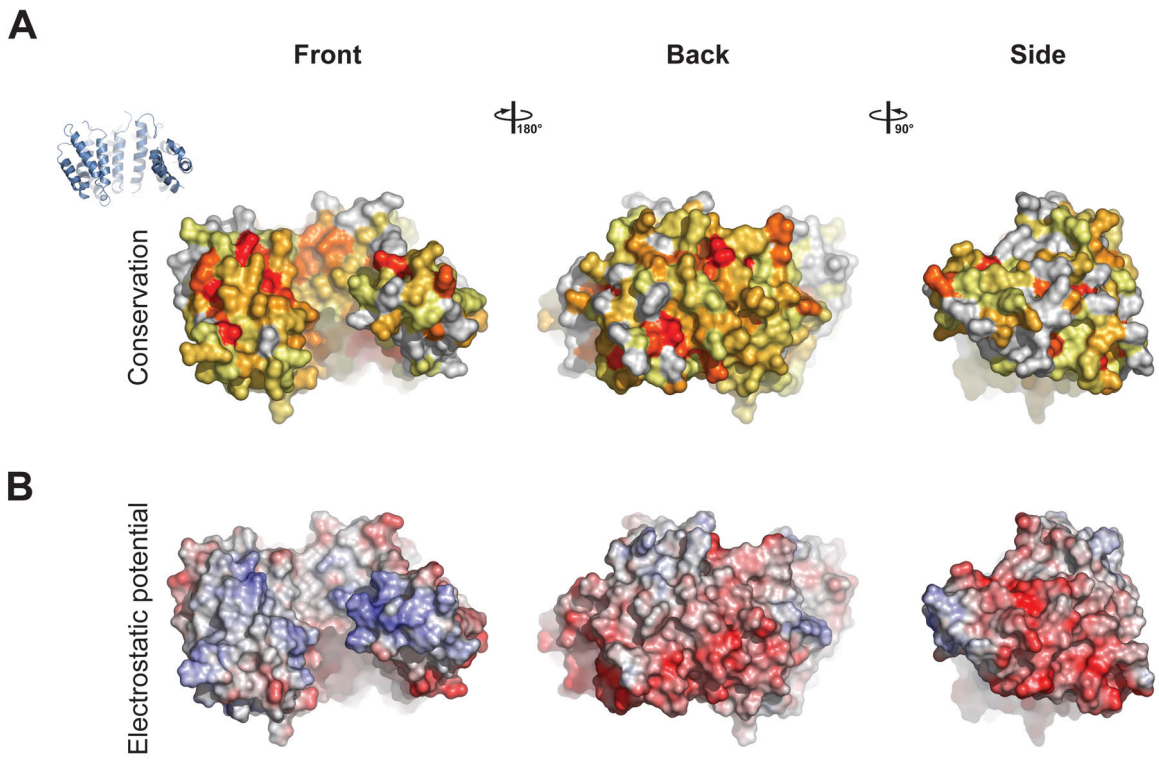
A
Front
Back
Side
180°
90°
Conservation
B
Electrostatic potential

Fig. S10.
Surface properties of Nup188^{TAIL}. Surface representation of Nup188^{TAIL} is shown in three different orientations, front, back and side. Rotations around the vertical axis are indicated between the respective views. (**A**) Surface representation colored according to sequence identity based on alignment in Figure S9. (**B**) Surface representation colored according to electrostatic potential from -10 k_BT/e (red) to +10 k_BT/e (blue).

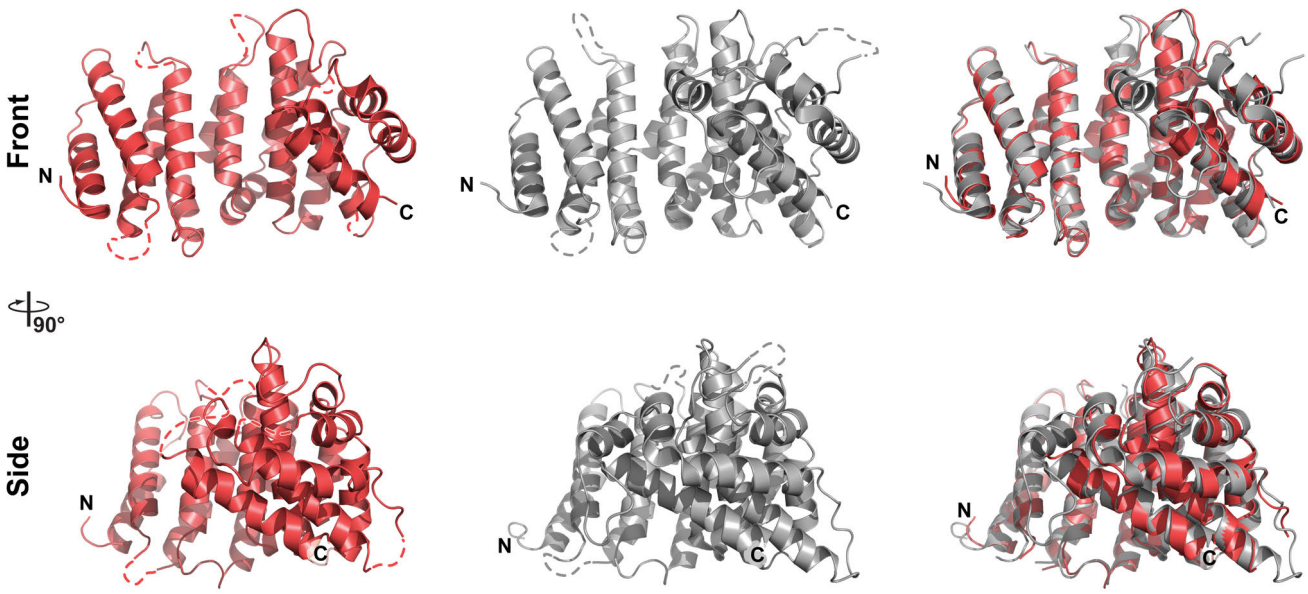
C.thermophilum Nup188 TAIL
M.thermophilia Nup188 TAIL
Superposition
Front
N
C
90°
Side

Fig. S11.
Comparison of *ct*Nup188^{TAIL} and *mt*Nup188^{TAIL} structures. Cartoon representations of (**A**) *C. thermophilum* Nup188^{TAIL} (red), (**B**) *M. thermophila* Nup188^{TAIL} (grey) (PDB ID: 4KF8) (*68*), and (**C**) a superposition of the two structures is shown in two different orientations.

A

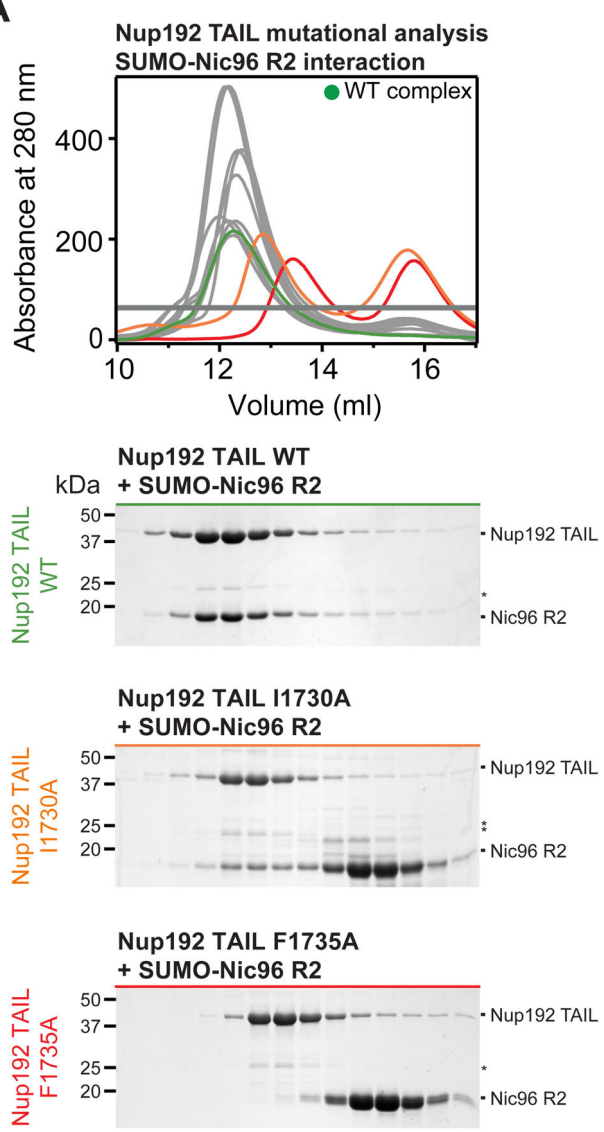

B

Nup192 TAIL mutations

Mutation	effect
L1597A	-
F1602A	insoluble
F1602W	-
F1611A	insoluble
DPE1614,15,16AAA	-
DPE1614,15,16APA	-
F1664A	insoluble
F1664W	-
V1673A	-
L1676A	insoluble
K1677A	-
M1727A	-
I1730A	+
F1735A	+++
Y1738A	-

Fig. S12.
Identification of Nup192^{TAIL} mutations that disrupt SUMO-Nic96^{R2} binding. (**A**) SEC interaction analysis between Nup192^{TAIL} mutants and SUMO-Nic96^{R2}. SEC profiles are colored according to the effect on SUMO-Nic96^{R2} binding; no effect (gray), mild effect (orange), or abolished binding (red). As reference, the wild type complex is shown (green). A gray bar indicates fractions that were resolved on SDS-PAGE gels and visualized by Coomassie staining. (**B**) Summary of tested Nup192^{TAIL} mutants and their effect on SUMO-Nic96^{R2} binding; (-) no effect, (+) decreased binding, (+++) abolished binding. The colors of the dots correspond to the color of the respective SEC profile in (A).

Nic96 R1-R2

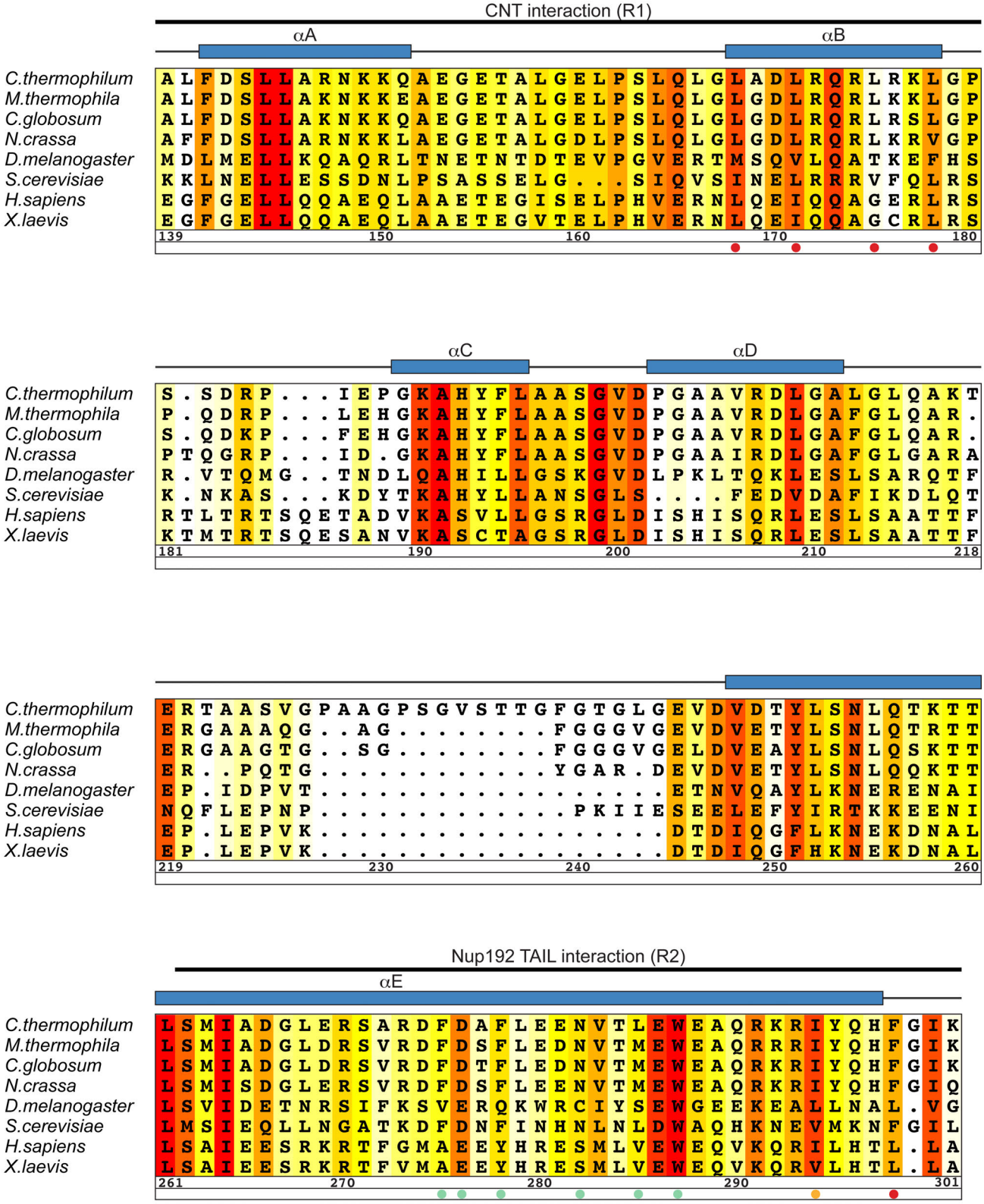
CNT interaction (R1)
αA
αB
C.thermophilum
M.thermophila
C.globosum
N.crassa
D.melanogaster
S.cerevisiae
H.sapiens
X.laevis
139
150
160
170
180
αC
αD
181
190
200
210
218
219
230
240
250
260
Nup192 TAIL interaction (R2)
αE
261
270
280
290
301

Fig. S13.
Multispecies sequence alignment of Nic96^{R1-R2}. Sequences from eight diverse species were aligned and colored by sequence similarity according to the BLOSUM62 matrix from white (less than 40 % similarity), to yellow (40 % similarity), to red (100 % identity). Numbering below alignment is relative to *C. thermophilum*. The secondary structure is shown above the alignment; α-helices are represented by blue bars. Black bars above the alignment indicate CNT-binding (R1) and Nup192-binding regions (R2). Dots below the alignment indicate the positions of mutations tested for CNT or Nup192^{TAIL} binding (Figures 3, S15, and S16); no effect (green), mild effect (orange), abolished binding (red).

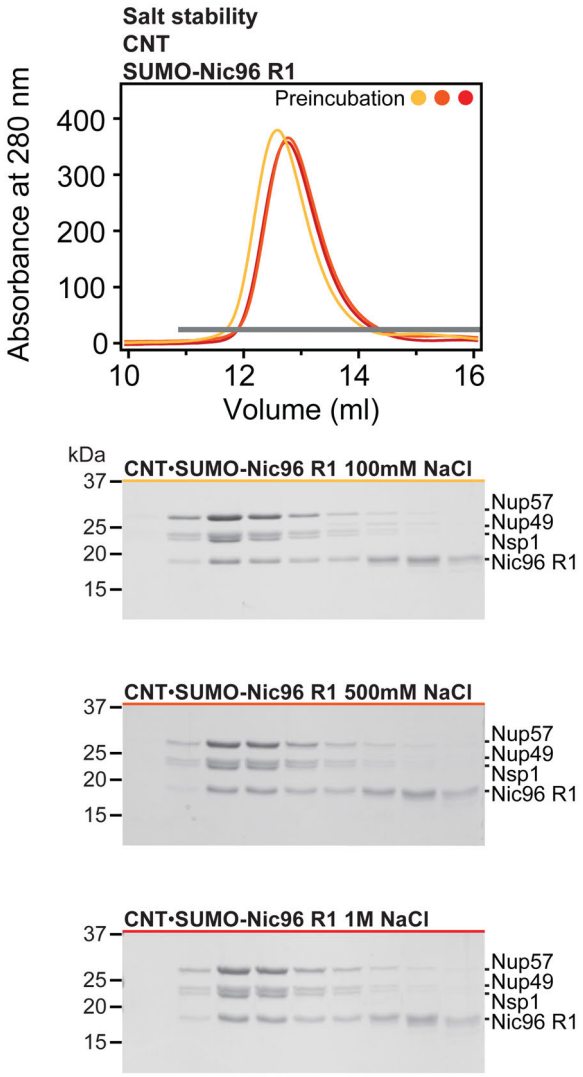
Salt stability
CNT
SUMO-Nic96 R1
Preincubation
Absorbance at 280 nm
400
300
200
100
0
10
12
14
16
Volume (ml)
kDa
CNT•SUMO-Nic96 R1 100mM NaCl
37
25
20
15
Nup57
Nup49
Nsp1
Nic96 R1
CNT•SUMO-Nic96 R1 500mM NaCl
37
25
20
15
Nup57
Nup49
Nsp1
Nic96 R1
CNT•SUMO-Nic96 R1 1M NaCl
37
25
20
15
Nup57
Nup49
Nsp1
Nic96 R1

Fig. S14.
Salt stability of the CNT•SUMO-Nic96^{R1} complex. SEC analysis of purified CNT•SUMO-Nic96^{R1} carried out in a buffer containing 0.1 M (yellow), 0.5 M (light orange) or 1.0 M NaCl (red). A gray bar indicates fractions that were resolved on a SDS-PAGE gel and visualized by Coomassie staining.

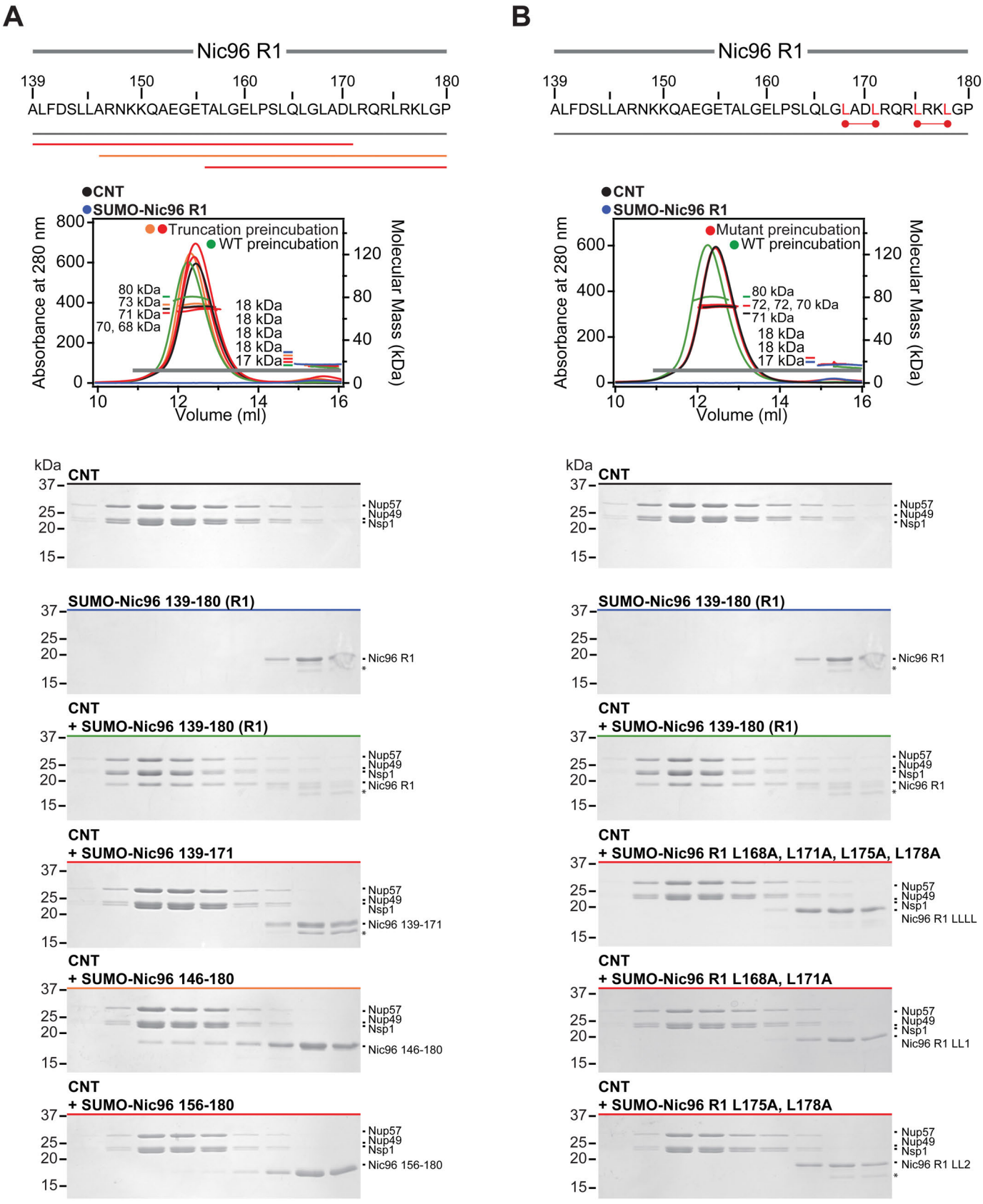
A
Nic96 R1
139
150
160
170
180
ALFDSLLARNKKQAEGETALGELPSLQLGLADLRQRLRKLGP
CNT
SUMO-Nic96 R1
Truncation preincubation
WT preincubation
Absorbance at 280 nm
Molecular Mass (kDa)
Volume (ml)
80 kDa
73 kDa
71 kDa
70, 68 kDa
18 kDa
17 kDa
B
Nic96 R1
ALFDSLLARNKKQAEGETALGELPSLQLGLADLRQRLRKLGP
CNT
SUMO-Nic96 R1
Mutant preincubation
WT preincubation
80 kDa
72, 72, 70 kDa
71 kDa
18 kDa
17 kDa
Volume (ml)
kDa
CNT
Nup57
Nup49
Nsp1
SUMO-Nic96 139-180 (R1)
Nic96 R1
CNT
+ SUMO-Nic96 139-180 (R1)
CNT
+ SUMO-Nic96 139-171
Nic96 139-171
CNT
+ SUMO-Nic96 146-180
Nic96 146-180
CNT
+ SUMO-Nic96 156-180
Nic96 156-180
CNT
+ SUMO-Nic96 R1 L168A, L171A, L175A, L178A
Nic96 R1 LLLL
CNT
+ SUMO-Nic96 R1 L168A, L171A
Nic96 R1 LL1
CNT
+ SUMO-Nic96 R1 L175A, L178A
Nic96 R1 LL2

Fig. S15.
Mapping and mutational analysis of the minimal Nic96^{R1} region required for CNT binding. (**A**, **B**) Analyzed Nic96^{R1} truncations and Nic96^{R1} leucine-alanine mutants are indicated below the primary Nic96^{R1} sequence. SEC-MALS profiles of SUMO-Nic96^{R1} fragments or mutants preincubated with CNT are shown and colored according to their effect on complex formation; mild effect (orange) or abolished binding (red). As reference, SEC profiles of CNT (black) and SUMO-Nic96^{R1} (blue) and their preincubation (green) are shown. Measured molecular masses are indicated for the peak fractions. Gray bars indicate fractions that were resolved on SDS-PAGE gels and visualized by Coomassie staining. LL1, LL2, and LLLL refer to the three combinations of SUMO-Nic96^{R1} leucine-alanine mutants tested. Asterisks indicate degradation products or contamination.

A

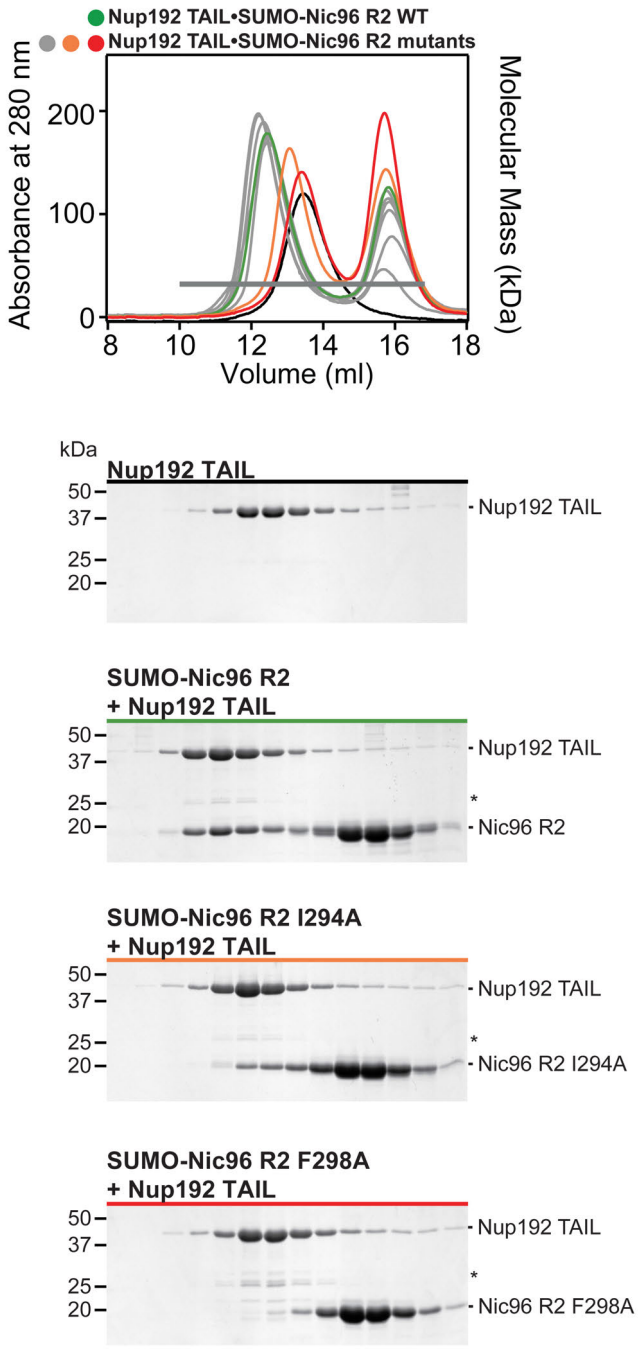

B

Nic96 R2 mutations

Mutation	effect
F275A	-
D276A	-
F278A	-
N282A	-
L285A	-
W287A	-
I294A	+
F298A	+++

Fig. S16.
Identification of Nic96^{R2} mutations that disrupt Nup192^{TAIL} binding. (**A**) SEC interaction analysis between SUMO-Nic96^{R2} mutants and Nup192^{TAIL}. SEC profiles are colored according to the effect on Nup192^{TAIL} binding; no effect (gray), mild effect (orange), or abolished binding (red). For reference, SEC profiles of wild type Nup192^{TAIL}•SUMO-Nic96^{R2} (green) and Nup192^{TAIL} (black) are shown. A gray bar indicates fractions that were resolved on SDS-PAGE gels and visualized by Coomassie staining. (**B**) Summary of tested SUMO-Nic96^{R2} mutants and their effect on Nup192^{TAIL} binding; (-) no effect, (+) decreased binding, (+++) abolished binding. The colors of the dots correspond to the color of the respective SEC profile in (A).

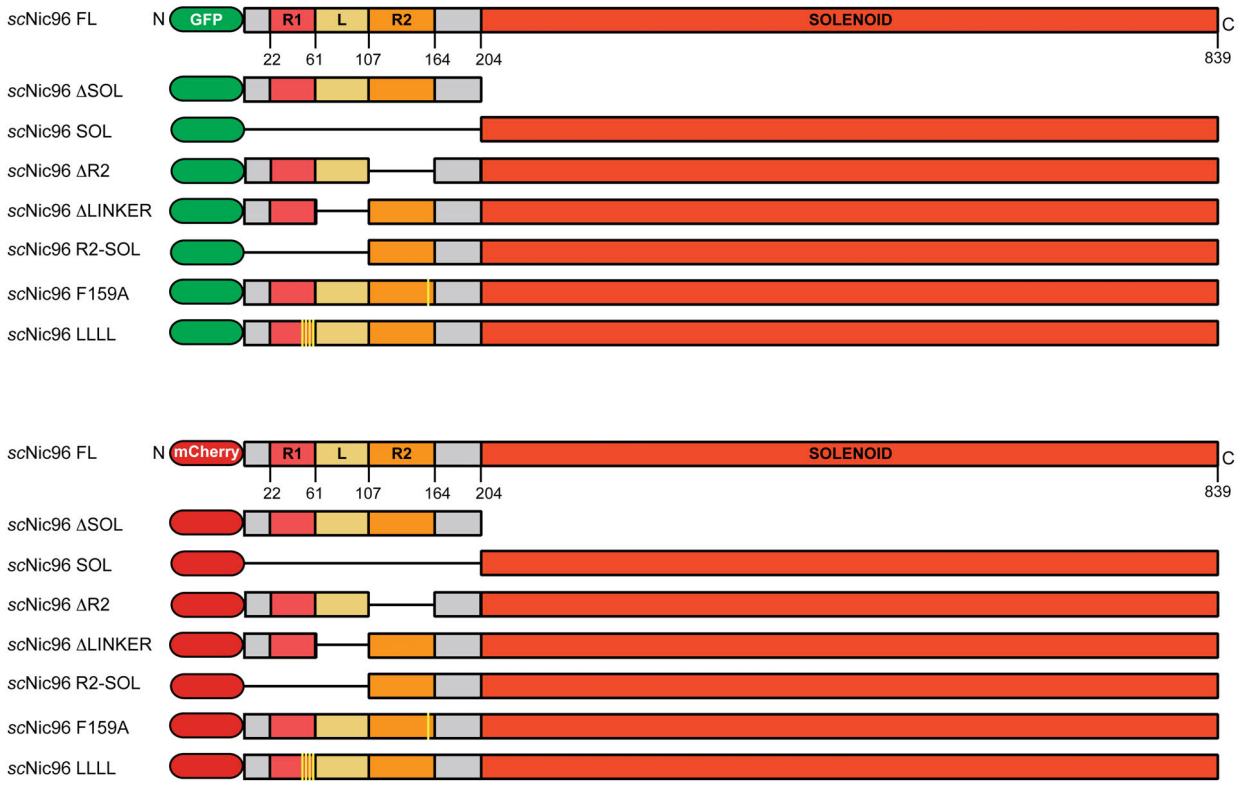
scNic96 FL
N
GFP
R1
L
R2
SOLENOID
C
22
61
107
164
204
839
scNic96 ΔSOL
scNic96 SOL
scNic96 ΔR2
scNic96 ΔLINKER
scNic96 R2-SOL
scNic96 F159A
scNic96 LLLL
scNic96 FL
N
mCherry
R1
L
R2
SOLENOID
C
22
61
107
164
204
839
scNic96 ΔSOL
scNic96 SOL
scNic96 ΔR2
scNic96 ΔLINKER
scNic96 R2-SOL
scNic96 F159A
scNic96 LLLL

Fig. S17.
***S. cerevisiae* GFP-Nic96 constructs used for *in vivo* analyses.** The domain architecture of *S. cerevisiae* Nic96 is shown and colored according to Figure 1. Black lines indicate the regions that were removed in various Nic96 deletion mutants. The positions of the F159A and LLLL mutants that abolish Nup192 and CNT binding, respectively, are highlighted in yellow.

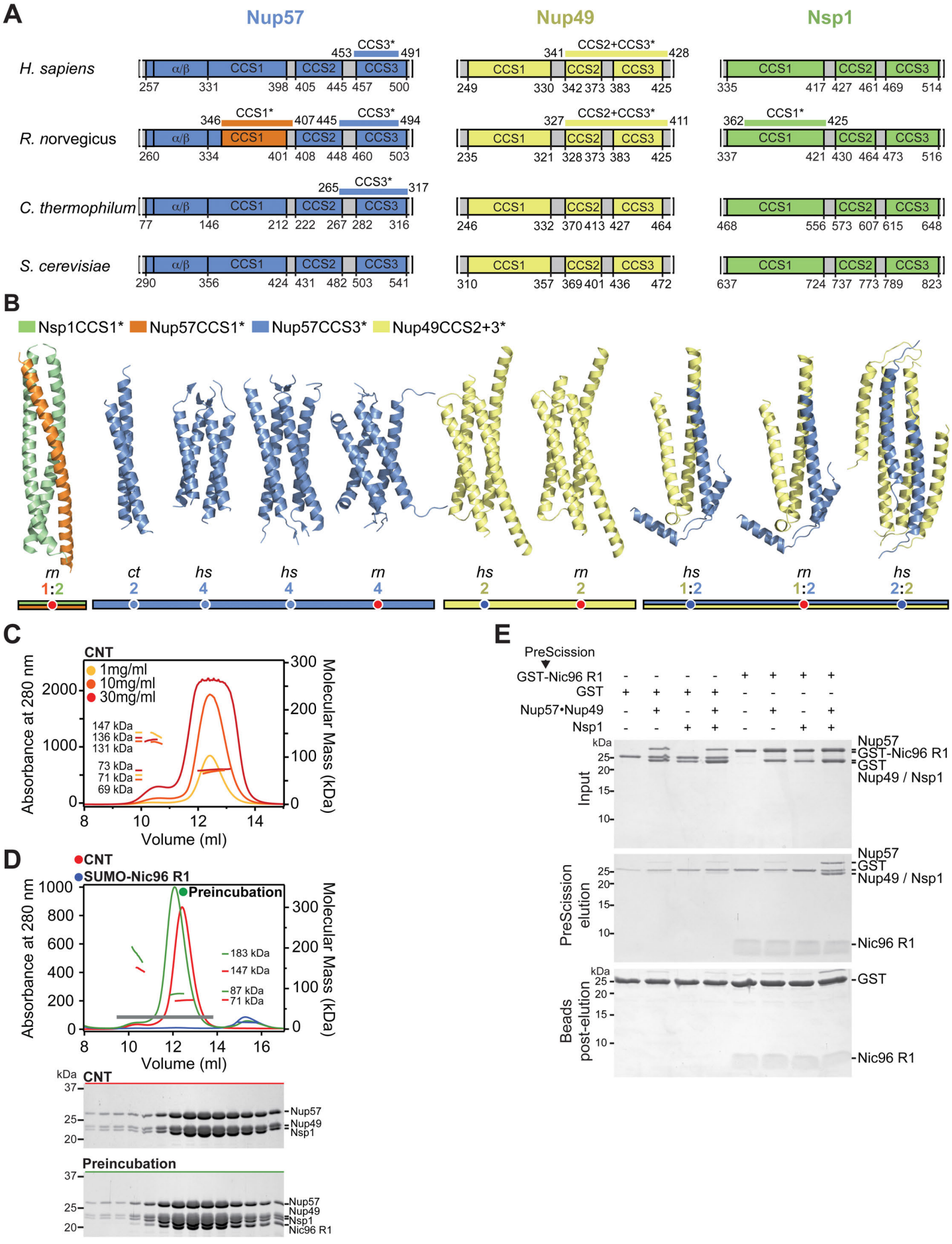
A
Nup57
Nup49
Nsp1
H. sapiens
R. norvegicus
C. thermophilum
S. cerevisiae
α/β
CCS1
CCS2
CCS3
CCS3*
CCS1*
CCS2+CCS3*
B
Nsp1CCS1*
Nup57CCS1*
Nup57CCS3*
Nup49CCS2+3*
rn 1:2
ct 2
hs 4
hs 4
rn 4
hs 2
rn 2
hs 1:2
rn 1:2
hs 2:2
C
CNT
1mg/ml
10mg/ml
30mg/ml
147 kDa
136 kDa
131 kDa
73 kDa
71 kDa
69 kDa
Absorbance at 280 nm
Molecular Mass (kDa)
Volume (ml)
D
CNT
SUMO-Nic96 R1
Preincubation
183 kDa
147 kDa
87 kDa
71 kDa
Nup57
Nup49
Nsp1
Nic96 R1
E
PreScission
GST-Nic96 R1
GST
Nup57•Nup49
Nsp1
Input
PreScission elution
Beads post-elution
Nup57
GST-Nic96 R1
GST
Nup49 / Nsp1
Nic96 R1

Fig. S18.
Characterization of channel nucleoporin fragments and the intact CNT. (**A**) Domain structures of the three CNT-forming channel nups from *H. sapiens*, *R. norvegicus*, and *C. thermophilum*. Bars indicate the boundaries of the crystallized Nup57 (blue, orange), Nup49 (yellow), and Nsp1 (green) fragments. (**B**) Crystal structures of seven channel nup fragments in isolation or in complex colored according to (A). The species and fragment stoichiometry are indicated for each structure. For clarity, only the homo-dimers of *H. sapiens* and *R. norvegicus* Nup49$^{CCS2+3*}$ are shown. The structures of Nup57^{CCS3*}, *hs*Nup57^{CCS3*} (two different states), *hs*Nup49$^{CCS2+3*}$, and *hs*Nup49$^{CCS2+3*}$•*hs*Nup57^{CCS3*} (with 1:2 and 2:2 stoichiometry) reported here are indicated with blue dots. The previously determined structure of *rn*Nup57^{CCS1*}•*rn*Nsp1^{CCS1*} (1:2 stoichiometry), *rn*Nup57^{CCS3*}, *rn*Nup49$^{CCS2+3*}$, and *rn*Nup49$^{CCS2+3*}$•*rn*Nup57^{CCS3*} (with 1:2 stoichiometry) are marked with red dots (*69-71*). (**C**) SEC-MALS profiles of the CNT at three different concentrations (yellow to red). Asterisks indicate that the crystallized channel nup fragments do not exactly correspond to the predicted coiled-coil regions. (**D**) SEC-MALS interaction analysis of CNT (red), SUMO-Nic96^{R1} (blue), and after their preincubation (green). Measured molecular masses are indicated for the peak fractions. Gray bars indicate fractions that were resolved on SDS-PAGE gels and visualized by Coomassie staining. **(E)** GST pull-down interaction analysis of Nsp1, Nup49•Nup57 or the premixed CNT with GST-Nic96^{R1} or GST as bait. The input, PreScission protease elution, and post-elution beads were analyzed by SDS-PAGE and Coomassie staining. Nic96^{R1} specifically pulls-down the intact CNT and fails to interact with Nsp1 or Nup49•Nup57.

A

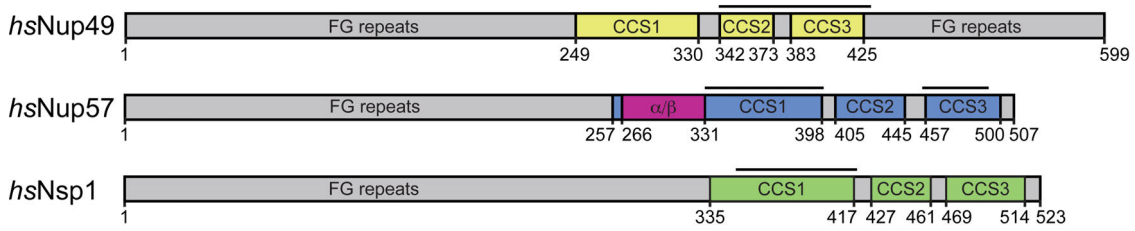

B

		GST		His_6		His_6-SUMO	
		Expression	Solubility	Expression	Solubility	Expression	Solubility
*hs*Nup49	250-299	++	++	-	N/A	+++	+++
	250-331	+++	++	-	N/A	+++	+++
	250-375	+++	+	++	-	+++	+++
	250-430	+++	+	+++	-	+++	++
	302-331	+++	++	-	N/A	+++	+++
	302-375	+++	++	++	-	++	++
	302-430	+++	++	+++	+	+++	+++
	341-375	+++	++	-	N/A	++	++
	341-430	+++	++	++	+	+++	+++
	383-430	+++	-	-	N/A	-	N/A
	●341-428	+++	++	++	-	+++	++
*hs*Nup57	331-364	++	++	-	N/A	++	++
	331-399	++	++	-	N/A	++	+
	331-450	+++	-	++	-	++	-
	331-493	+++	-	+++	-	+++	-
	343-364	+++	++	+	-	++	++
	●343-399	+	++	-	N/A	+++	-
	343-450	+++	-	++	-	+++	-
	343-493	+++	-	+++	-	+++	-
	365-399	+	++	-	N/A	+	++
	365-450	++	-	++	-	++	-
	365-493	+++	-	+++	-	+++	-
	404-450	++	++	-	N/A	+	++
	404-493	+++	++	++	+	+++	++
	456-493	+++	+++	-	N/A	++	++
	●453-491	+++	++	-	N/A	+++	+++
*hs*Nsp1	322-367	++	++	+	N/A	++	++
	322-420	+++	++	+	++	+++	++
	322-461	++	++	++	-	+	++
	322-522	+++	-	++	-	+++	-
	370-420	+	++	-	N/A	++	++
	370-461	+	++	-	N/A	+	++
	370-522	+	-	++	-	+++	-
	427-461	+	++	-	N/A	+	++
	427-522	+++	-	++	-	+++	++
	469-522	+++	-	+	-	+++	++
	●359-422	++	+++	-	N/A	++	++
*hs*Nic96	1-80	++	++	+	++	-	N/A
	1-151	+++	+	++	-	+++	+
	96-151	+++	-	+	-	++	++

●crystallized

Fig. S19.
Expression and solubility analysis of *H. sapiens* channel nups. (**A**) Domain architecture of the three human channel nups Nup49 (yellow), Nup57 (blue/purple), and Nsp1 (green) are shown. (**B**) The expression and solubility levels of individual CNT-fragments expressed as GST-fusions, hexahistidine (HIS_6) or HIS_6-SUMO tagged proteins are indicated; not expressed, insoluble (-) to highly expressed, highly soluble (+++). Crystallized fragments are highlighted with a black bar and a black dot.

A

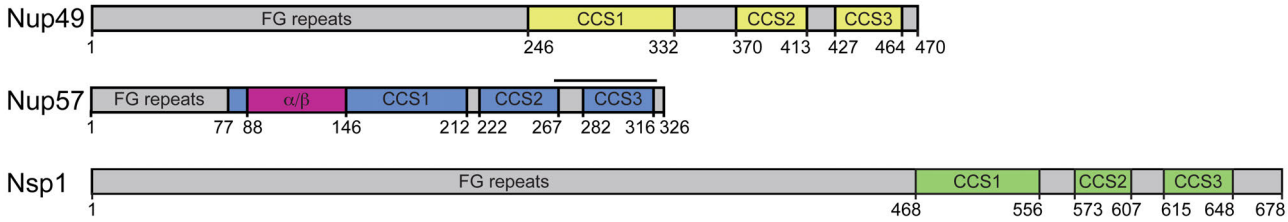

B

		GST		His_6		His_6-SUMO	
		Expression	Solubility	Expression	Solubility	Expression	Solubility
Nup49	246-281	++	-	-	N/A	+	+++
	246-333	++	+++	-	N/A	+	+++
	246-404	++	+++	+	-	+++	+++
	246-470	++	++	+++	-	+++	+++
	285-333	++	+++	+	-	+++	+++
	285-404	++	+	+	-	++	++
	285-470	++	++	++	-	+++	+
	370-404	+++	++	-	N/A	+++	++
	370-470	+++	+	+++	-	+++	+
	427-470	+++	+	-	N/A	+	++
Nup57	74-143	+	++	+	-	+	-
	74-220	++	-	++	-	+	-
	74-269	+++	-	+++	-	++	-
	74-317	+++	-	+++	-	++	-
	74-326	+++	-	+++	-	+++	+
	143-220	+++	-	-	N/A	++	-
	143-269	+++	-	++	-	+	-
	143-317	+++	-	+++	-	+++	+
	143-326	+++	-	+++	-	+	++
	158-220	+++	-	-	N/A	++	-
	158-269	+++	-	+	-	+++	+
	158-317	+++	++	++	++	+++	++
	158-326	+++	++	++	++	+++	++
	221-269	+++	+++	-	N/A	++	++
	221-317	+++	+++	+	+++	++	++
	221-326	+++	+++	+	++	+++	+++
	●265-317	+++	+++	-	N/A	+++	+++
	265-326	+++	+++	-	N/A	+++	+++
	58-216	++	-	-	N/A	++	++
	272-310	+++	++	-	N/A	+++	+++
Nsp1	467-501	++	++	-	N/A	+	++
	467-555	+++	++	-	N/A	++	++
	467-605	+++	++	+	+++	+++	++
	467-653	+++	+	++	+	+++	++
	467-678	+++	+	++	++	+++	++
	504-555	++	++	+	-	+++	++
	504-605	+++	++	++	-	++	++
	504-653	+++	++	+	+++	+++	++
	504-678	+++	+++	+++	-	+++	++
	569-605	+++	+++	-	N/A	++	++
	569-653	+++	++	+	-	+++	++
	569-678	+++	++	+	-	+++	++
	615-653	+++	+	-	N/A	+	++
	615-678	+++	+	-	N/A	++	++
	495-552	+-++	++	-	N/A	+++	+++
Nic96	110-153	+++	++	++	-	+++	+++
	110-180	++	+++	++	-	++	+++
	110-211	+	++	-	N/A	++-+	+++
	110-301	+++	-	+++	-	++	++
	139-180	++	++	-	N/A	++	++
	139-211	+	++	-	N/A	++	+++
	139-301	+++	-	++	-	++	++
	187-301	+++	-	+	-	++	++
	245-301	+++	-	+	-	+++	++

●crystallized

Fig. S20.
Expression and solubility analysis of *C. thermophilum* channel nups. (**A**) Domain architecture of the three *C. thermophilum* channel nups are shown and colored according to Figure S19. (**B**) The expression and solubility levels of individual CNT-fragments expressed as GST-fusions, hexahistidine (HIS_6) or HIS_6-SUMO tagged tagged proteins are indicated; not expressed, insoluble (-) to highly expressed, highly soluble (+++). Crystallized fragments are highlighted with a black bar and a black dot.

A

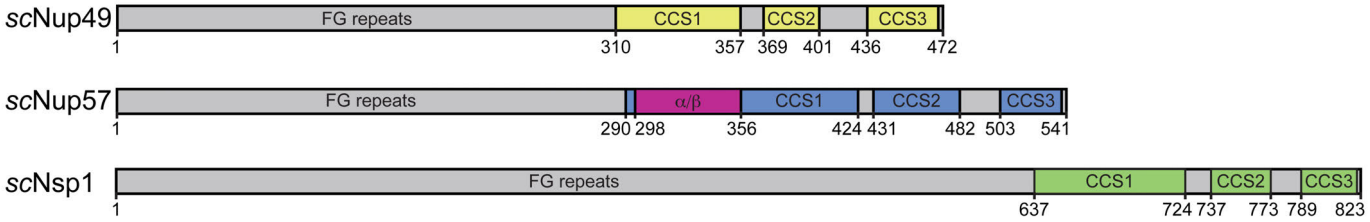

B

		GST		His_6		His_6-SUMO	
		Expression	Solubility	Expression	Solubility	Expression	Solubility
*sc*Nup49	310-356	++	+	++	-	+	++
	310-405	+++	++	+++	-	++	+
	310-472	+++	+	+++	-	+++	-
	366-405	+++	++	+++	-	++	++
	366-471	+++	+	+++	-	++	++
	425-472	+++	++	-	N/A	-	N/A
*sc*Nup57	333-389	+++	++	+	-	+++	+++
	333-425	+++	-	+++	-	++	-
	333-487	+++	+	+++	-	+++	+
	333-541	+++	-	+++	-	++	++
	356-389	+++	+++	+	-	+++	+++
	356-425	++	+	++	-	++	++
	356-487	+++	+	++	-	+++	+
	356-541	+++	+	+++	-	++	++
	391-425	+++	+++	+	-	+++	+++
	391-487	+	-	++	-	+++	-
	391-541	+++	++	++	-	++	+++
	433-487	++	++	+	-	+	+++
	433-541	+++	++	+	-	++	-
	500-541	+++	+++	+	+	+++	+++
	368-425	+++	++	-	N/A	++	+
	486-524	++	++	-	N/A	+++	+++
*sc*Nsp1	623-682	+	++	-	N/A	+++	++
	623-727	++	++	+	+++	+++	++
	623-773	+	++	+	-	+	++
	623-823	+++	-	+	-	+++	-
	649-682	+	++	-	N/A	++	++
	649-727	++	++	+	-	+++	+++
	649-773	+	++	+	-	+	++
	649-823	+++	+	++	-	+++	++
	694-727	+++	++	-	N/A	++	+++
	694-773	+	++	-	N/A	+	+++
	694-823	+++	++	+	++	+++	++
	738-773	+	++	-	N/A	+	++
	738-823	++	+	++	-	+++	++
	787-823	+++	++	-	N/A	+++	++
	665-722	+	++	-	N/A	++	++
*sc*Nic96	1-60	+++	-	+	-	++	++
	1-160	+++	-	+++	-	+++	+
	16-60	++	++	++	-	++	++
	16-160	+++	-	+++	-	+++	+
	107-160	++	+	++	-	++	++

Fig. S21.
Expression and solubility analysis of *S. cerevisiae* channel nups. (**A**) Domain architecture of the three *S. cerevisiae* channel nups are shown and colored according to Figure S19. (**B**) The expression and solubility levels of individual CNT-fragments expressed as GST-fusions, hexahistidine (HIS_6) or HIS_6-SUMO tagged proteins are indicated; not expressed, insoluble (-) to highly expressed, highly soluble (+++). Crystallized fragments are highlighted with a black bar and a black dot.

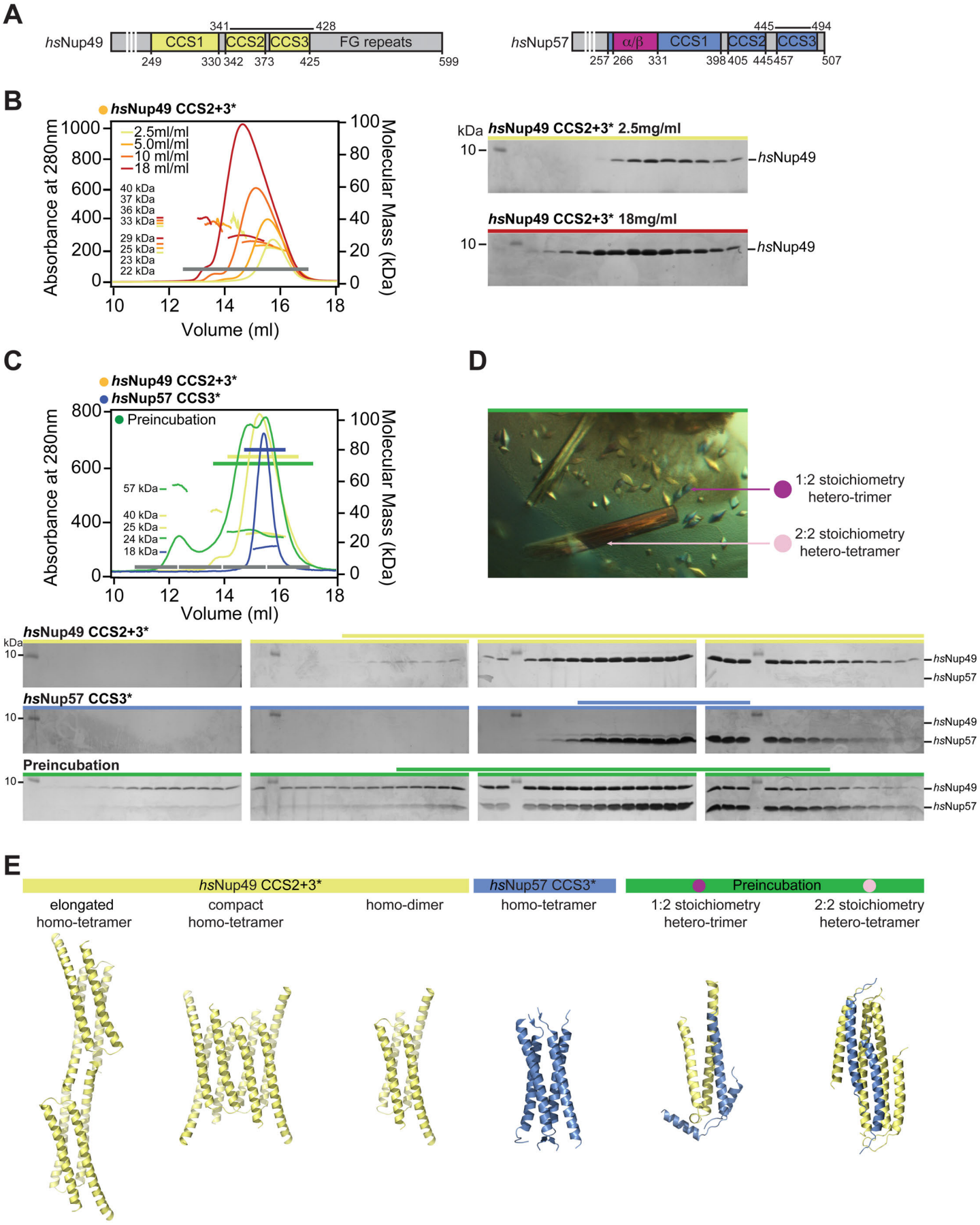
A
hsNup49
341
428
CCS1
CCS2
CCS3
FG repeats
249
330
342
373
425
599
hsNup57
445
494
α/β
CCS1
CCS2
CCS3
257
266
331
398
405
445
457
507
B
hsNup49 CCS2+3*
2.5ml/ml
5.0ml/ml
10 ml/ml
18 ml/ml
40 kDa
37 kDa
36 kDa
33 kDa
29 kDa
25 kDa
23 kDa
22 kDa
Absorbance at 280nm
Molecular Mass (kDa)
Volume (ml)
kDa
hsNup49 CCS2+3* 2.5mg/ml
hsNup49
hsNup49 CCS2+3* 18mg/ml
hsNup49
C
hsNup49 CCS2+3*
hsNup57 CCS3*
Preincubation
57 kDa
40 kDa
25 kDa
24 kDa
18 kDa
Absorbance at 280nm
Molecular Mass (kDa)
Volume (ml)
D
1:2 stoichiometry
hetero-trimer
2:2 stoichiometry
hetero-tetramer
hsNup49 CCS2+3*
hsNup57 CCS3*
Preincubation
kDa
hsNup49
hsNup57
E
hsNup49 CCS2+3*
hsNup57 CCS3*
Preincubation
elongated
homo-tetramer
compact
homo-tetramer
homo-dimer
homo-tetramer
1:2 stoichiometry
hetero-trimer
2:2 stoichiometry
hetero-tetramer

Fig. S22.
Biochemical and structural analysis of different *hs*Nup49$^{CCS2+3*}$ and *hs*Nup57^{CCS3*} complexes reveal different oligomerization states. (**A**) Domain architecture of *hs*Nup49 and *hs*Nup57 is shown and colored according to Figure S19. (**B**) SEC-MALS profiles of *hs*Nup49$^{CCS2+3*}$ are shown at increasing protein concentrations (yellow to red). (**C**) SEC-MALS profiles of *hs*Nup57^{CCS3*} and *hs*Nup49$^{CCS2+3*}$ are shown individually (blue and yellow) and after their preincubation (green). Measured molecular masses are indicated for the peak fractions. Gray bars indicate fractions that were resolved on SDS-PAGE gels and visualized by Coomassie staining. Colored bars indicate the fractions that were pooled for crystallization. (**D**) Crystallization drop showing two different crystal forms of the *hs*Nup57^{CCS3*}•*hs*Nup49$^{CCS2+3*}$ complex with 1:2 (purple) and 2:2 (magenta) stoichiometry. (**E**) The structure of the three different homo-oligomers of *hs*Nup49$^{CCS2+3*}$ (elongated homo-tetramer, compact homo-tetramer, and homo-dimer), the homo-tetramer of *hs*Nup57^{CCS3*}, and the *hs*Nup57^{CCS3*}•*hs*Nup49$^{CCS2+3*}$ complexes with 2:1 and 2:2 stoichiometry are shown from left to right.

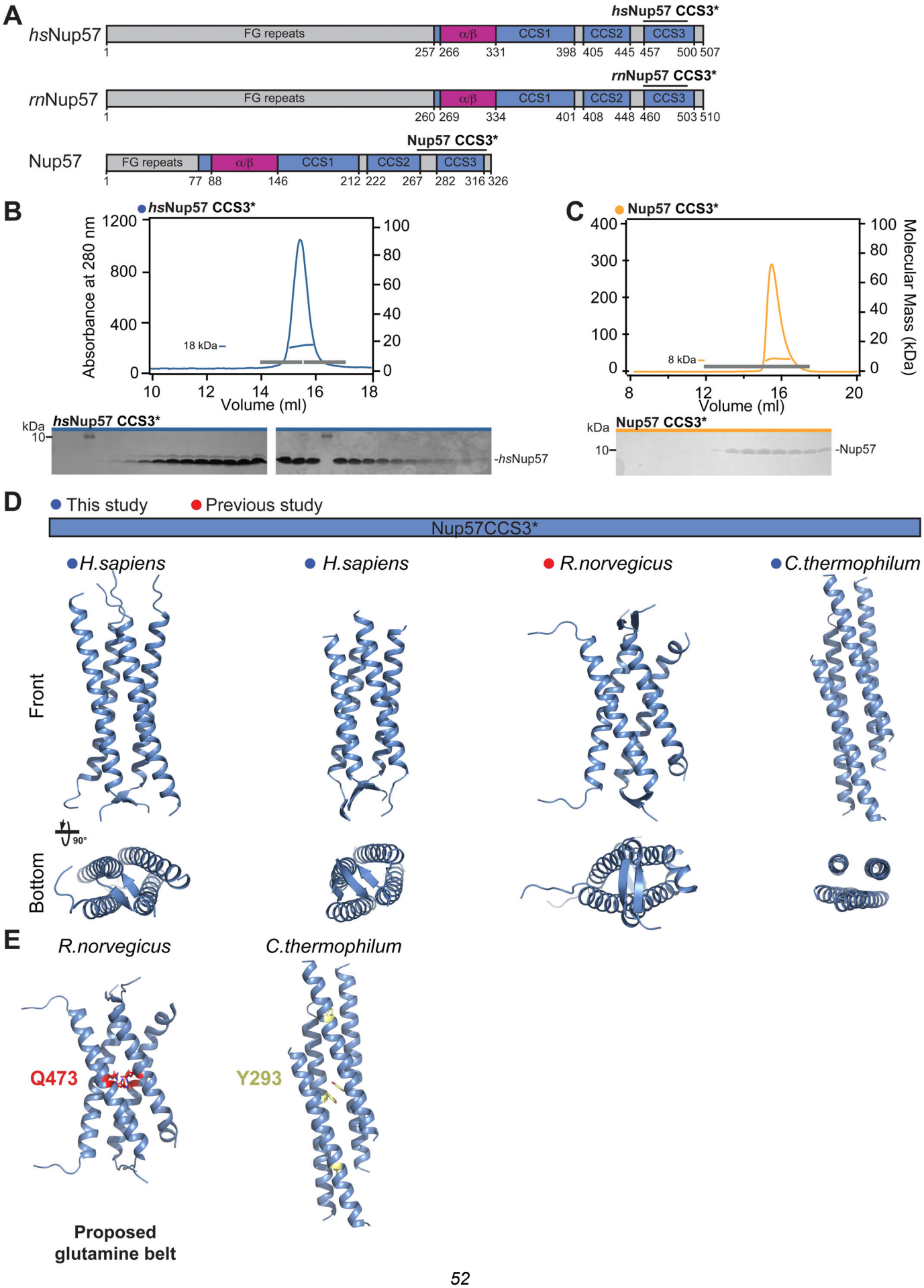
A
hsNup57
FG repeats
α/β
CCS1
CCS2
CCS3
hsNup57 CCS3*
1
257 266
331
398 405
445 457
500 507
rnNup57
rnNup57 CCS3*
1
260 269
334
401 408
448 460
503 510
Nup57
Nup57 CCS3*
1
77 88
146
212 222
267
282 316 326
B
hsNup57 CCS3*
Absorbance at 280 nm
1200
800
400
0
100
80
60
40
20
0
18 kDa
10
12
14
16
18
Volume (ml)
kDa
10
hsNup57 CCS3*
-hsNup57
C
Nup57 CCS3*
400
300
200
100
0
100
80
60
40
20
0
Molecular Mass (kDa)
8 kDa
8
12
16
20
Volume (ml)
kDa
10
Nup57 CCS3*
-Nup57
D
This study
Previous study
Nup57CCS3*
H.sapiens
H.sapiens
R.norvegicus
C.thermophilum
Front
Bottom
90°
E
R.norvegicus
C.thermophilum
Q473
Y293
Proposed
glutamine belt

Fig. S23.
Biochemical and structural analysis of the Nup57^{CCS3*} segment from different species. (**A**) Domain architectures of the *C. thermophilum*, *H. sapiens, and R. norvegicus* Nup57 are shown and colored according to Figure S19. SEC-MALS profiles of (**B**) Nup57^{CCS3*} and (**C**) *hs*Nup57^{CCS3*}. Measured molecular masses are indicated for the peak fractions. Gray bars indicate fractions that were resolved on SDS-PAGE gels and visualized by Coomassie staining. (**D**) Structures of human and *C. thermophilum* Nup57^{CCS3*} shown in cartoon representation, shown in the same orientations as the previously determined rat Nup57^{CCS3*} (*70*). Two different states of *hs*Nup57^{CCS3*} were obtained in different crystal packing arrangements. (**E**) Structural comparison of the *R. norvegicus and C. thermophilum* Nup57^{CCS3*} homo-tetramers. The Nup57^{CCS3*} and *hs*Nup57^{CCS3*} homo-tetramers possess different helical packing arrangements and fail to superpose. As a reference, two corresponding residues Q473 (red) and Y293 of the *C. thermophilum and R. norvegicus* homo-tetramers, respectively, are indicated, illustrating their distinct helical packing. Notably, the *C. thermophilum* Nup57^{CCS3*} is homo-dimeric in solution, whereas the human homologue forms a homo-tetramer.

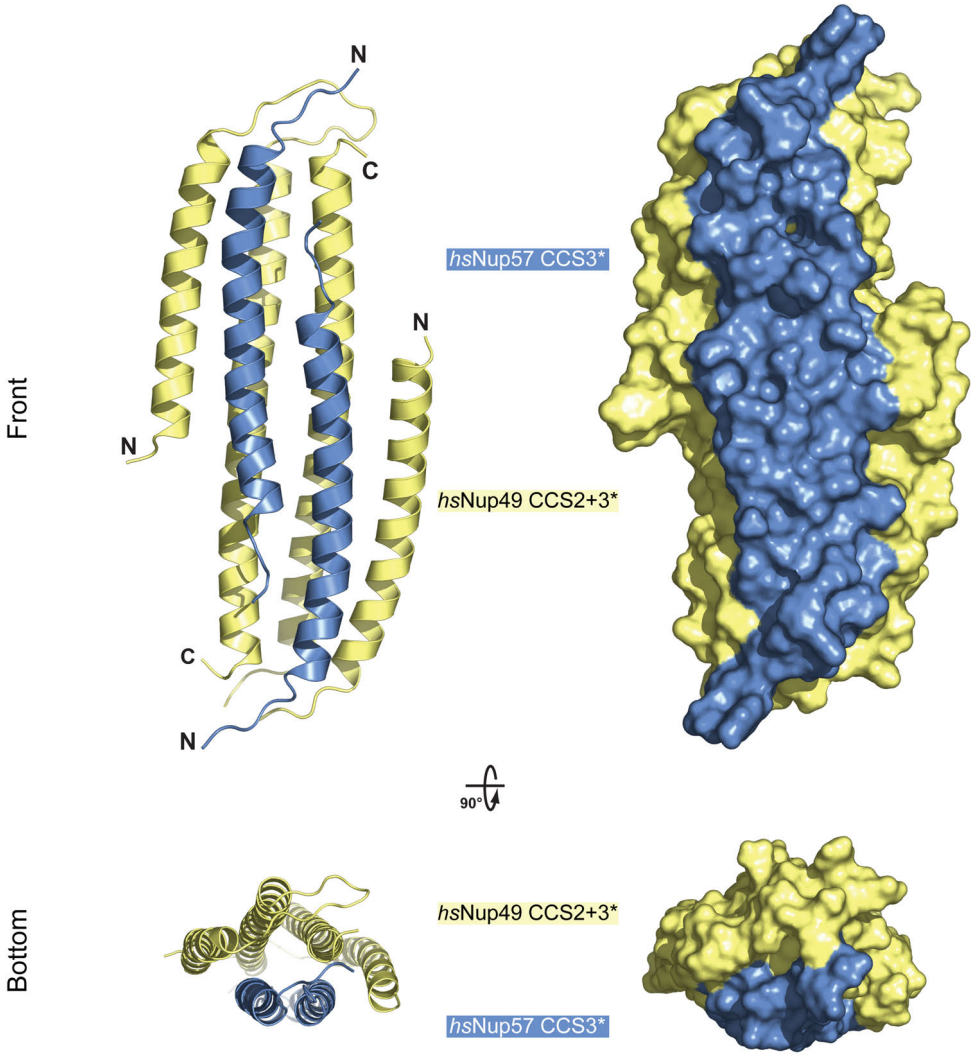
Front
N
C
N
N
C
N
hsNup57 CCS3*
hsNup49 CCS2+3*
90°
Bottom
hsNup49 CCS2+3*
hsNup57 CCS3*

Fig. S24.
Structure of *hs*Nup49•Nup57 with 2:2 stoichiometry. Cartoon representation of the *hs*Nup57^{CCS3*}•*hs*Nup49$^{CCS2+3*}$ hetero-dimer with 2:2 stoichiometry. Two orientations are shown from the front and side; *hs*Nup57^{CCS3*} (blue) and *hs*Nup49$^{CCS2+3*}$ (yellow). A surface representation of the two views is shown on the right.

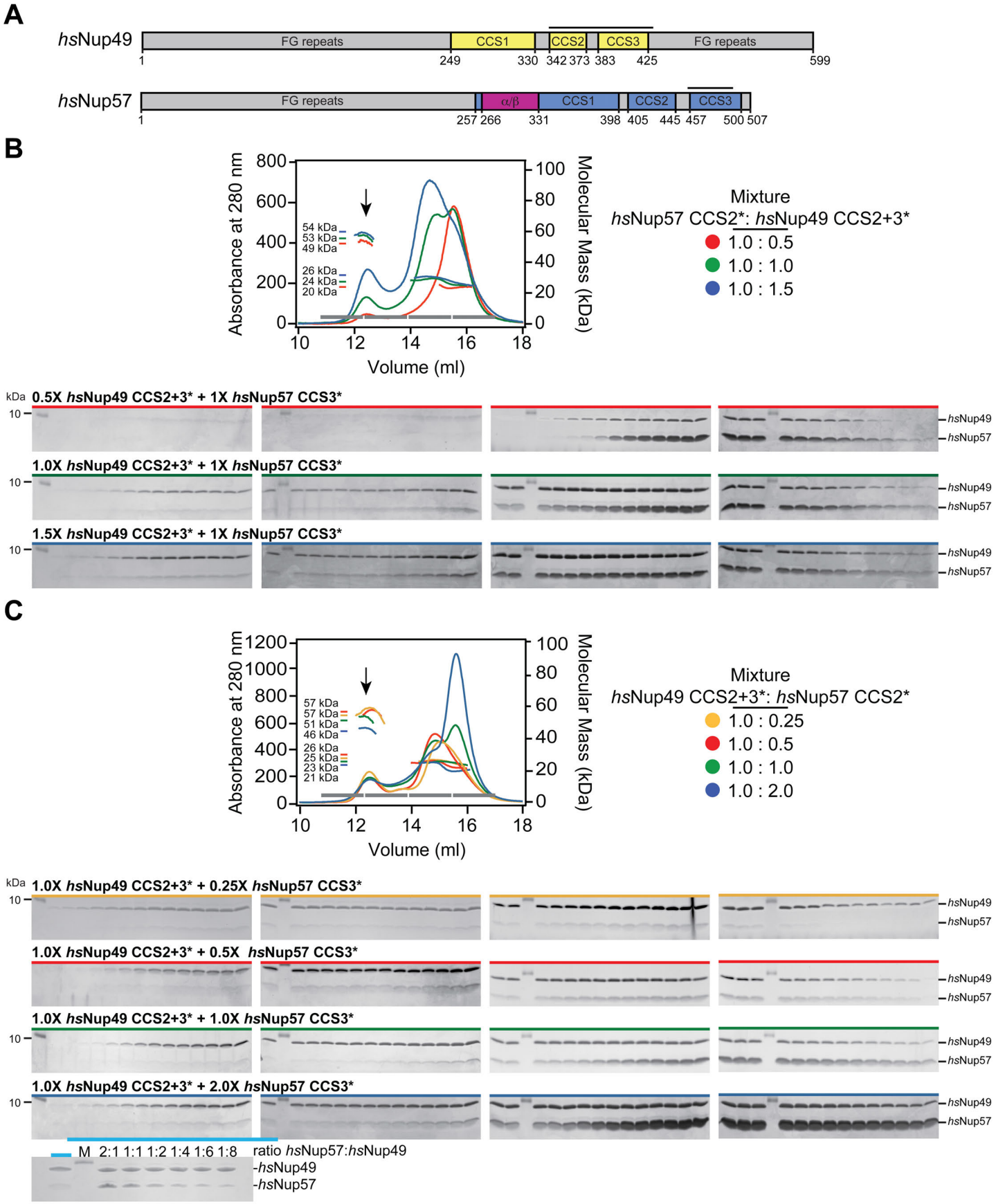
A
hsNup49
FG repeats
CCS1
CCS2
CCS3
FG repeats
1
249
330
342 373
383
425
599
hsNup57
FG repeats
α/β
CCS1
CCS2
CCS3
1
257 266
331
398
405
445
457
500 507
B
Absorbance at 280 nm
Molecular Mass (kDa)
Volume (ml)
54 kDa
53 kDa
49 kDa
26 kDa
24 kDa
20 kDa
Mixture
hsNup57 CCS2*: hsNup49 CCS2+3*
1.0 : 0.5
1.0 : 1.0
1.0 : 1.5
kDa
0.5X hsNup49 CCS2+3* + 1X hsNup57 CCS3*
1.0X hsNup49 CCS2+3* + 1X hsNup57 CCS3*
1.5X hsNup49 CCS2+3* + 1X hsNup57 CCS3*
hsNup49
hsNup57
C
Absorbance at 280 nm
Molecular Mass (kDa)
Volume (ml)
57 kDa
57 kDa
51 kDa
46 kDa
26 kDa
25 kDa
23 kDa
21 kDa
Mixture
hsNup49 CCS2+3*: hsNup57 CCS2*
1.0 : 0.25
1.0 : 0.5
1.0 : 1.0
1.0 : 2.0
kDa
1.0X hsNup49 CCS2+3* + 0.25X hsNup57 CCS3*
1.0X hsNup49 CCS2+3* + 0.5X hsNup57 CCS3*
1.0X hsNup49 CCS2+3* + 1.0X hsNup57 CCS3*
1.0X hsNup49 CCS2+3* + 2.0X hsNup57 CCS3*
hsNup49
hsNup57
M 2:1 1:1 1:2 1:4 1:6 1:8 ratio hsNup57:hsNup49
-hsNup49
-hsNup57

Fig. S25.
Analysis of oligomeric state of human channel nup fragment mixtures. (**A**) Domain architectures of the *H. sapiens* Nup49 and Nup57 are shown and colored according to Figure S19. (**B**) SEC-MALS profiles of *hs*Nup57^{CCS3*} preincubated with increasing molar amounts of *hs*Nup49 $^{CCS2+3*}$ (red, green, and blue). (**C**) SEC-MALS profiles of *hs*Nup49$^{CCS2+3*}$ preincubated with increasing molar amounts of *hs*Nup57^{CCS3*} (yellow, red, green, and blue). Measured molecular masses are indicated for the peak fractions. Gray bars indicate fractions that were resolved on SDS-PAGE gels and visualized by Coomassie staining. An arrow indicates the position of a higher molecular mass peak, which was previously described as a Nup57^{CCS3*}•Nup49$^{CCS2+3*}$ complex with 6:4 stoichiometry, which constitutes the keystone for the open ring structure in the "ring model" (*71*). The abundance of this peak increases with increasing amounts of *hs*Nup49$^{CCS2+3*}$, whereas it stays constant in the presence of increasing amounts of *hs*Nup57^{CCS3*}. The corresponding SDS-PAGE analysis shows that Nup49 is substantially more abundant in this peak. To rule out that differential staining of the two proteins causes a perceived excess of *hs*Nup49$^{CCS2+3*}$, *hs*Nup49$^{CCS2+3*}$ was mixed with different molar amounts of *hs*Nup57^{CCS3*}, analyzed by SDS-PAGE and compared to the protein in the unknown peak (cyan). This analysis confirms an abundance of *hs*Nup49$^{CCS2+3*}$ in the peak.

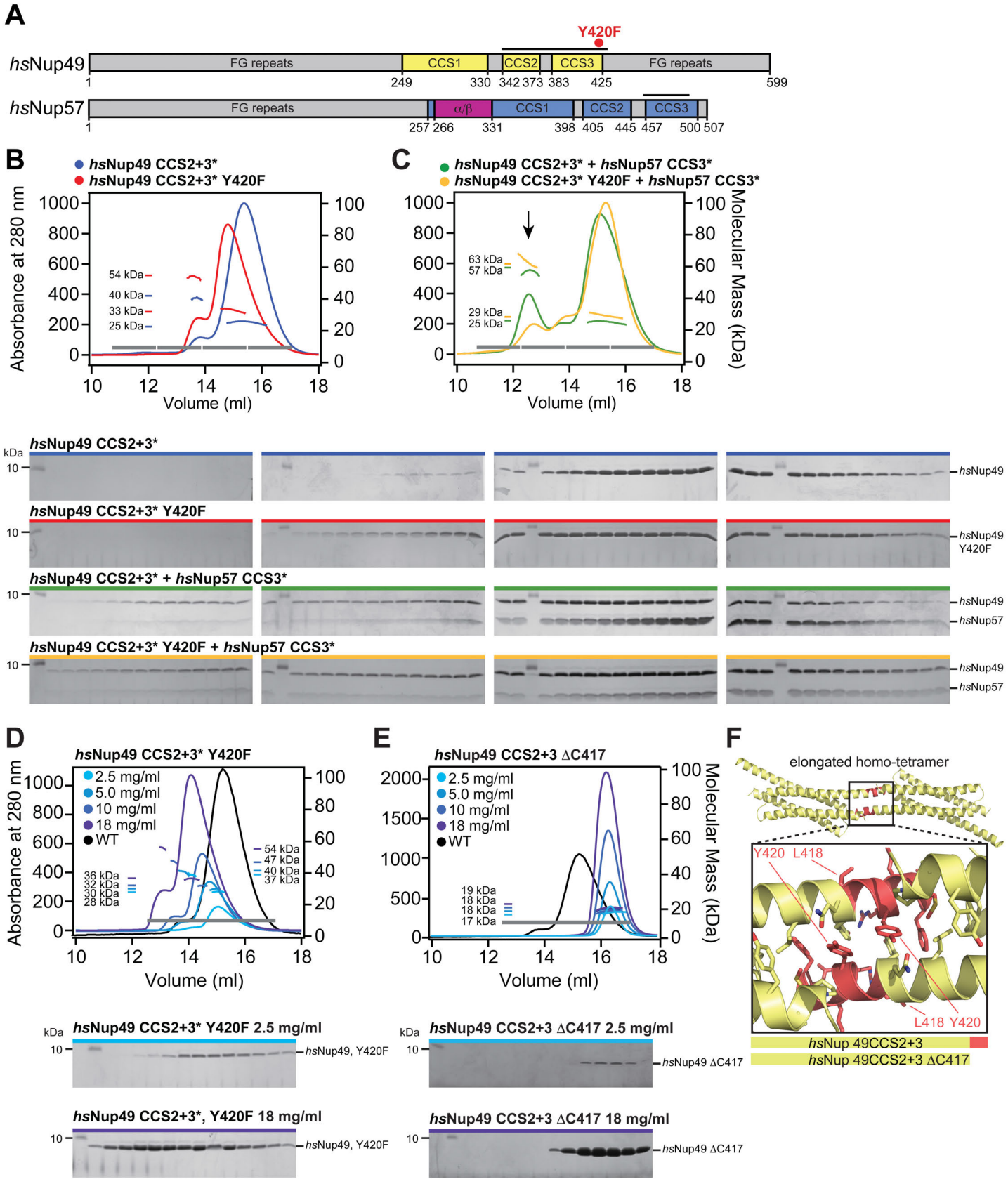
A
Y420F
hsNup49
FG repeats
CCS1
CCS2
CCS3
FG repeats
1
249
330
342 373
383
425
599
hsNup57
FG repeats
α/β
CCS1
CCS2
CCS3
1
257 266
331
398
405
445
457
500 507
B
hsNup49 CCS2+3*
hsNup49 CCS2+3* Y420F
Absorbance at 280 nm
54 kDa
40 kDa
33 kDa
25 kDa
Volume (ml)
C
hsNup49 CCS2+3* + hsNup57 CCS3*
hsNup49 CCS2+3* Y420F + hsNup57 CCS3*
63 kDa
57 kDa
29 kDa
25 kDa
Molecular Mass (kDa)
Volume (ml)
kDa
hsNup49 CCS2+3*
hsNup49
hsNup49 CCS2+3* Y420F
hsNup49 Y420F
hsNup49 CCS2+3* + hsNup57 CCS3*
hsNup49
hsNup57
hsNup49 CCS2+3* Y420F + hsNup57 CCS3*
hsNup49
hsNup57
D
hsNup49 CCS2+3* Y420F
2.5 mg/ml
5.0 mg/ml
10 mg/ml
18 mg/ml
WT
36 kDa
32 kDa
30 kDa
28 kDa
54 kDa
47 kDa
40 kDa
37 kDa
Absorbance at 280 nm
Volume (ml)
E
hsNup49 CCS2+3 ΔC417
2.5 mg/ml
5.0 mg/ml
10 mg/ml
18 mg/ml
WT
19 kDa
18 kDa
18 kDa
17 kDa
Molecular Mass (kDa)
Volume (ml)
F
elongated homo-tetramer
Y420
L418
L418
Y420
hsNup 49CCS2+3
hsNup 49CCS2+3 ΔC417
kDa
hsNup49 CCS2+3* Y420F 2.5 mg/ml
hsNup49, Y420F
hsNup49 CCS2+3 ΔC417 2.5 mg/ml
hsNup49 ΔC417
hsNup49 CCS2+3*, Y420F 18 mg/ml
hsNup49, Y420F
hsNup49 CCS2+3 ΔC417 18 mg/ml
hsNup49 ΔC417

Fig. S26.
Analysis of *hs*Nup49$^{CCS2+3*}$ mutants that affect the formation of higher oligomeric states. (**A**) Domain architectures of the *H. sapiens* Nup49 and Nup57 are shown and colored according to Figure S19. A red dot indicates the position of the Y420F mutant in *hs*Nup49, which was previously suggested to stabilize a *hs*Nup57^{CCS3*}•*hs*Nup49$^{CCS2+3*}$ assembly with 6:4 stochiometry (*71*). (**B**) SEC-MALS profiles of wild type *hs*Nup49$^{CCS2+3*}$ (blue) and *hs*Nup49$^{CCS2+3*}$ Y420F (red) in isolation and (**C**) preincubated with equimolar amounts of *hs*Nup57^{CCS3*} (green and yellow; right). The Nup49^{CCS3*} Y420F mutant decreases the height of the ~60 kDa peak (black arrow) in the presence of Nup57^{CCS3*}, contrary to a previous report (*71*). SEC-MALS profiles of (**D**) *hs*Nup49$^{CCS2+3*}$ Y420F and (**E**) *hs*Nup49$^{CCS2+3*}$ ΔC417 at increasing protein concentrations. As reference, the wild type *hs*Nup49$^{CCS2+3*}$ SEC profile at a protein concentration of 18 mg/ml is shown (black). Measured molecular masses are indicated for the peak fractions. Gray bars indicate fractions that were resolved on SDS-PAGE gels and visualized by Coomassie staining. (**F**) Close-up view of the elongated hetero-tetramer interface of *hs*Nup49$^{CCS2+3*}$ in cartoon representation. The C-terminal two helical turns that are absent in the *hs*Nup49$^{CCS2+3*}$ ΔC417 mutant are colored in red. The *hs*Nup49$^{CCS2+3*}$ Y420F mutant forms higher order homo-oligomers with increasing molecular masses which is abolished in the *hs*Nup49$^{CCS2+3*}$ ΔC417 mutant.

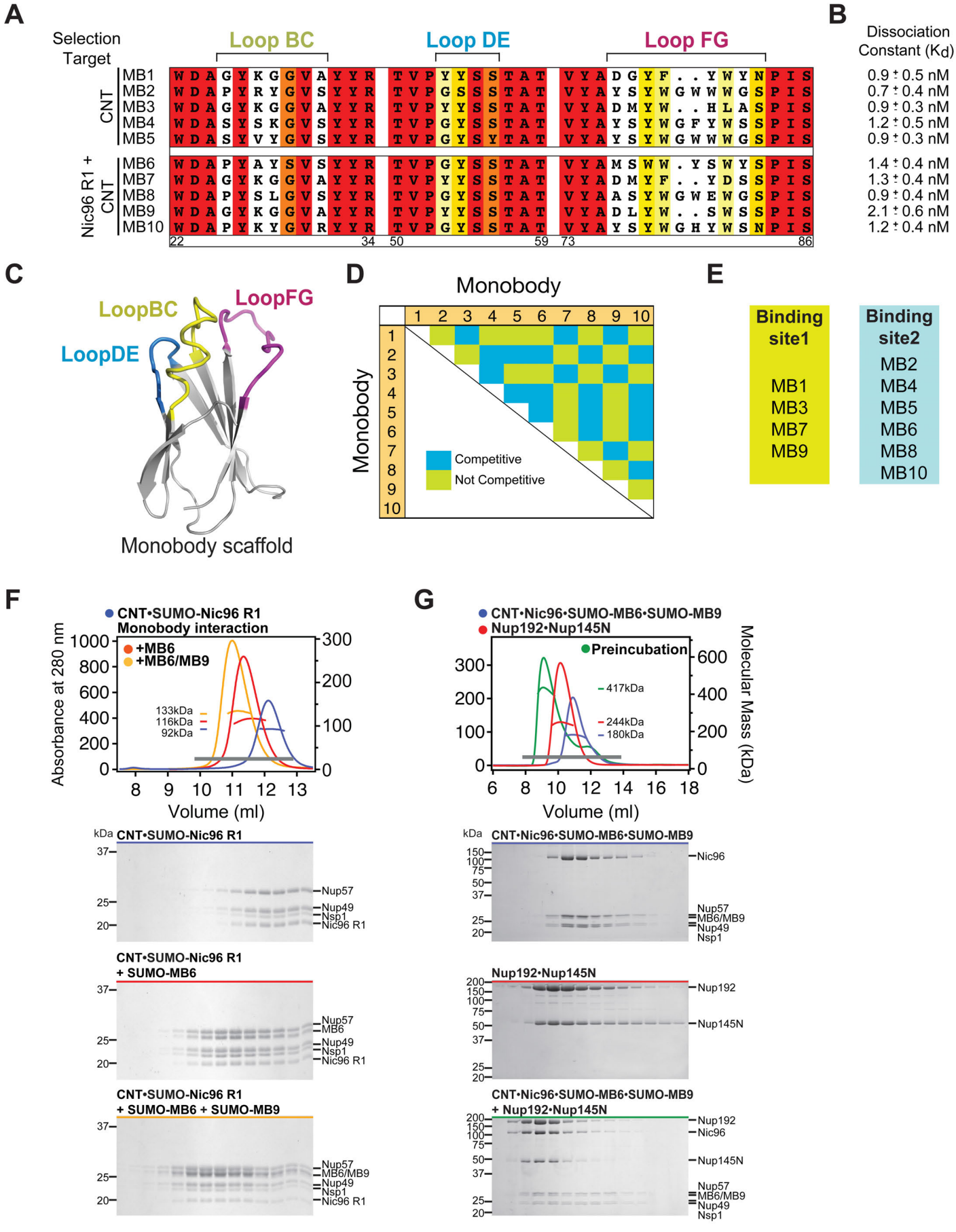
A
Selection Target
Loop BC
Loop DE
Loop FG
CNT
Nic96 R1 + CNT
MB1 WDAGYKGGVAYYR TVPYYSSTAT VYADGYF..YWYNPIS
MB2 WDAPYRYGVSYYR TVPGSSSTAT VYAYSYWGWWWGSPIS
MB3 WDAGYKGGVAYYR TVPYYSSTAT VYADMYW..HLASPIS
MB4 WDASYSKGVSYYR TVPGYSSTAT VYAYSYWGFYWSSPIS
MB5 WDASYVYGVSYYR TVPGYSYTAT VYAYSYWGWWWGSPIS
MB6 WDAPYAYSVSYYR TVPGYSSTAT VYAMSWW..YSWYSPIS
MB7 WDAGYKGGVAYYR TVPYYSSTAT VYADMYF..YDSSPIS
MB8 WDAPYSLGVSYYR TVPGYSSTAT VYAASYWGWEWGSPIS
MB9 WDAGYKGGVAYYR TVPYYSSTAT VYADLYW..SWSSPIS
MB10 WDAPYKYGVRYYR TVPGYSSTAT VYAYSYWGHYWSNPIS
22 34 50 59 73 86
B
Dissociation Constant (Kd)
0.9 ± 0.5 nM
0.7 ± 0.4 nM
0.9 ± 0.3 nM
1.2 ± 0.5 nM
0.9 ± 0.3 nM
1.4 ± 0.4 nM
1.3 ± 0.4 nM
0.9 ± 0.4 nM
2.1 ± 0.6 nM
1.2 ± 0.4 nM
C
LoopBC
LoopFG
LoopDE
Monobody scaffold
D
Monobody
Competitive
Not Competitive
E
Binding site1
MB1
MB3
MB5
MB7
MB9
Binding site2
MB2
MB4
MB6
MB8
MB10
F
CNT•SUMO-Nic96 R1
Monobody interaction
+MB6
+MB6/MB9
133kDa
116kDa
92kDa
Absorbance at 280 nm
Volume (ml)
kDa
CNT•SUMO-Nic96 R1
Nup57
Nup49
Nsp1
Nic96 R1
CNT•SUMO-Nic96 R1
+ SUMO-MB6
Nup57
MB6
CNT•SUMO-Nic96 R1
+ SUMO-MB6 + SUMO-MB9
Nup57
MB6/MB9
G
CNT•Nic96•SUMO-MB6•SUMO-MB9
Nup192•Nup145N
Preincubation
417kDa
244kDa
180kDa
Molecular Mass (kDa)
Volume (ml)
CNT•Nic96•SUMO-MB6•SUMO-MB9
Nic96
Nup57
MB6/MB9
Nup49
Nsp1
Nup192•Nup145N
Nup192
Nup145N
CNT•Nic96•SUMO-MB6•SUMO-MB9
+ Nup192•Nup145N

Fig. 27.

Probing the CNT accessibility and assembly state in the IRC with synthetic monobodies. (**A**) Sequence alignment of the variable loops (BC, DE, FG) of 10 monobodies generated against either the CNT or the CNT•Nic96^{R1} complex. White bars indicate gaps in the alignment between loops. Single residue similarity is shaded from white (less than 40 % similarity), to yellow (40 % similarity), to red (100 % identity) using the BLOSUM62 matrix. (**B**) The dissociation constant of each monobody for CNT binding is shown. (**C**) The monobody scaffold is shown in cartoon representation highlighting the variable DE (blue), BC (yellow) and FG (magenta) loops. (**D**) A pairwise protein interaction matrix indicating competitive (blue) and non-competitive (green) binding to the CNT for the tested monobodies as determined by SEC-MALS analysis. (**E**) The monobodies are grouped according to their competitive CNT binding properties, indicating two distinct binding sites. (**F**) SEC-MALS profiles of CNT•SUMO-Nic96^{R1} (blue), CNT•SUMO-Nic96^{R1} bound to a single monobody (SUMO-MB6; red), and bound to 2 monobodies (SUMO-MB6 and SUMO-MB9; yellow) are shown. (**G**) SEC-MALS profiles of CNT•Nic96•SUMO-MB6•SUMO-MB9 (blue), Nup192•Nup145N (red), and after their preincubation (green) are shown. Measured molecular masses are indicated for the peak fractions. Gray bars indicate fractions that were resolved on SDS-PAGE gels and visualized by Coomassie staining. MALS and SDS-PAGE confirm the presence of the two monobodies MB6 and MB10 in the peak fractions of the IRC, confirming the steric accessibility of the CNT for monobody binding in solution.

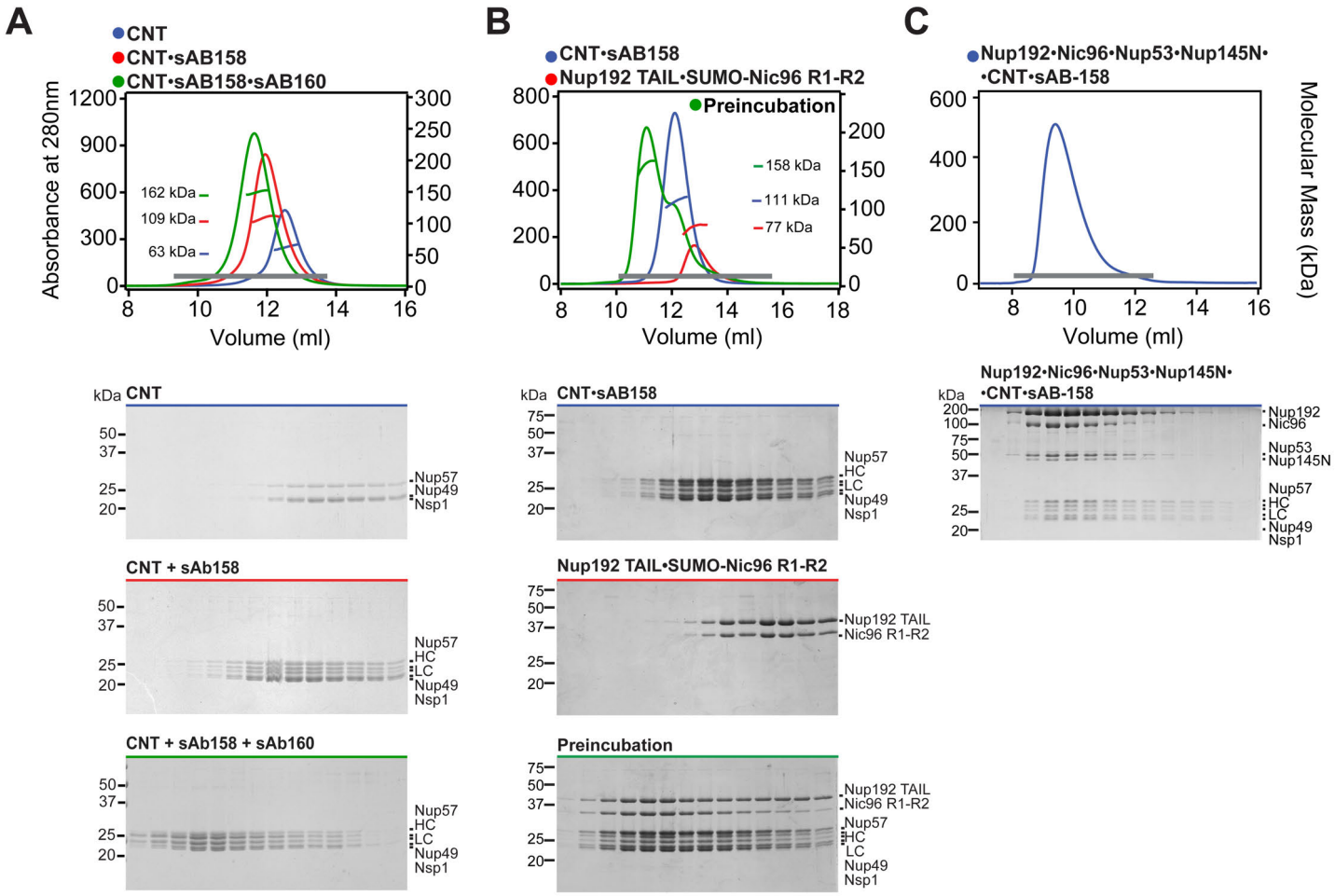
A
CNT
CNT•sAB158
CNT•sAB158•sAB160
Absorbance at 280nm
Volume (ml)
162 kDa
109 kDa
63 kDa
B
CNT•sAB158
Nup192 TAIL•SUMO-Nic96 R1-R2
Preincubation
158 kDa
111 kDa
77 kDa
Volume (ml)
C
Nup192•Nic96•Nup53•Nup145N•
•CNT•sAB-158
Molecular Mass (kDa)
Volume (ml)
kDa
CNT
CNT + sAb158
CNT + sAb158 + sAb160
Nup57
HC
LC
Nup49
Nsp1
CNT•sAB158
Nup192 TAIL•SUMO-Nic96 R1-R2
Preincubation
Nup192 TAIL
Nic96 R1-R2
Nup192•Nic96•Nup53•Nup145N•
•CNT•sAB-158
Nup192
Nic96
Nup53
Nup145N

Fig. S28.
Probing the CNT accessibility and assembly state in the IRC with synthetic antibodies. (**A**) SEC-MALS profiles of the CNT (blue), the CNT preincubated with sAB-158 (red) and the CNT preincubated with sAB-158 and sAB-160 (green) are shown. (**B**) SEC-MALS profiles of the CNT•sAB-158 (blue), the $Nup192^{TAIL}$•SUMO-$Nic96^{R1-R2}$ (red) and after their preincubation (green) are shown. (**C**) SEC-MALS profile of Nup192•Nic96•Nup145N•CNT•sAB-158 (blue). Measured molecular masses are indicated for the peak fractions. Gray bars indicate fractions that were resolved on SDS-PAGE gels and visualized by Coomassie staining. MALS and SDS-PAGE confirm stoichiometric complexes and the presence of sAb-158 in the peak fractions of the minimal and intact IRC, indicating the accessibility of the CNT for synthetic antibody binding and confirming that the CNT adopts the same assembly state in the IRC as observed in the crystal structure.

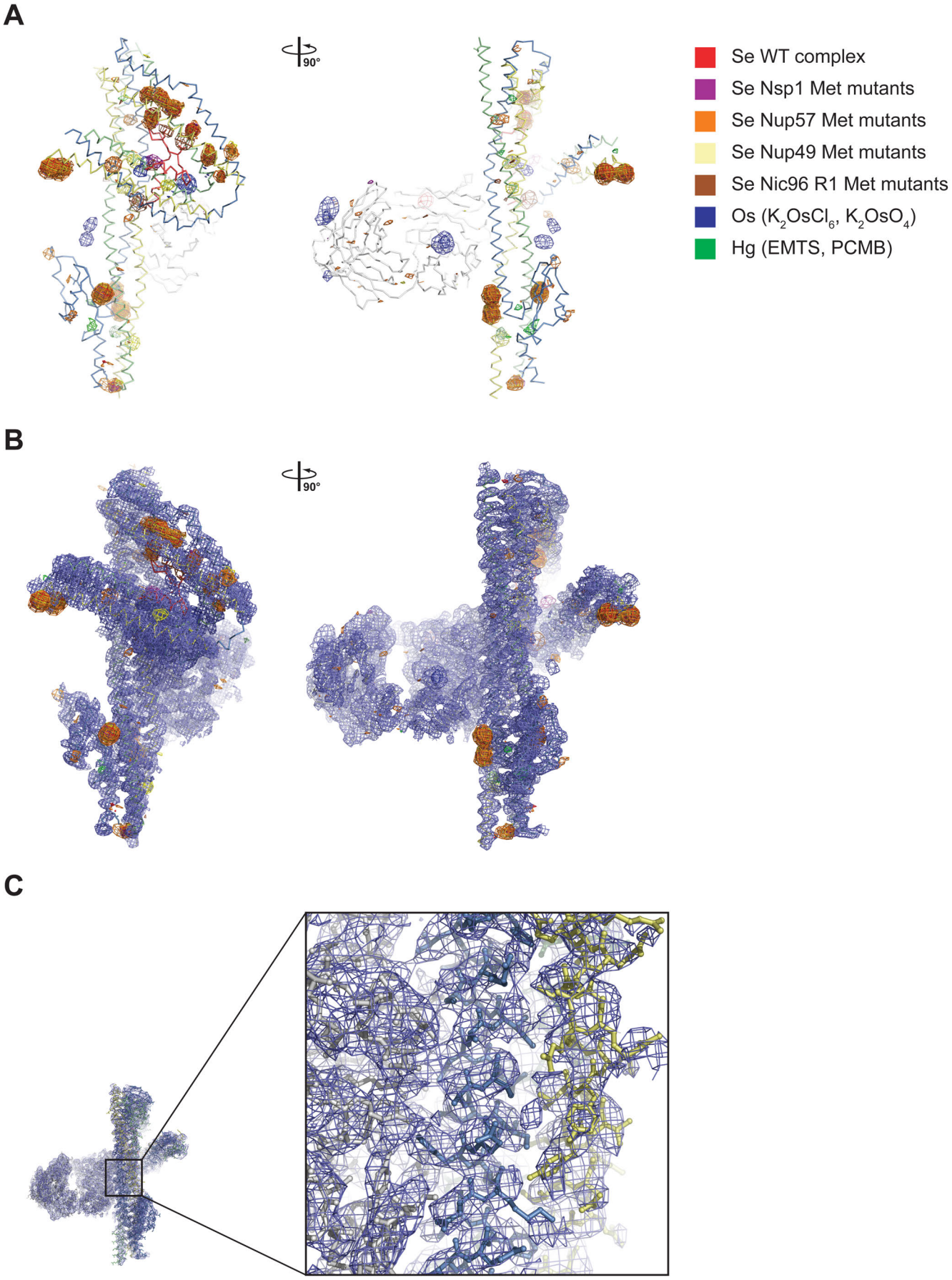
A
90°
Se WT complex
Se Nsp1 Met mutants
Se Nup57 Met mutants
Se Nup49 Met mutants
Se Nic96 R1 Met mutants
Os (K_2OsCl_6, K_2OsO_4)
Hg (EMTS, PCMB)
B
90°
C

Fig. S29.
Experimental phasing of the CNT•Nic96^{R1}•sAB-158 structure. (**A**) Anomalous difference Fourier maps were calculated from X-ray diffraction data collected at the selenium, osmium and mercury peak wavelengths. A ribbon representation of the structure of the CNT•Nic96^{R1}•sAB-158 complex with the indicated anomalous difference Fourier maps contoured at 3.5 σ is shown. The 29 introduced methionine mutants in Nsp1, Nup49, Nup57, and Nic96^{R1} yielded additional 22 selenium sites, validating the sequence register. (**B**) Experimental electron density map after density modification of the CNT•Nic96^{R1}•sAB-158 complex phased with the anomalous signal from crystals soaked with potassium hexachloroosmate (K_2OsCl_6), contoured at 1.0 σ. The anomalous difference Fourier maps of the various heavy metal derivatives (panel A) are overlaid and contoured at 3.5 σ. (**C**) Close-up view of a representative section of the experimental electron density map from panel B overlaid with a stick representation of the final model.

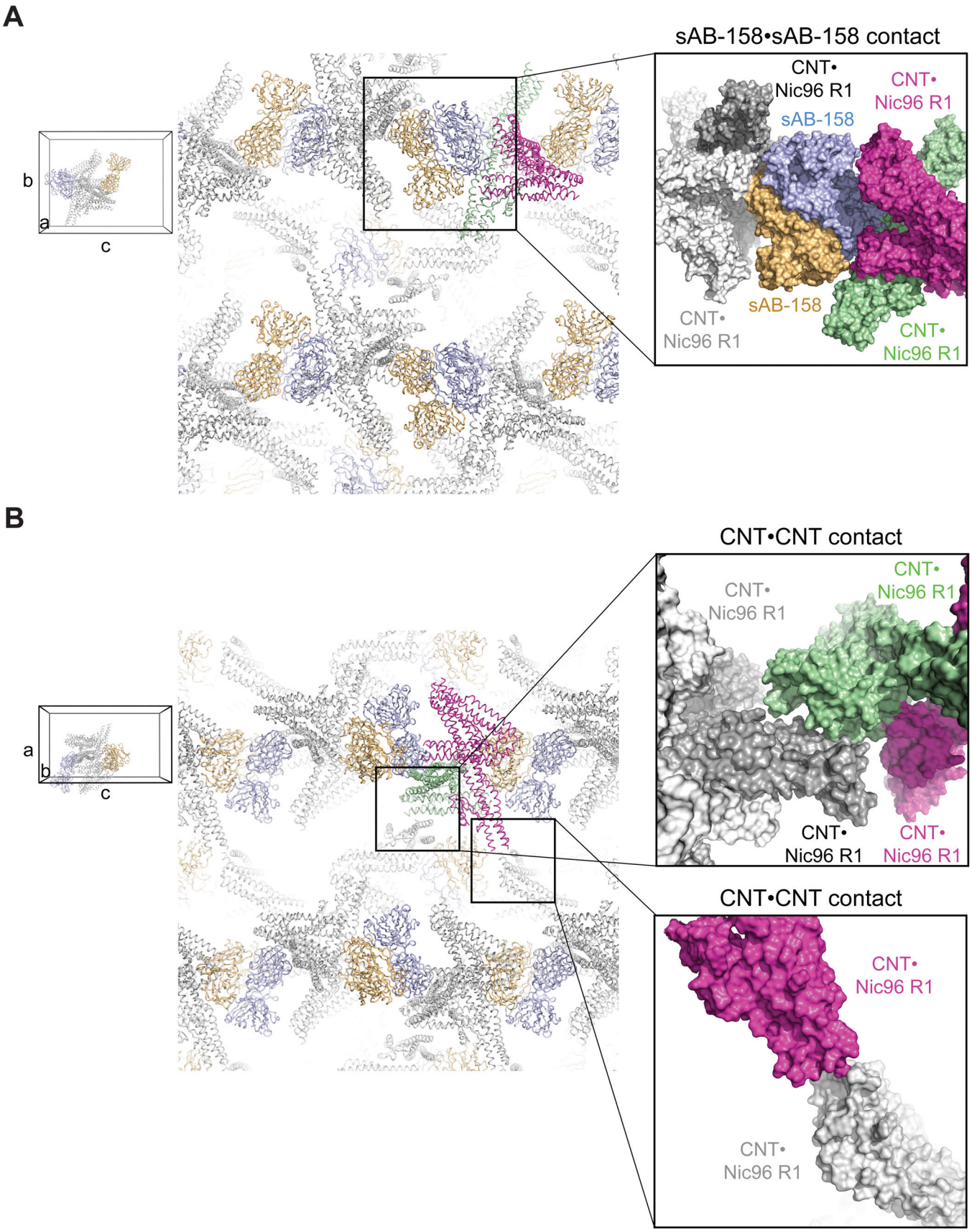
A
sAB-158•sAB-158 contact
CNT•
Nic96 R1
CNT•
Nic96 R1
sAB-158
sAB-158
CNT•
Nic96 R1
CNT•
Nic96 R1
b
a
c
B
CNT•CNT contact
CNT•
Nic96 R1
CNT•
Nic96 R1
CNT•
Nic96 R1
CNT•
Nic96 R1
CNT•CNT contact
CNT•
Nic96 R1
CNT•
Nic96 R1
a
b
c

Fig. S30.
Crystal packing interactions in the CNT•Nic96^{R1}•sAB-158 crystals. (**A**, **B**) Crystal packing interactions in the CNT•Nic96^{R1}•sAB-158 crystal shown in two different orientations. Each asymmetric unit is composed of two CNT•Nic96^{R1}•sAB-158 complexes that dimerize in a cross-handshake fashion. The major crystal contact is formed by an interaction between sAB-158 molecules (blue and orange) from adjacent asymmetric units along the c axis. Two additional minor crystal contacts are formed by CNT-CNT interactions along the a and b axes. CNT•Nic96^{R1} complexes of one asymmetric unit are colored in green and magenta and their symmetry mates in light and dark gray. As references, units cell diagrams are shown to indicate the orientation of each view. The *Insets* mark the locations of the three crystal contact regions that are enlarged and shown in surface representation.

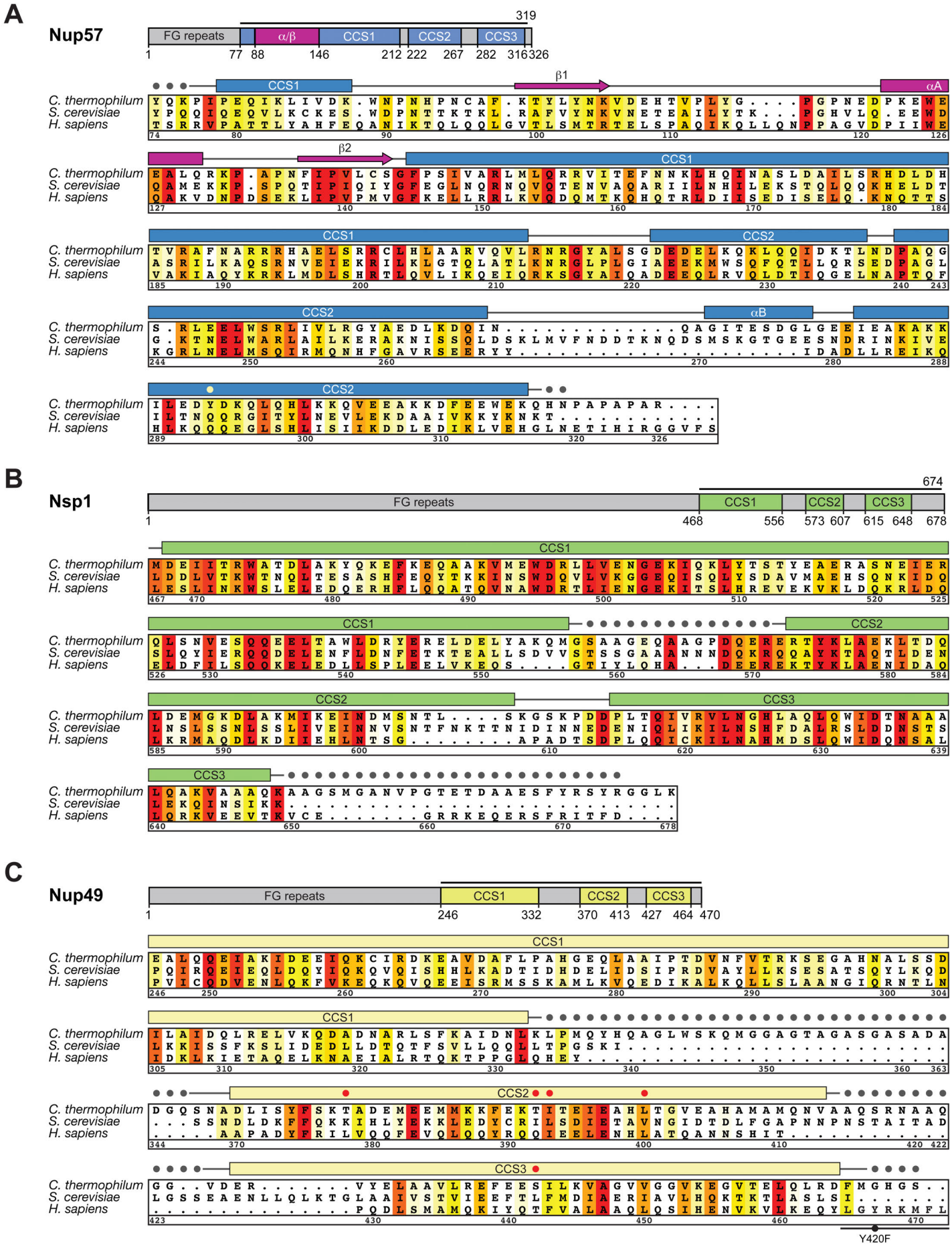
A
Nup57
319
FG repeats
α/β
CCS1
CCS2
CCS3
1
77
88
146
212
222
267
282
316
326
β1
αA
β2
αB
C. thermophilum
S. cerevisiae
H. sapiens
B
Nsp1
674
468
556
573
607
615
648
678
525
584
639
678
C
Nup49
246
332
370
413
427
464
470
Y420F

Fig. S31.
Multispecies sequence alignment of the CNT coiled-coil segments. Sequences of the three coiled-coil segments of (**A**) Nup57, (**B**) Nsp1 and (**C**) Nup49 from *C. thermophilum*, *S. cerevisiae, and H. sapiens* were aligned based on the secondary structure elements observed in the CNT•Nic96^{R1} structure and colored by sequence similarity according to the BLOSUM62 (Blocks Substitution Matrix) matrix from white (less than 40 % similarity), to yellow (40 % similarity), to red (100 % identity). The numbering is according to the *C. thermophilum* channel nups. The secondary structure is indicated above the sequence as rectangles (α-helices), arrows (β-strands), and lines (unstructured regions). Gray dots indicate residues with no observed electron density in the crystal structure, which are presumed disordered. Secondary structure elements are colored according to Figure 4A with the exception of the Nup57α/β domain (magenta). A yellow dot in the secondary structure plot of Nup57 (A) indicates the position of Q473 and Y293, which are used as positional markers in the structural comparison of Nup57^{CCS3*} and *hs*Nup57^{CCS3*} (Figure S23E). Residues of the EVPIP mutant are indicated by red dots in the secondary structure plot of Nup49 (panel C). A black dot and a black bar indicate the position of the Y420F mutant and the residues removed in the ΔC417 mutant of *hs*Nup49$^{CCS2+3*}$, which increases the abundance (Figure S26, A to C) and abolishes the formation (Figure S26, D and E) of higher homo-oligomeric states, respectively.

Nup57

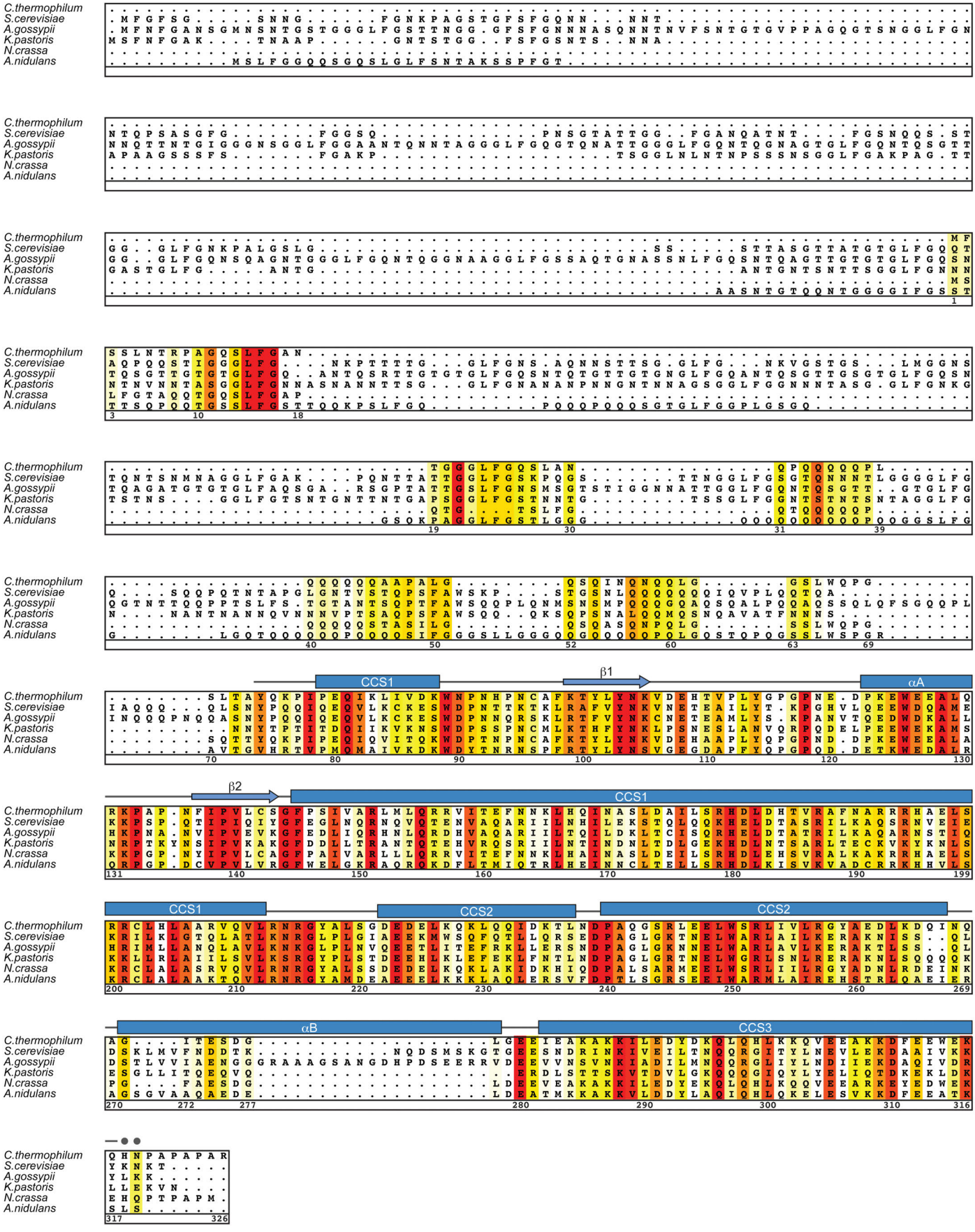
C.thermophilum
S.cerevisiae
A.gossypii
K.pastoris
N.crassa
A.nidulans
CCS1
β1
αA
β2
CCS1
CCS1
CCS2
CCS2
αB
CCS3

Fig. S32.
Multispecies sequence alignment of full-length Nup57. Sequences from six diverse fungal species were aligned and colored by sequence similarity according to the BLOSUM62 matrix from white (less than 40 % similarity), to yellow (40 % similarity), to red (100 % identity). The numbering is according to *C. thermophilum* proteins. The secondary structure is indicated above the sequence as rectangles (α-helices), arrows (β-strands), and lines (unstructured regions). Gray dots indicate residues with no observed electron density in the crystal structure, which are presumed disordered. Secondary structure elements of Nup57 are colored according to Figure 4.

Nsp1

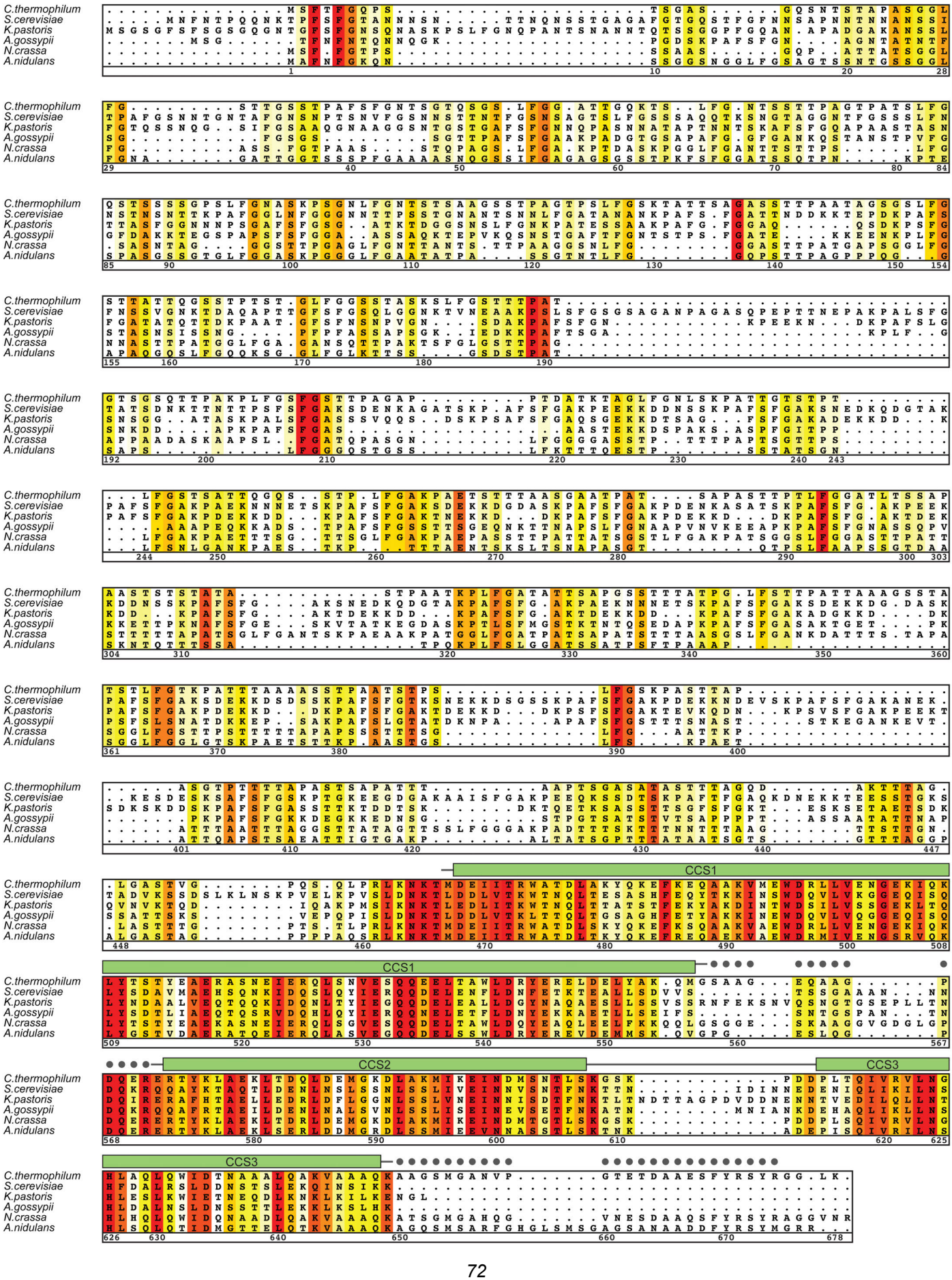
C.thermophilum
S.cerevisiae
K.pastoris
A.gossypii
N.crassa
A.nidulans
CCS1
CCS2
CCS3

Fig. S33.
Multispecies sequence alignment of full-length Nsp1. Sequences from six species were aligned and colored by sequence similarity according to the BLOSUM62 matrix from white (less than 40 % similarity), to yellow (40 % similarity), to red (100 % identity). The numbering is according to *C. thermophilum* proteins. The secondary structure is indicated above the sequence as rectangles (α-helices), arrows (β-strands), and lines (unstructured regions). Gray dots indicate residues with no observed electron density in the crystal structure, which are presumed disordered. Secondary structure elements of Nsp1 are colored according to Figure 4.

Nup49

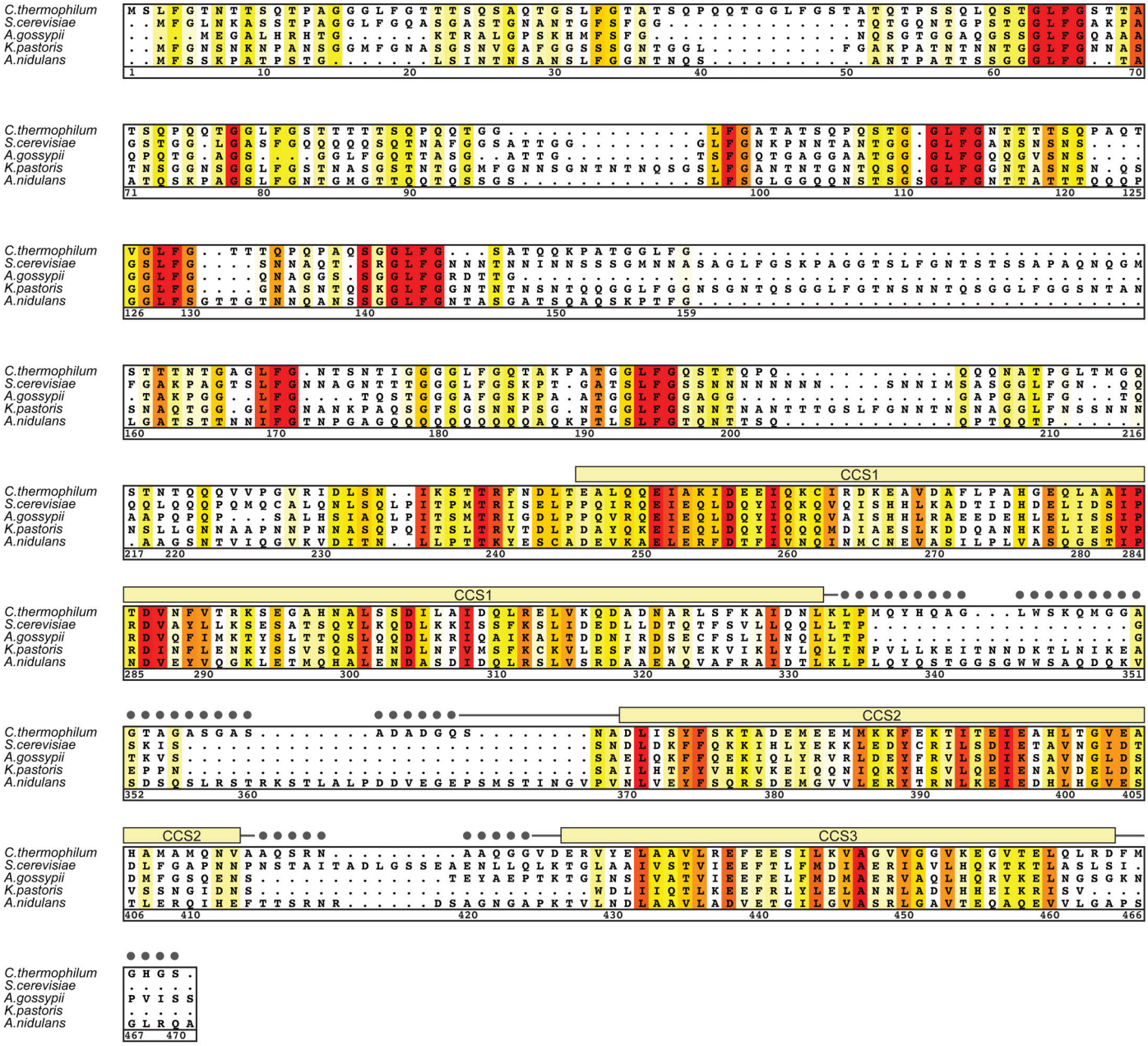
C.thermophilum
S.cerevisiae
A.gossypii
K.pastoris
A.nidulans
CCS1
CCS2
CCS3

Fig. S34.
Multispecies sequence alignment of full-length Nup49. Sequences from six diverse fungal species were aligned and colored by sequence similarity according to the BLOSUM62 matrix from white (less than 40 % similarity), to yellow (40 % similarity), to red (100 % identity). The numbering is according to *C. thermophilum* proteins. The secondary structure is indicated above the sequence as rectangles (α-helices), arrows (β-strands), and lines (unstructured regions). Gray dots indicate residues with no observed electron density in the crystal structure, which are presumed disordered. Secondary structure elements of Nup49 are colored according to Figure 4.

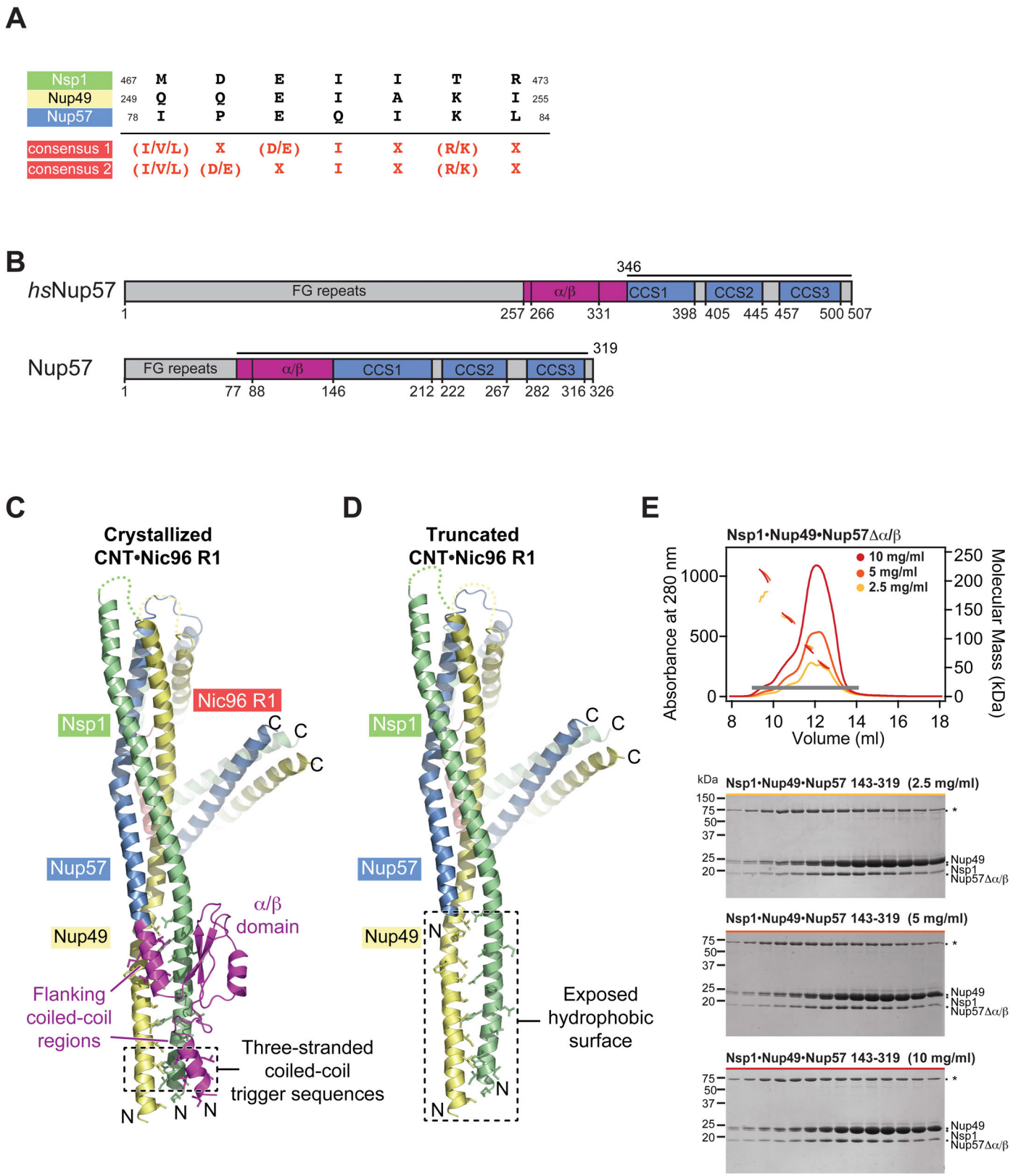
A
Nsp1 467 M D E I I T R 473
Nup49 249 Q Q E I A K I 255
Nup57 78 I P E Q I K L 84
consensus 1 (I/V/L) X (D/E) I X (R/K) X
consensus 2 (I/V/L) (D/E) X I X (R/K) X
B
hsNup57
FG repeats
α/β
CCS1
CCS2
CCS3
1 257 266 331 346 398 405 445 457 500 507
Nup57
FG repeats
α/β
CCS1
CCS2
CCS3
1 77 88 146 212 222 267 282 316 319 326
C
Crystallized CNT•Nic96 R1
Nic96 R1
Nsp1
Nup57
Nup49
α/β domain
Flanking coiled-coil regions
Three-stranded coiled-coil trigger sequences
D
Truncated CNT•Nic96 R1
Nsp1
Nup57
Nup49
Exposed hydrophobic surface
E
Nsp1•Nup49•Nup57Δα/β
10 mg/ml
5 mg/ml
2.5 mg/ml
Absorbance at 280 nm
Molecular Mass (kDa)
Volume (ml)
kDa
Nsp1•Nup49•Nup57 143-319 (2.5 mg/ml)
Nsp1•Nup49•Nup57 143-319 (5 mg/ml)
Nsp1•Nup49•Nup57 143-319 (10 mg/ml)
Nup49
Nsp1
Nup57Δα/β

Fig. S35.

Removal of the Nup57 α/β insertion domain results in non-stoichiometric higher-order CNT oligomers. (**A**) Alignment of the putative three-stranded coiled-coil trigger sequences of Nsp1 (green), Nup49 (yellow) and Nup57 (blue) is shown. The consensus sequence is depicted in red (X, any residue) (*72*). (**B**) Domain structures of *H. sapiens* and *C. thermophilum* Nup57. Bars above the domain structures indicate the domain boundaries of intact Nup57 as observed in the CNT•Nic96^{R1}•sAB-158 crystal structure and of *rn*Nup57 and *hs*Nup57 fragments that were reported previously to form various vastly different CNT oligomerization states in solution (*69, 71, 73, 74*). (**C**) CNT•Nic96^{R1}•sAB-158 structure is shown in cartoon representation colored according to Figure 4. The Nup57 α/β insertion domain and flanking coiled-coil regions that were excluded in previous mammalian CNT reconstitutions are colored in magenta. Hydrophobic residues in the coiled-coil center are represented in ball-and-stick representation. The location of the putative three-stranded coiled-coil trigger sequences is highlighted on the bottom. For clarity, sAB-158 was removed from the illustration. (**D**) Model of the CNT lacking an N-terminal Nup57 region that encodes the α/β insertion domain and flanking coiled-coil regions, corresponding to the mammalian Nup57 fragments used in previous studies. (**E**) SEC-MALS profiles of a *C. thermophilum* CNT variant using a Nup57 fragment that lacks the N-terminal coiled-coil region and the α/β insertion domain (residues 146-319) at three different concentrations. Measured molecular masses are indicated for the peak fractions. Gray bar indicates fractions that were resolved on SDS-PAGE gels and visualized by Coomassie staining. Asterisks indicate degradation products or contaminations. MALS and SDS-PAGE analysis establish that the removal of the Nup57 α/β insertion domain results in a CNT that adopts various different oligomeric states in solution, as previously observed for the mammalian truncated CNT (*69, 71, 73, 74*).

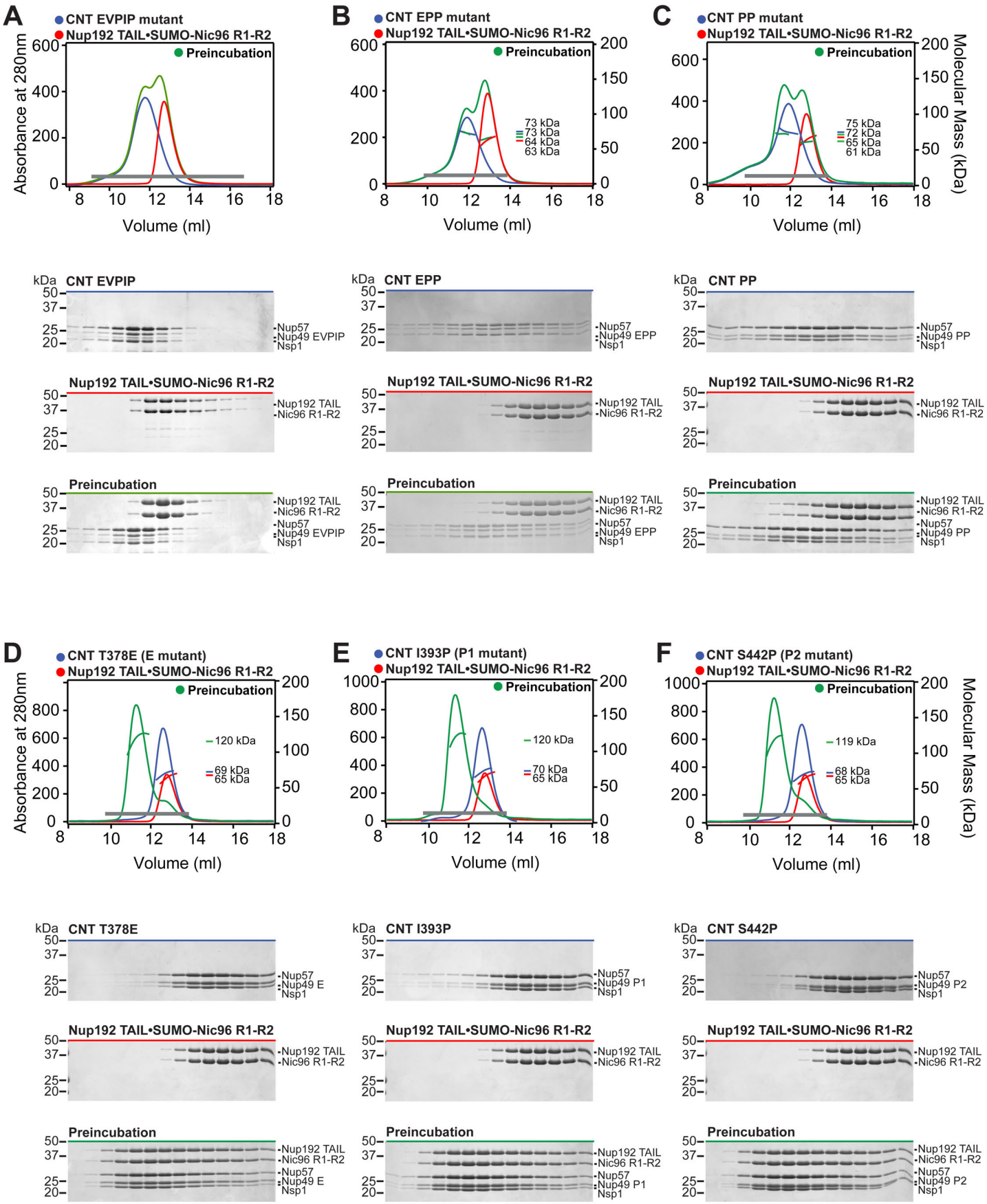
A
CNT EVPIP mutant
Nup192 TAIL•SUMO-Nic96 R1-R2
Preincubation
Absorbance at 280nm
Volume (ml)
B
CNT EPP mutant
Nup192 TAIL•SUMO-Nic96 R1-R2
Preincubation
73 kDa
73 kDa
64 kDa
63 kDa
Volume (ml)
C
CNT PP mutant
Nup192 TAIL•SUMO-Nic96 R1-R2
Preincubation
75 kDa
72 kDa
65 kDa
61 kDa
Molecular Mass (kDa)
Volume (ml)
kDa
CNT EVPIP
Nup57
Nup49 EVPIP
Nsp1
CNT EPP
Nup57
Nup49 EPP
Nsp1
CNT PP
Nup57
Nup49 PP
Nsp1
Nup192 TAIL•SUMO-Nic96 R1-R2
Nup192 TAIL
Nic96 R1-R2
Preincubation
D
CNT T378E (E mutant)
120 kDa
69 kDa
65 kDa
E
CNT I393P (P1 mutant)
120 kDa
70 kDa
65 kDa
F
CNT S442P (P2 mutant)
119 kDa
68 kDa
65 kDa
CNT T378E
Nup49 E
CNT I393P
Nup49 P1
CNT S442P
Nup49 P2

Fig. S36.
Identification of CNT mutations that disrupt binding to the IRC. (**A-F**) SEC-MALS and SDS-PAGE analysis corresponding to Figure 5. SEC-MALS profiles of mutant CNT or Nup192^{TAIL}•SUMO-Nic96^{R1-R2} complexes are shown individually (blue and red) and after their preincubation (green). Measured molecular masses are indicated for the peak fractions. Gray bars indicate fractions that were resolved on SDS-PAGE gels and visualized by Coomassie staining.

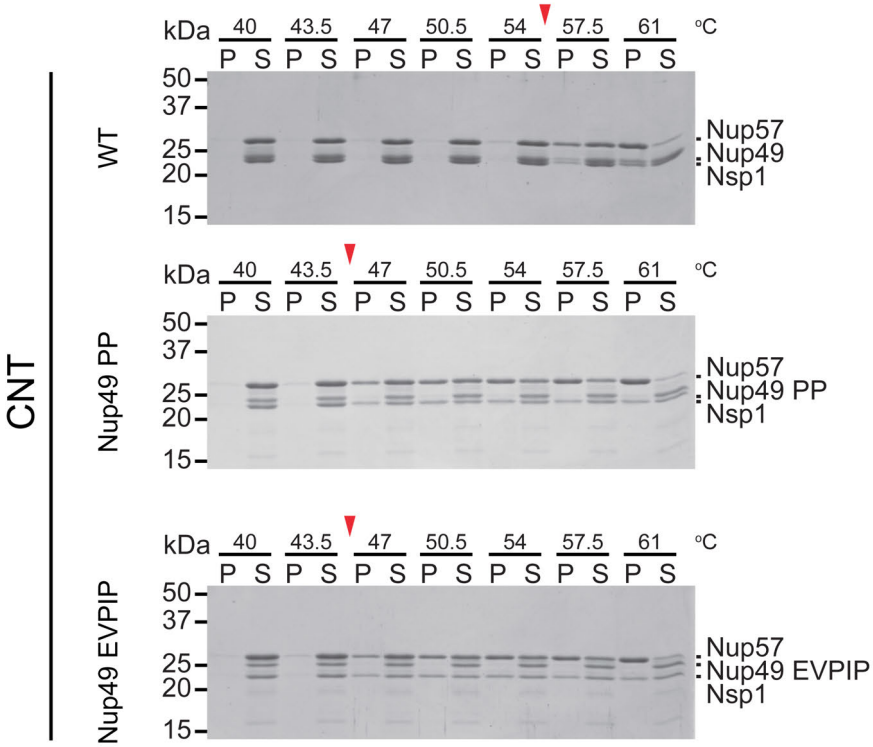
CNT
WT
Nup49 PP
Nup49 EVPIP
kDa
40
43.5
47
50.5
54
57.5
61
°C
P S P S P S P S P S P S P S
50
37
25
20
15
Nup57
Nup49
Nsp1
Nup49 PP
Nup49 EVPIP

Fig. S37.
Nup49 PP and EVPIP mutants decrease CNT thermostability. Wild type CNT and CNT carrying either the Nup49 PP or EVPIP mutant were incubated at the indicated temperatures for 30 minutes prior to centrifugation. Soluble (S) and pelleted (P) fractions were analyzed by SDS-PAGE and visualized by Coomassie staining. Red arrows indicate temperature increment at which *in vitro* aggregation ensued.

A

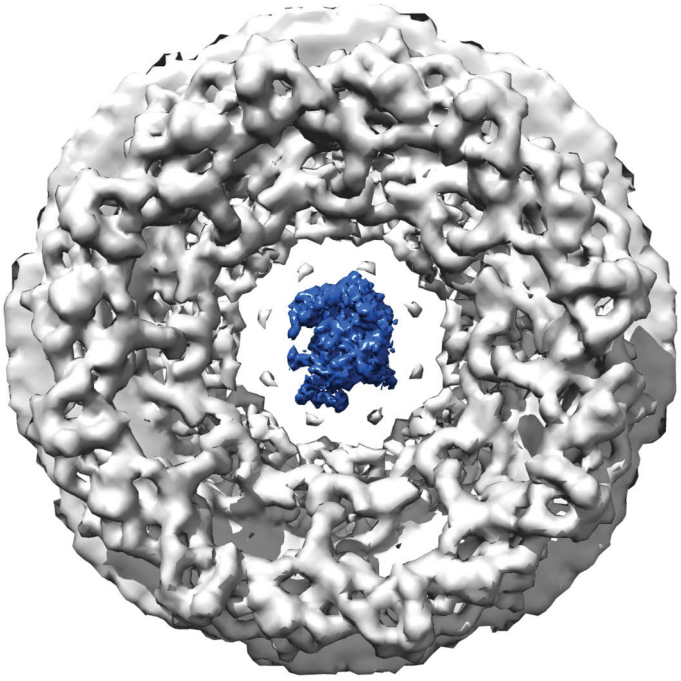

Arx1 pre-60S particle

human NPC

B

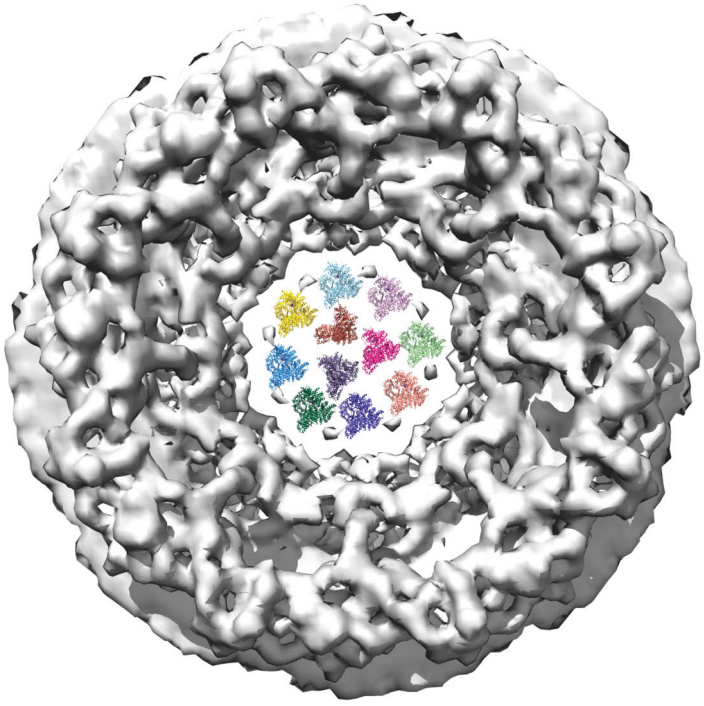

Cse1•Kap-α•RanGTP

human NPC

Fig. S38.
The human NPC can accommodate the 60S pre-ribosomal particle. A top view of the cryoelectron tomography reconstruction of the human NPC is shown (EMD 2444; gray). The central transport channel is large enough to accommodate (**A**) the 60S pre-ribosomal particle (EMD 2528; blue) and (**B**) eleven Cse1•Kap-α•RanGTP nuclear export complexes (1WA5). (*75*-*77*).

Table S1.

SEC-MALS analysis

Figure	Nucleoporin or nucleoporin complex	Experimental Mass (kDa)	Theoretical Mass (kDa)	Stoichiometry
Fig. 1B Fig. S1A	CNT•Nic96	180	187	equimolar
	Nup192•Nup145N	250	239	equimolar
	Nup192•Nup145N •CNT•Nic96	425	426	equimolar
Fig. 1C Fig. S1B	CNT•Nic96•Nup192•Nup53	320	424	below measurement limit
	Nup82•SUMO-Nup159^{T}•Nup145N	110	123	equimolar
	Nup82•SUMO-Nup159^{T}•Nup145N•CNT•Nic96•Nup192 •Nup53	440	547	below measurement limit
Fig. 1D Fig. S1C	CNT•Nup192•Nup145N•SUMO-Nic96^{R1-R2}	291	345	below measurement limit
	Nic96^{SOL}	75	81	n/a
	CNT•Nup192•Nup145N•SUMO-Nic96^{R1-R2} •Nic96^{SOL}	301, 74	426	no interaction
Fig. 1E Fig. S1D	CNT	74	77	equimolar
	Nup192^{TAIL}•SUMO-Nic96^{R1-R2}	69	72	equimolar
	Nup192^{TAIL}•SUMO-Nic96^{R1-R2}•CNT	135	149	equimolar
Fig. 1F Fig. S1E	CNT	74	77	equimolar
	SUMO-Nic96^{R1}	18	18	n/a
	CNT•SUMO-Nic96^{R1}	87, 18	95	equimolar
Fig. 1G Fig. S1F	Nup192^{TAIL}	39	41	n/a
	SUMO-Nic96^{R2}	18	19	n/a
	Nup192^{TAIL}•SUMO-Nic96^{R2}	54, 19	60	equimolar
Fig. 1H Fig. S1G	CNT	68	77	equimolar
	Nup192•Nup145N•Nic96^{R2-SOL}	358	336	equimolar
	Nup192•Nup145N•Nic96^{R2-SOL}•CNT	360, 73	413	no interaction
Fig. 1I Fig. S1H	CNT	70	77	equimolar
	Nup192•Nup53•Nic96^{R2-SOL}	355	333	equimolar
	Nup192•Nup53•Nic96^{R2-SOL}•CNT	350, 70	410	no interaction
Fig. S2A	Nup82^{NTD}•SUMO-Nup159^{T}	79	80	equimolar
	Nup145N	42	42	n/a
	Nup82^{NTD}•SUMO-Nup159^{T}•Nup145N	110	122	equimolar
Fig. S2B	Nup82^{NTD}•SUMO-Nup159^{T}	79	80	equimolar
	Nup145N^{APD}	16	16	n/a
	Nup82^{NTD}•SUMO-Nup159^{T}•Nup145N^{APD}	97	96	equimolar
Fig. S2D	CNT	71	77	equimolar
	Nup145N	48	42	n/a
	CNT•Nup145N	105	119	equimolar
Fig. S2F	CNT•Nup145N	78	119	equimolar
	Nup192	182	197	n/a
	Nup192• CNT•Nup145N	210, 76	316	no interaction
Fig. S4A	CNT	74	77	equimolar
	SUMO-Nic96^{R2}	18	19	n/a
	CNT•SUMO-Nic96^{R2}	75, 18	96	No interaction
Fig. S4B	Nup192^{TAIL}	39	41	n/a
	SUMO-Nic96^{R1}	18	18	n/a
	Nup192^{TAIL}•SUMO-Nic96^{R1}	29	59	No interaction
Fig. S4C	CNT	74	77	equimolar
	Nup192^{TAIL}	39	41	n/a
	CNT•Nup192^{TAIL}	74, 40	118	No interaction
Fig. 3B Fig. S15B	CNT	71	77	equimolar
	SUMO-Nic96^{R1}	18	18	n/a
	Preincubation - LLLL	18, 70	95	no interaction
	Preincubation - wt	17, 80	95	equimolar
Fig. S15A	CNT	71	77	equimolar
	SUMO-Nic96^{R1} wt and truncations	18	18, 17, 18, 17	n/a
	Preincubation - wt	17, 80	95	equimolar
	Preincubation - truncations	18, 18, 18, 73, 70, 68	94-95	sub-stoichiometric / no interaction
Fig. S18C	CNT 1 mg/ml	147, 71	77 for monomer	equimolar
	CNT 10 mg/ml	131, 69	77 for monomer	equimolar
	CNT 30 mg/ml	136, 73	77 for monomer	equimolar

Figure	Nucleoporin or nucleoporin complex	Experimental Mass (kDa)	Theoretical Mass (kDa)	Stoichiometry
Fig. S18D	CNT	147, 71	77 for monomer	equimolar
	SUMO-Nic96^{R1}	---	18	n/a
	CNT•SUMO-Nic96^{R1}	183, 87	95 for monomer	equimolar
Fig. S15A	CNT	71	77	equimolar
	SUMO-Nic96^{R1} wt and truncations	18	18, 17, 18, 17	n/a
	Preincubation - wt	17, 80	95	equimolar
	Preincubation - truncations	18, 18, 18, 73, 70, 68	94-95	sub-stoichiometric / no interaction
Fig. S22B	*hs*Nup49 CCS2+3*	22, 23, 25, 29, 33, 36, 37, 40	10 for monomer	n/a
Fig. S22C	*hs*Nup57 CCS3*	18	5 for monomer	n/a
	*hs*Nup49 CCS2+3*	25, 40	10 for monomer	n/a
	*hs*Nup57 CCS3*• *hs*Nup49 CCS2+3*	24, 57	various	polydisperse
Fig. S23B	*hs*Nup57 CCS3*	18	5 for monomer	tetramer
Fig. S23C	Nup57 CCS3*	8	4 for monomer	dimer
Fig. S25B	*hs*Nup57 CCS3*	---	5 for monomer	n/a
	*hs*Nup49 CCS2+3*	---	10 for monomer	n/a
	*hs*Nup57 CCS3*• *hs*Nup49 CCS2+3*	20, 24, 26, 49, 53, 54	various	polydisperse
Fig. S25C	*hs*Nup57 CCS3*	---	5 for monomer	n/a
	*hs*Nup49 CCS2+3*	---	10 for monomer	n/a
	Preincubation	21, 23, 25, 26, 46, 51, 57, 57	various	polydisperse
Fig. S26B	*hs*Nup57 CCS3*	---	5 for monomer	n/a
	*hs*Nup49 CCS2+3*	---	10 for monomer	n/a
	*hs*Nup49 CCS2+3*, Y420F	---	10 for monomer	n/a
	*hs*Nup57 CCS3*•*hs*Nup49 CCS2+3*	25, 57	various	polydisperse
	*hs*Nup57 CCS3*•*hs*Nup49 CCS2+3*, Y420F	29, 63	various	polydisperse
Fig. S26C	*hs*Nup49 CCS2+3*	25, 40	10 for monomer	polydisperse
	*hs*Nup49 CCS2+3*, Y420F	33, 54	10 for monomer	polydisperse
Fig. S26D	*hs*Nup49 CCS2+3*, Y420F	28, 30, 32, 36, 37, 40, 47, 54	10 for monomer	polydisperse
Fig. S26E	*hs*Nup49 CCS2+3* ΔC417	17, 18, 18, 19	10 for monomer	polydisperse
Fig. S27F	CNT•SUMO-Nic96^{R1}	92	95	n/a
	CNT•SUMO-Nic96^{R1}•MB6	116	119	equimolar
	CNT•SUMO-Nic96^{R1}•MB6•MB9	133	143	equimolar
Fig. S27G	CNT•Nic96•SUMO-MB6•SUMO-MB9	180	236	equimolar
	Nup192•Nup145N	244	239	equimolar
	CNT•Nic96•SUMO-MB6•SUMO-MB9• Nup192•Nup145N	417	475	equimolar
Fig. S28A	CNT	63	77	equimolar
	CNT•sAB158	109	128	equimolar
	CNT•sAB158•sAB160	162	179	equimolar
Fig. S28B	CNT•sAB158	111	128	equimolar
	Nup192^{TAIL}•SUMO-Nic96^{R1-R2}	77	72	equimolar
	CNT•sAB158•Nup192^{TAIL}•SUMO-Nic96^{R1-R2}	158	200	equimolar
Fig. 5C Fig. S36B	CNT EPP	73	77	equimolar
	Nup192^{TAIL}•SUMO-Nic96^{R1-R2}	63	72	equimolar
	Preincubation - wt	135	149	equimolar
	Preincubation – EPP mutant	73, 64	149	no interaction
Fig. S36C	CNT PP	75	77	equimolar
	Nup192^{TAIL}•SUMO-Nic96^{R1-R2}	65	72	equimolar
	Preincubation	72, 61	149	below measurement limit
Fig. S36D	CNT T378E	69	77	equimolar
	Nup192^{TAIL}•SUMO-Nic96^{R1-R2}	65	72	equimolar
	Preincubation	120	149	equimolar
Fig. S36E	CNT I393P	70	77	equimolar
	Nup192^{TAIL}•SUMO-Nic96^{R1-R2}	65	72	equimolar
	Preincubation	120	149	equimolar
Fig. S36F	CNT S442P	68	77	equimolar
	Nup192^{TAIL}•SUMO-Nic96^{R1-R2}	65	72	equimolar
	Preincubation	119	149	equimolar

Table S2.

Crystallographic analysis Nup188^{TAIL}, Nup192^{TAIL}, Nup82^{NTD}•Nup159^{T}•Nup145N^{APD}

Data collection				
Protein(s)	Nup192^{TAIL}	Nup188^{TAIL}	Nup82^{NTD} Nup159^{T} Nup145N^{APD}	Nup82^{NTD} Nup159^{T} Nup145N^{APD}
PDB code	5CWV	5CWU	5CWW	
Synchrotron	SSRL[a]	APS[c]	APS	SSRL
Beamline	BL12-2	23-ID-D	23ID-D	BL12-2
Space group	$P2_12_12_1$	P1	C2	C2
Cell parameters				
a (Å)	64.7	65.2	122.3	122.1
b (Å)	114.4	65.3	108	108.2
c (Å)	114.7	155.5	69.6	69.6
α (°)	90.0	90.0	90.0	90.0
β (°)	90.0	89.9	108.6	108.4
γ (°)	90.0	90.0	90.0	90.0
	Se peak	*Se peak*	*Native*	*Se peak*
Wavelength (Å)	0.97930	0.97944	1.0000	0.97940
Resolution (Å)	20.0 – 3.15	20.0 – 3.35	30.0 – 2.2	40.0 – 2.5
R_{sym} (%)[d]	7.5 (95.8)	5.4 (90.0)	8.4 (154.6)	6.6 (76.4)
$\langle I \rangle / \langle \sigma I \rangle$[d]	21.8 (1.7)	23.4 (1.5)	13.6 (1.2)	13.2 (1.7)
Completeness (%)[d]	99.5 (99.0)	99.0 (97.9)	99.0 (97.1)	97.4 (96.2)
No. observations	183,279	294,471	300,689	202,782
No. unique reflections	28,157 (2,819)	74,517 (7,493)	43,372 (6,846)	57,257 (9,135)
Redundancy	6.5 (4.7)	4.0 (3.9)	6.9 (6.7)	3.5 (3.4)
Refinement				
Resolution (Å)	20.0 – 3.15	20.0 – 3.35	30.0 – 2.2	
No. reflections total	28,095	72,752	43,204	
No. reflections test set	2,843 (10.1%)	3,632 (5.0%)	2,959 (6.8%)	
R_{work} / R_{free}	18.5 / 24.07	24.6 / 27.9	21.4 / 24.0	
No. atoms	4167	18,312	5,537	
Protein	4167	18,264	5,463	
Ligand	0	48	0	
Water	0	0	74	
B-factors				
Protein	121.0	103.5	52.8	
Ligand	N/A	79.8	N/A	
Water	N/A	N/A	57.3	
R.m.s. deviations				
Bond lengths (Å)	0.003	0.004	0.005	
Bond angles (°)	0.6	0.7	1.0	
Ramachandran plot[e]				
Favored (%)	94.2	89.4	98.2	
Additionally allowed (%)	5.8	10.6	1.8	
Outliers (%)	0.0	0.0	0.0	

[a] SSRL, Stanford Synchrotron Radiation Lightsource
[b] APS, Advanced Photon Source
[c] Highest-resolution shell is shown in parentheses
[d] As determined by MolProbity (*63*)

Table S3.

Crystallographic analysis of channel nup fragments

Data collection							
Protein 1	*hs*Nup57^{CCS3}*	*hs*Nup57^{CCS3}*	*hs*Nup49^{CCS2+3}*	*hs*Nup49^{CCS2+3}*	*hs*Nup49^{CCS2+3}*	Nup57^{CCS3}*	Nup57^{CCS3}* I289M
Protein 2				*hs*Nup57^{CCS3}*	*hs*Nup57^{CCS3}*		
Stoichiometry	Homotetramer	Homotetramer	Homotetramer	2:2 stoichiometry	1:2 stoichiometry	Homodimer	Homotetramer
PDB code	4JNV	4JNU	4JQ5	4JO7	4JO9	5CWT	
Synchrotron	SSRL[a]	ALS[b]	SSRL	SSRL	SSRL	SSRL	SSRL
Beamline	BL12-2	BL8.2.1	BL12-2	BL12-2	BL12-2	BL12-2	BL12-2
Space group	C2	$P2_1$	P1	P1	$P4_122$	$P2_12_12_1$	$P2_12_12_1$
Cell parameters							
a (Å)	70.5	39.9	63.8	47.7	55.5	42.3	42.2
b (Å)	36.6	45.1	77.1	47.7	55.5	42.4	42.2
c (Å)	63.2	46.4	77.2	71.3	191.2	138.7	139.6
α (°)	90.0	90.0	120.0	88.9	90.0	90.0	90.0
β (°)	104.4	113.8	90.1	83.4	90.0	90.0	90.0
γ (°)	90.0	90.0	89.9	81.4	90.0	90.0	90.0
	Se peak	*Native*	*Native*	*Se peak*	*Native*	*Native*	*Se peak*
Wavelength (Å)	0.97940	1.0000	1.0000	0.97940	1.0000	1.00010	0.97920
Resolution (Å)	20.0 – 1.85	20.0 – 1.45	20.0 – 2.2	50.0 – 1.75	50.0 – 2.5	20.0 – 2.5	20.0 – 2.75
R_{sym} (%)[c]	8.5 (51.5)	9.9 (59.0)	6.4 (52.8)	11.6 (74.0)	13.6 (74.3)	4.3 (24.2)	14.1 (80.9)
$\langle I \rangle / \langle \sigma I \rangle$[c]	12.4 (2.7)	15.5 (2.1)	17.8 (2.1)	10.0 (2.2)	19.8 (2.1)	58.3 (6.3)	12.0 (1.9)
Completeness (%)[c]	96.9 (94.4)	97.2 (81.6)	97.3 (87.7)	97.4 (95.2)	98.8 (89.1)	98.0 (88.2)	99.7 (98.7)
No. observations	82,655	174,150	242,553	205,417	169,333	136,374	79,570
No. unique reflections	25,273 (2,494)	26,320 (2,198)	63,140 (5,724)	117,121 (11,189)	11,003 (953)	8,970 (759)	12,635 (1,297)
Redundancy	3.3 (2.8)	6.6 (3.6)	3.8 (3.5)	1.8 (1.6)	15.4 (10.0)	15.2 (10.2)	6.4 (4.5)
Refinement							
Resolution (Å)	20.0 – 1.85	20.0 – 1.45	20.0 – 2.2	50.0 – 1.75	50.0 – 2.5	20.0 – 2.5	
No. reflections total	25,266	26,274	63,070	116,939	10,891	8,126	
No. reflections test set	2,508 (9.93%)	1,990 (7.57%)	1,990 (3.16%)	3,925 (3.36%)	1,092 (10.0%)	809 (9.9%)	
R_{work} / R_{free}	23.7 / 27.7	18.3 / 21.8	28.5 / 29.3	18.6 / 21.4	24.7 / 29.4	24.1 / 29.3	
No. atoms	1,108	3,121	8,526	4,592	1,355	1,323	
Protein	1,086	2,989	8,526	4,138	1,338	1,305	
Ligand	0	0	0	0	0	0	
Water	22	132	0	454	17	18	
B-factors							
Protein	30.4	24.5	51.3	18.6	88.7	58.2	
Ligand	N/A	N/A	N/A	N/A	N/A	N/A	
Water	29.7	36.5	N/A	32.2	60.6	54.2	
R.m.s. deviations							
Bond lengths (Å)	0.009	0.007	0.002	0.008	0.002	0.002	
Bond angles (°)	0.9	1.0	0.5	0.8	0.4	0.4	
Ramachandran plot[d]							
Favored (%)	99.2	100.0	96.1	99.2	97.4	99.3	
Additionally allowed (%)	0.8	0.0	3.9	0.8	2.6	0.7	
Outliers (%)	0.0	0.0	0.0	0.0	0.0	0.0	

[a] SSRL, Stanford Synchrotron Radiation Lightsource
[b] ALS, Advanced Light Source
[c] Highest-resolution shell is shown in parentheses
[d] As determined by MolProbity (*63*)

Table S4.

Crystallographic analysis of the CNT•Nic96^{R1}•sAB-158 structure

Data collection	K_2OsCl_6	K_2OsCl_6	*K_2OsO_4*	*SeMet*[e]	*PCMB*	*EMTS*	*Native*
Synchrotron[a]	SSRL	SSRL	SSRL	SSRL	SSRL	SSRL	APS
Beamline	BL12-2	BL12-2	BL12-2	BL12-2	BL12-2	BL12-2	GM/CA
Space group	$P2_12_12_1$	$P2_12_12_1$	$P2_12_12_1$	$P2_12_12_1$	$P2_12_12_1$	$P2_12_12_1$	$P2_12_12_1$
Cell dimensions							
a (Å)	123.2	123.2	122.5	122.9	123.3	121.5	123.7
b (Å)	162.8	162.8	162.8	162.2	163.8	162.4	162.9
c (Å)	212.9	212.9	215.2	214.0	214.5	215.5	214.1
α (°)	90.0	90.0	90.0	90.0	90.0	90.0	90.0
β (°)	90.0	90.0	90.0	90.0	90.0	90.0	90.0
γ (°)	90.0	90.0	90.0	90.0	90.0	90.0	90.0
	Os peak	*Os peak*	*Os peak*	*Se peak*	*Hg peak*	*Hg peak*	
Wavelength (Å)	1.1400	1.1400	1.1400	0.9793	1.0078	1.0054	1.033
Resolution (Å)	50.0 – 3.77	50.0 – 3.95	40.0 – 4.4	40.0 – 3.77	40.0 – 5.6	40.0 – 4.8	40.0 – 3.95
*R*meas (%)[b]	20.4 (585.7)	17.2 (308.4)	16.3 (302.1)	18.1 (495.9)	11.9 (330.3)	15.5 (304.6)	11.3 (373.9)
CC1/2 [b]	100.0 (54.4)	100.0 (74.6)	100.0 (57.2)	100.0 (57.6)	99.9 (53.0)	99.0 (64.7)	100.0 (59.5)
$< I / \sigma I >$[b]	17.0 (1.00)	19.36 (1.84)	14.26 (1.42)	14.49 (1.01)	14.31 (1.02)	11.68 (1.16)	17.79 (1.17)
Completeness (%)[b]	99.9 (99.9)	99.9 (100.0)	99.7 (100.0)	99.8 (99.8)	99.4 (99.8)	98.7 (97.9)	99.5 (98.9)
No. of observations	1,765,669	1,538,483	740,306	1,167,642	181,671	283,261	1,024,643
No. of unique reflections[b]	43,896 (7,063)	38,253 (6,105)	27,912 (4,495)	43,765 (7,006)	13,837 (2,144)	21,204 (3,350)	38,491 (6,087)
Redundancy[b]	40.2 (40.2)	40.2 (40.4)	26.5 (27.7)	26.7 (27.1)	13.1 (13.8)	13.4 (13.1)	26.6 (26.0)

Refinement	
Resolution (Å)	50 – 3.77
No. of reflections	43,876
No. of reflections test set	2,000 (4.56%)
*R*work / *R*free	22.9 / 26.5
No. atoms	16,564
Protein	16,562
Ions	2
R.m.s deviations	
Bond lengths (Å)	0.003
Bond angles (°)	0.7
B-factors[c]	
Protein	241.9
Ions	299.4
Ramachandran plot[d]	
Favored (%)	93.1
Additionally allowed (%)	6.9
Outliers (%)	0.0

[a]SSRL, Stanford Synchrotron Radiation Lightsource; APS, Advanced Photon Source
[b]Highest-resolution shell is shown in parentheses
[c]B-factors include overall B-factor of the crystal
[d]As determined by MolProbity (*63*)
[e]Representative statistics for all 23 datasets (wild type and 22 methionine mutants)

Table S5.

Bacterial expression constructs and expression conditions

#	Protein	Residues	Expression vector	Restriction sites 5', 3'	N-terminal overhang	C-terminal overhang	Expression conditions
1♦	*hs*Nup49 CCS2+3*	341-428	pET28a-Sumo	BamHI, NotI	S	none	18 °C / 18 hours
2	*hs*Nup49	341-428 (Y420F)	pET28a-Sumo	BamHI, NotI	S	none	18 °C / 18 hours
3♦	*hs*Nup57 CCS3*	453-491	pET28a-Sumo	BamHI, NotI	S	none	18 °C / 18 hours
4♦	*hs*Nup57	453-491 (I478M)	pET28a-Sumo	BamHI, NotI	S	none	18 °C / 18 hours
5♦	Nsp1 Nup57	467-674 74-319	pETDuet1	NcoI/NotI NdeI/XhoI	None M	none none	18 °C / 18 hours
6	Nsp1 Nup57 Δα/β	467-674 146-319	pETDuet1	NcoI/NotI NdeI/XhoI	None M	none none	18 °C / 18 hours
7♦■	Nsp1 Nup57	467-674 (L527M) 74-319	pETDuet1	NcoI/NotI	None M	none	18 °C / 18 hours
8♦■	Nsp1 Nup57	467-674 (L548M) 74-319	pETDuet1	NdeI/XhoI	None M	none	18 °C / 18 hours
9♦■	Nsp1 Nup57	467-674 (A628M) 74-319	pETDuet1	NcoI/NotI	None M	none	18 °C / 18 hours
10♦■	Nsp1 Nup57	467-674 74-319 (I82M)	pETDuet1	NdeI/XhoI	None M	none	18 °C / 18 hours
11♦■	Nsp1 Nup57	467-674 74-319 (H109M)	pETDuet1	NcoI/NotI	None M	none	18 °C / 18 hours
12♦■	Nsp1 Nup57	467-674 74-319 (L113M)	pETDuet1	NdeI/XhoI	None M	none	18 °C / 18 hours
13♦■	Nsp1 Nup57	467-674 74-319 (E127M)	pETDuet1	NcoI/NotI	None M	none	18 °C / 18 hours
14♦■	Nsp1 Nup57	467-674 74-319 (I138M)	pETDuet1	NcoI/NotI	None M	none	18 °C / 18 hours
15♦■	Nsp1 Nup57	467-674 74-319 (L198M)	pETDuet1	NcoI/NotI	None M	none	18 °C / 18 hours
16♦■	Nsp1 Nup57	467-674 74-319 (I233M)	pETDuet1	NcoI/NotI	None M	none	18 °C / 18 hours
17♦■	Nsp1 Nup57	467-674 74-319 (L253M)	pETDuet1	NcoI/NotI	None M	none	18 °C / 18 hours
18♦■	Nsp1 Nup57	467-674 74-319 (V303M)	pETDuet1	NcoI/NotI	None M	none	18 °C / 18 hours
19	Nsp1	467-678	pET28a-Sumo	BamHI, NotI	S	none	18 °C / 18 hours
20	Nup57	74-326	pGEX-6P1	BamHI, NotI	GPLGS	none	18 °C / 18 hours
21♦	Nup57	265-317	pET28a-Sumo	BamHI, NotI	S	none	18 °C / 18 hours
22♦	Nup57	265-317 (I289M)	pET28a-Sumo	BamHI, NotI	S	none	18 °C / 18 hours
23♦	Nup49	246-470	pET28a-Sumo	BamHI, NotI	S	none	18 °C / 18 hours
24♦■	Nup49	246-470 (I263M)	pET28a-Sumo	BamHI, NotI	S	none	18 °C / 18 hours
25♦■	Nup49	246-470 (H276M)	pET28a-Sumo	BamHI, NotI	S	none	18 °C / 18 hours
26♦■	Nup49	246-470 (L301M)	pET28a-Sumo	BamHI, NotI	S	none	18 °C / 18 hours
27♦■	Nup49	246-470 (A307M)	pET28a-Sumo	BamHI, NotI	S	none	18 °C / 18 hours
28♦■	Nup49	246-470 (L332M)	pET28a-Sumo	BamHI, NotI	S	none	18 °C / 18 hours
29♦■	Nup49	246-470 (E438M)	pET28a-Sumo	BamHI, NotI	S	none	18 °C / 18 hours
30#	Avi-Nup49	246-470	pET28a-PreS	BamHI, NotI	GPLMSGLNDIFEAQKI EWHEGSAGGSGHM	none	18 °C / 18 hours
31	Nup49 E	246-470 (T378E)	pET28a-Sumo	BamHI, NotI	S	none	18 °C / 18 hours
32	Nup49 P1	246-470 (I393P)	pET28a-Sumo	BamHI, NotI	S	none	18 °C / 18 hours
33	Nup49 P2	246-470 (S442P)	pET28a-Sumo	BamHI, NotI	S	none	18 °C / 18 hours
34	Nup49 PP	246-470 (I393P, S442P)	pET28a-Sumo	BamHI, NotI	S	none	18 °C / 18 hours
35	Nup49 EPP	246-470 (T378E, I393P, S442P)	pET28a-Sumo	BamHI, NotI	S	none	18 °C / 18 hours
36	Nup49 EVPIP	246-470 (T378E, T292V, I393P, L400I, S442P)	pET28a-Sumo	BamHI, NotI	S	none	18 °C / 18 hours
37	Nic96	110-1112	pET28a-Sumo	BamHI, NotI	S	AAALEHHHHHH	18 °C / 18 hours
38#	Nic96	139-201	pET28a-Sumo	BamHI, NotI	S	none	18 °C / 18 hours
39♦#	Nic96 R1	139-180	pET28a-Sumo	BamHI, NotI	S	none	18 °C / 18 hours
40♦■	Nic96 R1	139-180 (L178M)	pET28a-Sumo	BamHI, NotI	S	none	18 °C / 18 hours
41♦■	Nic96 R1	139-180 (L140M)	pET28a-Sumo	BamHI, NotI	S	none	18 °C / 18 hours
42♦■	Nic96 R1	139-180 (L161M)	pET28a-Sumo	BamHI, NotI	S	none	18 °C / 18 hours
43♦■	Nic96 R1	139-180 (L164M)	pET28a-Sumo	BamHI, NotI	S	none	18 °C / 18 hours
44	Nic96	139-164	pET28a-Sumo	BamHI, NotI	S	none	18 °C / 18 hours
45	Nic96	139-171	pET28a-Sumo	BamHI, NotI	S	none	18 °C / 18 hours
46	Nic96	146-180	pET28a-Sumo	BamHI, NotI	S	none	18 °C / 18 hours
47	Nic96	156-180	pET28a-Sumo	BamHI, NotI	S	none	18 °C / 18 hours
48	Nic96	165-180	pET28a-Sumo	BamHI, NotI	S	none	18 °C / 18 hours
49	Nic96	139-180 (L168A, L171A, L175A, L178A)	pET28a-Sumo	BamHI, NotI	S	none	18 °C / 18 hours
50	Nic96	139-180 (L168A, L171A)	pET28a-Sumo	BamHI, NotI	S	none	18 °C / 18 hours
51	Nic96	139-180 (L175A, L178A)	pET28a-Sumo	BamHI, NotI	S	none	18 °C / 18 hours
52	Nic96 R1-R2	139-301	pET-MCN-Sumo	BamHI, NotI	S	none	N/A
53	Nic96 R2-SOL	245-1112	pGEX-6P1	BamHI, NotI	GPHM	none	23 °C / 18 hours

#	Protein	Residues	Expression vector	Restriction sites 5', 3'	N-terminal overhang	C-terminal overhang	Expression conditions
54	Nic96 SOL	391-1112	pET28a-SUMO	BamHI, NotI	S	none	18 °C / 18 hours
55	Nic96 R2	245-301	pET-MCN-Sumo	BamHI, NotI	S	none	37 °C / 2 hours
56	Nic96 R2	245-301 (F275A)	pET-MCN-Sumo	BamHI, NotI	S	none	37 °C / 2 hours
57	Nic96 R2	245-301 (D276A)	pET-MCN-Sumo	BamHI, NotI	S	none	37 °C / 2 hours
58	Nic96 R2	245-301 (F278A)	pET-MCN-Sumo	BamHI, NotI	S	none	37 °C / 2 hours
59	Nic96 R2	245-301 (N282A)	pET-MCN-Sumo	BamHI, NotI	S	none	37 °C / 2 hours
60	Nic96 R2	245-301 (L285A)	pET-MCN-Sumo	BamHI, NotI	S	none	37 °C / 2 hours
61	Nic96 R2	245-301 (W287A)	pET-MCN-Sumo	BamHI, NotI	S	none	37 °C / 2 hours
62	Nic96 R2	245-301 (I294A)	pET-MCN-Sumo	BamHI, NotI	S	none	37 °C / 2 hours
63	Nic96 R2	245-301 (F298A)	pET-MCN-Sumo	BamHI, NotI	S	none	37 °C / 2 hours
64	MB1	1-91	pET28a-Sumo	BamHI, NotI	S	none	18 °C / 18 hours
65	MB2	1-93	pET28a-Sumo	BamHI, NotI	S	none	18 °C / 18 hours
66	MB3	1-91	pET28a-Sumo	BamHI, NotI	S	none	18 °C / 18 hours
67	MB4	1-93	pET28a-Sumo	BamHI, NotI	S	none	18 °C / 18 hours
68	MB5	1-93	pET28a-Sumo	BamHI, NotI	S	none	18 °C / 18 hours
69	MB6	1-92	pET28a-Sumo	BamHI, NotI	S	none	18 °C / 18 hours
70	MB7	1-91	pET28a-Sumo	BamHI, NotI	S	none	18 °C / 18 hours
71	MB8	1-93	pET28a-Sumo	BamHI, NotI	S	none	18 °C / 18 hours
72	MB9	1-91	pET28a-Sumo	BamHI, NotI	S	none	18 °C / 18 hours
73	MB10	1-93	pET28a-Sumo	BamHI, NotI	S	none	18 °C / 18 hours
74♦	sAB-158-LC sAB-158-HC	1-204 1-258	pSV4	NcoI, SalI	none	VDKKVEPKSCDKT HTGGSHHHHHH	37 °C / 2 hours
75	sAB-160-LC sAB-160-HC	1-204 1-258	pSV4	NcoI, SalI	none	VDKKVEPKSCDKT HTGGSHHHHHH	37 °C / 2 hours
76	Nup145N	606-993	pET28a-Sumo	BamHI, NotI	S	none	23 °C / 18 hours
77♦	Nup145N APD	858-993	pET28a-PreS	NdeI, XhoI	GPHM	none	23 °C / 18 hours
78	Nup53 ΔC	1-361	pET28a-Sumo	BamHI, XhoI	S	LEHHHHHH	23 °C / 18 hours
79♦	Nup82 NTD	1-595	pET28a-PreS	NdeI, NotI	GPH	none	18 °C / 18 hours
80♦	Nup159 T	1440-1481	pET28a-Sumo	BamHI, NotI	S	none	18 °C / 18 hours
81	Nup192	1-1756	pET28a-PreS	NdeI, NotI	GPLMSGLNDIFEAQKI EWHEGSAGGSGH	none	23 °C / 18 hours
82	Nup192 CTD	944-1756	pET28a-PreS	NdeI, NotI	GPHM	none	23 °C / 18 hours
83♦	Nup192 TAIL	1397-1756	pET28a-PreS	NdeI, NotI	GPHM	none	37 °C / 2 hours
84*	Nup192 TAIL	1397-1756 (L1403E, I1427E)	pET28a-PreS	NdeI, NotI	GPHM	none	37 °C / 2 hours
85	Nup192 TAIL	1397-1756 (L1597A)	pET28a-PreS	NdeI, NotI	GPHM	none	37 °C / 2 hours
86	Nup192 TAIL	1397-1756 (F1602A)	pET28a-PreS	NdeI, NotI	GPHM	none	37 °C / 2 hours
87	Nup192 TAIL	1397-1756 (F1602W)	pET28a-PreS	NdeI, NotI	GPHM	none	37 °C / 2 hours
88	Nup192 TAIL	1397-1756 (F1611A)	pET28a-PreS	NdeI, NotI	GPHM	none	37 °C / 2 hours
89	Nup192 TAIL	1397-1756 (D1614A, P1615A, E1616A)	pET28a-PreS	NdeI, NotI	GPHM	none	37 °C / 2 hours
90	Nup192 TAIL	1397-1756 (D1614A, E1616A)	pET28a-PreS	NdeI, NotI	GPHM	none	37 °C / 2 hours
91	Nup192 TAIL	1397-1756 (F1664A)	pET28a-PreS	NdeI, NotI	GPHM	none	37 °C / 2 hours
92	Nup192 TAIL	1397-1756 (F1664W)	pET28a-PreS	NdeI, NotI	GPHM	none	37 °C / 2 hours
93	Nup192 TAIL	1397-1756 (V1673A)	pET28a-PreS	NdeI, NotI	GPHM	none	37 °C / 2 hours
94	Nup192 TAIL	1397-1756 (L1676A)	pET28a-PreS	NdeI, NotI	GPHM	none	37 °C / 2 hours
95	Nup192 TAIL	1397-1756 (K1677A)	pET28a-PreS	NdeI, NotI	GPHM	none	37 °C / 2 hours
96	Nup192 TAIL	1397-1756 (M1727A)	pET28a-PreS	NdeI, NotI	GPHM	none	37 °C / 2 hours
97	Nup192 TAIL	1397-1756 (I1730A)	pET28a-PreS	NdeI, NotI	GPHM	none	37 °C / 2 hours
98	Nup192 TAIL	1397-1756 (F1735A)	pET28a-PreS	NdeI, NotI	GPHM	none	37 °C / 2 hours
99	Nup192 TAIL	1397-1756 (Y1738A)	pET28a-PreS	NdeI, NotI	GPHM	none	37 °C / 2 hours
100♦	Nup188 TAIL	1447-1858	pET28a-SUMO	BamHI, NotI	SM	none	18 °C / 18 hours

* Nup192 TAIL used for SEC-MALS analyses harbored two mutations to prevent non-physiological dimerization. These mutants were designed based on observed crystal packing interactions in the $Nup192^{TAIL}$ structure

♦ Constructs that were used for crystallization

Constructs that were used for sAB and MB selection

■ Constructs that were used for ascertaining sequence register by Se-Met labeling

Table S6.

Protein purification protocols

Protein(s)	Expression constructs	Purification step	Buffer A	Buffer B
Nup192 TAIL♦	Individual (#83)	1. Ni-NTA 2. Dialysis/Cleavage 3. Ni-NTA 4. HiLoad Superdex 200 16/60 PG	Ni-A1, 5 mM β-ME Ni-A3, 5 mM β-ME / PreS Ni-A3, 5 mM β-ME SEC-B, 1 mM DTT	Ni-B1, 5 mM β-ME N/A Ni-B1, 5 mM β-ME N/A
His_6-Nup192 TAIL wild type and mutants	Individual (#83, #85-99)	1. Ni-NTA 2. Dialysis 3. HiTrap Q HP 4. HiLoad Superdex 200 16/60 PG	Ni-A1, 5 mM β-ME IEX-A1, pH 9.0, 5 mM β-ME IEX-A1, pH 9.0, 1 mM DTT SEC-B, 1 mM DTT	Ni-B1, 5 mM β-ME N/A IEX-B, pH 9.0, 1 mM DTT N/A
His_6-Nup192 TAIL•SUMO-Nic96 R1-R2	Co-expression (#84+#52)	1. Ni-NTA 2. Dialysis 3. HiTrap Q HP 4. HiLoad Superdex 200 16/60 PG	Ni-A1, 5 mM β-ME IEX-A1, pH 9.0, 5 mM β-ME IEX-A1, pH 9.0, 1 mM DTT SEC-B, 1 mM DTT	Ni-B1, 5 mM β-ME N/A IEX-B, pH 9.0, 1 mM DTT N/A
Nup188 TAIL♦	Individual (#100)	1. Ni-NTA 2. Dialysis/Cleavage 3. Ni-NTA 4. MonoQ 10/100 GL 5. HiLoad Superdex 200 16/60 PG	Ni-A1, 5 mM β-ME Ni-A2, 5 mM β-ME / ULP1 Ni-A2, 5 mM β-ME IEX-A2, pH 8.0, 1 mM DTT SEC-A, 1 mM DTT	Ni-B1, 5 mM β-ME N/A Ni-B1, 5 mM β-ME IEX-B, pH 8.0, 1 mM DTT N/A
SUMO-Nup188 TAIL	Individual (#100)	1. Ni-NTA 2. Dialysis 3. MonoQ 10/100 GL 4. HiLoad Superdex 200 16/60 PG	Ni-A1, 5 mM β-ME IEX-A2, pH 8.0, 5 mM β-ME IEX-A2, pH 8.0, 1 mM DTT SEC-B, 1 mM DTT	Ni-B1, 5 mM β-ME N/A IEX-B, pH 8.0, 1 mM DTT N/A
SUMO-Nup188 TAIL•SUMO-Nic96 R1-R2	Co-expression (#100+#52)	1. Ni-NTA 2. Dialysis 3. MonoQ 10/100 GL 4. HiLoad Superdex 200 16/60 PG	Ni-A1, 5 mM β-ME IEX-A2, pH 8.0, 5 mM β-ME IEX-A2, pH 8.0, 1 mM DTT SEC-B, 1 mM DTT	Ni-B1, 5 mM β-ME N/A IEX-B, pH 8.0, 1 mM DTT N/A
SUMO-Nic96 R1♦ wild type, mutants, and truncations	Individual (#39-#51)	1. Ni-NTA 2. HiPrep 26/20 Desalting 3. HiLoad Superdex 75 16/60 PG	Ni-A1, 5 mM β-ME SEC-A, 5 mM DTT SEC-A, 5 mM DTT	Ni-B1, 5 mM β-ME N/A N/A
SUMO-Nic96 R2 wild type and mutants	Individual (#55-63)	1. Ni-NTA 2. Dialysis 3. HiTrap Q HP 4. HiLoad Superdex 75 16/60 PG	Ni-A1, 5 mM β-ME IEX-A2, pH 8.0, 5 mM β-ME IEX-A2, pH 8.0, 1 mM DTT SEC-B, 1 mM DTT	Ni-B1, 5 mM β-ME N/A IEX-B, pH 8.0, 1 mM DTT N/A
Nup145N	Individual (#76)	1. Ni-NTA 2. Dialysis/Cleavage 3. MonoS 5/50 GL 4. HiLoad Superdex 75 16/60 PG	Ni-A1, 5 mM β-ME IEX-A2, pH 7.0, 5 mM DTT / ULP1 IEX-A2, pH 7.0, 5 mM DTT SEC-A, 5 mM DTT	Ni-B1, 5 mM β-ME N/A IEX-B, pH 7.0, 5 mM DTT N/A
Nup145N APD♦	Individual (#77)	1. Ni-NTA 2. Dialysis/cleavage 3. Ni-NTA 4. Superdex 75 16/60 PG	Ni-A1, 5 mM β-ME IEX-A2, pH 8.0, 5 mM β-ME / PreS Ni-A2, 5 mM β-ME SEC-A, 5 mM DTT	Ni-B1, 5 mM β-ME N/A Ni-B1, 5 mM β-ME N/A
Nup53	Individual (#78)	1. Ni-NTA 2. HiPrep 26/20 Desalting/Cleavage 3. Ni-NTA 4. HiPrep 26/20 Desalting 5. MonoS 5/50 GL 6. HiLoad Superdex 75 16/60 PG	Ni-A1, 5 mM β-ME Ni-A1, 5 mM β-ME / ULP1 Ni-A1, 5 mM β-ME IEX-A2, pH 7.0, 5 mM DTT IEX-A2, pH 7.0, 5 mM DTT SEC-A, 5 mM DTT	Ni-B1, 5 mM β-ME N/A Ni-B1, 5 mM β-ME N/A IEX-B, pH 7.0, 5 mM DTT N/A
hsNup49 CCS2+3*♦ wild type and mutant	Individual (#1-2)	1. Ni-NTA 2. HiPrep 26/20 Desalting/Cleavage 3. Ni-NTA 4. HiLoad Superdex 75 16/60 PG	Ni-A1, 5 mM β-ME SEC-A, 4 mM β-ME / ULP1 Ni-A2, pH 8.0, 4 mM β-ME SEC-A, 4 mM DTT	Ni-B1, 5 mM β-ME N/A Ni-B1, 5 mM β-ME N/A
hsNup57 CCS3*♦ wild type and mutant	Individual (#3-4)	1. Ni-NTA 2. HiPrep 26/20 Desalting/Cleavage 3. Ni-NTA 4. HiLoad Superdex 75 16/60 PG	Ni-A1, 5 mM β-ME SEC-A, 4 mM β-ME / ULP1 Ni-A2, pH 8.0, 4 mM β-ME SEC-A, 4 mM DTT	Ni-B1, 5 mM β-ME N/A Ni-B1, 5 mM β-ME N/A
ctNup57 CCS3*♦ wild type and mutant	Individual (#21-22)	1. Ni-NTA 2. HiPrep 26/20 Desalting/Cleavage 3. Ni-NTA 4. HiLoad Superdex 75 16/60 PG	Ni-A1, 5 mM β-ME SEC-A, 4 mM β-ME / ULP1 Ni-A2, pH 8.0, 4 mM β-ME SEC-A, 4 mM DTT	Ni-B1, 5 mM β-ME N/A Ni-B1, 5 mM β-ME N/A
Nic96 SOL	Individual (#54)	1. Ni-NTA 2. Dialysis/Cleavage 3. Ni-NTA 4. MonoQ 10/100 GL 5. HiLoad Superdex 200 16/60 PG	Ni-A1, 5 mM β-ME IEX-A2, pH 8.0, 5 mM β-ME / ULP1 Ni-A2, 5 mM β-ME IEX-A2, pH 8.0, 5 mM DTT SEC-A, 5 mM DTT	Ni-B1, 5 mM β-ME N/A Ni-B1, 5 mM β-ME IEX-B, pH 8.0, 5 mM DTT N/A
avi-Nup192	Individual (#81)	1. Ni-NTA 2. Dialysis/Cleavage 3. Ni-NTA 4. MonoQ 10/100 GL 5. HiLoad Superdex 200 16/60 PG	Ni-A1, 5 mM β-ME IEX-A2, pH 8.0, 5 mM β-ME / PreS Ni-A2, pH 8.0, 5 mM β-ME IEX-A2, pH 8.0, 5 mM DTT SEC-A, 5 mM DTT	Ni-B1, 5 mM β-ME N/A Ni-B1, 5 mM β-ME IEX-B, pH 8.0, 5 mM DTT N/A
CNT♦ wild type mutants avi-tagged variant Met mutants	Co-expression (#5+#23) (#5+#31-36) (#5+#12) (#5+#24-29)	1. Ni-NTA 2. HiPrep 26/20 Desalting/Cleavage 3. Ni-NTA 4. HiTrap Q HP 5. HiLoad Superdex 200 16/60 PG	Ni-A1, 4 mM β-ME IEX-A2, pH 8.0, 4 mM β-ME / ULP1 Ni-A2, pH 8.0, 4 mM β-ME IEX-A2, pH 8.0, 5 mM DTT SEC-A, 5 mM DTT	Ni-B1, 4 mM β-ME N/A Ni-B1, 4 mM β-ME IEX-B, pH 8.0, 5 mM DTT N/A
Nsp1	Individual (#19)	1. Ni-NTA 2. HiPrep 26/20 Desalting/Cleavage 3. Ni-NTA 4. HiLoad Superdex 200 16/60 PG	Ni-A1, 5 mM β-ME SEC-A, 5 mM β-ME / ULP1 Ni-A2, 5 mM β-ME SEC-A, 5 mM DTT	Ni-B1, 5 mM β-ME N/A Ni-B1, 5 mM β-ME N/A

Protein(s)	Expression constructs	Purification step	Buffer A	Buffer B
Nup49•Nup57	Co-expression (#23+#20)	1. GST-Sepharose fastflow 2. HiPrep 26/20 Desalting/Cleavage 3. Ni-NTA 4. HiPrep 26/20 Desalting/Cleavage 5. Ni-NTA 6. HiTrap Desalting	GST-A, 5 mM β-ME IEX-A2: pH 8.0, 5 mM β-ME / PreS Ni-A2, 5 mM β-ME IEX-A2: pH 8.0, 5 mM β-ME / ULP1 Ni-A2, 5 mM β-ME SEC-A, 5 mM β-ME	GST-B, 5 mM β-ME N/A Ni-B2, 5 mM β-ME N/A Ni-B2, 5 mM β-ME N/A
Nup82 NTD•Nup159 T♦	Individual (#79) (#80) co-lysis (1:1)	1. Ni-NTA 2. HiPrep 26/20 Desalting/Cleavage 3. Ni-NTA 4. HiLoad Superdex 200 16/60 PG	Ni-A1, 5 mM β-ME Ni-A1, 5 mM β-ME/ PreS / ULP1 Ni-A1, 5 mM β-ME SEC-A, 5 mM DTT	Ni-B1, 4 mM β-ME N/A Ni-B1, 4 mM β-ME N/A
SUMO-MBs	Individual (#64-73)	1. Ni-NTA 2. HiPrep 26/20 Desalting	Ni-A1, 4 mM β-ME SEC-B, 4 mM β-ME	Ni-B1, 4 mM β-ME N/A
sABs	(#74-75)	Detailed description in SI methods		
CNT•Nic96 CNT Nic96	Individual (#5+#23) (#37) co-lysis (1:1)	Detailed description in SI methods		
Nic96 R2-SOL•avi-Nup192 Nic96 R2-SOL avi-Nup192	Individual (#53) (#81) co-lysis (1:1)	Detailed description in SI methods		
CNT•SUMO-Nic96 R1	Biochemical reconstitution	Detailed description in SI methods		
CNT•Nic96 R1•sAB-158	Biochemical reconstitution	Detailed description in SI methods		
Nup82 NTD•Nup159 T•Nup145N APD	Biochemical reconstitution	Detailed description in SI methods		

♦ Constructs that were used for crystallization
Ni-A1: 20 mM TRIS (pH 8.0), 500 mM NaCl, 20 mM imidazole
Ni-A2: 20 mM TRIS (pH 8.0), 100 mM NaCl, 20 mM imidazole
Ni-A3: 20 mM TRIS (pH 8.0), 200 mM NaCl, 20 mM imidazole
Ni-B1: 20 mM TRIS (pH 8.0), 500 mM NaCl, 500 mM imidazole
Ni-B2: 20 mM TRIS (pH 8.0), 100 mM NaCl, 500 mM imidazole
GST-A: 20 mM TRIS (pH 8.0), 300 mM NaCl
GST-B: 20 mM TRIS (pH 8.0), 300 mM NaCl, 20 mM glutathione
IEX-A1: 20 mM TRIS, 50 mM NaCl
IEX-A2: 20 mM TRIS, 100 mM NaCl
IEX-A3: 20 mM TRIS, 80 mM NaCl
IEX-B: 20 mM TRIS, 2.0 M NaCl
SEC-A: 20 mM TRIS (pH 8.0), 100 mM NaCl
SEC-B: 20 mM TRIS (pH 8.0), 200 mM NaCl

Table S7.

Yeast expression constructs

Plasmid	Protein	Residues (Mutations)	Vector	Restriction sites 5', 3'	Selection Marker	Reference
pRS415-P_{Nop1}-eGFP-*scNUP192*	*sc*Nup192	1-1683	pRS415	NotI, SacII	*LEU2*	(*53*)
pRS415-P_{Nop1}-eGFP-*scnup192 ΔTAIL*	*sc*Nup192	1-1316	pRS415	NotI, SacII	*LEU2*	(*53*)
pRS415-P_{Nop1}-eGFP-*scnup192 Y1679A*	*sc*Nup192	1-1683, Y1679A	pRS415	NotI, SacII	*LEU2*	this study
pRS415-P_{Nop1}-mCherry-*scNUP192*	*sc*Nup192	1-1683	pRS415	NotI, SacII	*LEU2*	this study
pRS415-P_{Nop1}-mCherry-*scnup192 ΔTAIL*	*sc*Nup192	1-1316	pRS415	NotI, SacII	*LEU2*	this study
pRS415-P_{Nop1}-mCherry-*scnup192* Y1679A	*sc*Nup192	1-1683, Y1679A	pRS415	NotI, SacII	*LEU2*	this study
pRS416-P_{Nop1}-mCherry-*scNUP192*	*sc*Nup192	1-1683	pRS416	NotI, SacII	*URA3*	(*53*)
pRS415-P_{Nop1}-eGFP-*scNIC96*	*sc*Nic96	1-839	pRS415	BamHI, NotI	*LEU2*	this study
pRS415-P_{Nop1}-eGFP-*scnic96 ΔSOL*	*sc*Nic96	1-203	pRS415	BamHI, NotI	*LEU2*	this study
pRS415-P_{Nop1}-eGFP-*scnic96 R2*-SOL	*sc*Nic96	107-839	pRS415	BamHI, NotI	*LEU2*	this study
pRS415-P_{Nop1}-eGFP-*scnic96 SOL*	*sc*Nic96	204-839	pRS415	BamHI, NotI	*LEU2*	this study
pRS415-P_{Nop1}-eGFP-*scnic96 ΔR2*	*sc*Nic96	1-108, 166-839	pRS415	BamHI, NotI	*LEU2*	this study
pRS415-P_{Nop1}-eGFP-*scnic96 F159A*	*sc*Nic96	1-839, F159A	pRS415	BamHI, NotI	*LEU2*	this study
pRS415-P_{Nop1}-eGFP-*scnic96 ΔLINKER*	*sc*Nic96	1-60, 107-839	pRS415	BamHI, NotI	*LEU2*	this study
pRS415-P_{Nop1}-eGFP-*scnic96 LLLL*	*sc*Nic96	1-839, I46A, L49A, V53A, L56A	pRS415	BamHI, NotI	*LEU2*	this study
pRS415-P_{Nop1}-mCherry-*scNIC96*	*sc*Nic96	1-839	pRS415	BamHI, NotI	*LEU2*	this study
pRS415-P_{Nop1}-mCherry-*scnic96 R2-SOL*	*sc*Nic96	107-839	pRS415	BamHI, NotI	*LEU2*	this study
pRS415-P_{Nop1}-mCherry-*scnic96 R2*	*sc*Nic96	1-108, 166-839	pRS415	BamHI, NotI	*LEU2*	this study
pRS415-P_{Nop1}-mCherry-*scnic96 F159A*	*sc*Nic96	1-839, F159A	pRS415	BamHI, NotI	*LEU2*	this study
pRS415-P_{Nop1}-mCherry-*scnic96 ΔLINKER*	*sc*Nic96	1-60, 107-839	pRS415	BamHI, NotI	*LEU2*	this study
pRS415-P_{Nop1}-mCherry-*scnic96 LLLL*	*sc*Nic96	1-839, I46A, L49A, V53A, L56A	pRS415	BamHI, NotI	*LEU2*	this study
pRS416-P_{Nop1}-mCherry-*scNIC96*	*sc*Nic96	1-839	pRS416	BamHI, NotI	*URA3*	this study
pRS415-P_{Nop1}-eGFP-*scNUP49*	*sc*Nup49	1-472	pRS415	BamHI, NotI	*LEU2*	this study
pRS415-P_{Nop1}-eGFP-*scnup49 E*	*sc*Nup49	1-472, K376E	pRS415	BamHI, NotI	*LEU2*	this study
pRS415-P_{Nop1}-eGFP-*scnup49 P1*	*sc*Nup49	1-472, I391P	pRS415	BamHI, NotI	*LEU2*	this study
pRS415-P_{Nop1}-eGFP-*scnup49 P2*	*sc*Nup49	1-472, L449P	pRS415	BamHI, NotI	*LEU2*	this study
pRS415-P_{Nop1}-eGFP-*scnup49 PP*	*sc*Nup49	1-472, I391P, L449P	pRS415	BamHI, NotI	*LEU2*	this study
pRS415-P_{Nop1}-eGFP-*scnup49 EPP*	*sc*Nup49	1-472, K376E, I391P, L449P	pRS415	BamHI, NotI	*LEU2*	this study
pRS415-P_{Nop1}-eGFP-*scnup49 EVPIP*	*sc*Nup49	1-472, K376E, I390V, I391P, V398I, L449P	pRS415	BamHI, NotI	*LEU2*	this study*
pRS415-P_{Nop1}-mCherry-*scNUP49*	*sc*Nup49	1-472	pRS415	BamHI, NotI	*LEU2*	this study
pRS415-P_{Nop1}-mCherry-*scnup49 E*	*sc*Nup49	1-472, K376E	pRS415	BamHI, NotI	*LEU2*	this study
pRS415-P_{Nop1}-mCherry-*scnup49 P1*	*sc*Nup49	1-472, I391P	pRS415	BamHI, NotI	*LEU2*	this study
pRS415-P_{Nop1}-mCherry-*scnup49 P2*	*sc*Nup49	1-472, L449P	pRS415	BamHI, NotI	*LEU2*	this study
pRS415-P_{Nop1}-mCherry-*scnup49 PP*	*sc*Nup49	1-472, I391P, L449P	pRS415	BamHI, NotI	*LEU2*	this study
RS415-P_{Nop1}-mCherry-*scnup49 EPP*	*sc*Nup49	1-472, K376E, I391P, L449P	pRS415	BamHI, NotI	*LEU2*	this study
pRS415-P_{Nop1}-mCherry-*scnup49 EVPIP*	*sc*Nup49	1-472, K376E, I390V, I391P, V398I, L449P	pRS415	BamHI, NotI	*LEU2*	this study*
pRS411-P_{RPL25}-*scRPL25*-mCherry	*sc*Rpl25	1-142	pRS411	SacII, BamHI	*MET15*	this study
pRS413-P_{RPL25}-*scRPL25*-mCherry	*sc*Rpl25	1-142	pRS413	SacII, BamHI	*HIS3*	this study
pFA6a-natNT2	N/A	N/A	pFA6a	N/A	N/A	(*51*)
pRS413	N/A	N/A	pRS413	N/A	*HIS3*	(*52*)

*mutations based on nup49-313 (*54*)

Table S8.

Yeast strains

Strain	Parental strain	Genotype	Plasmid	Transformed with	Analyses	Reference
*sc*nup192Δ	BY4741	MATa, *his3Δ1, leu2Δ0, met15Δ0, ura3Δ0, scnup192::HIS3*	pRS416-P_{Nop1}-mcherry-*scNUP192*	pRS415-P_{Nop1}-eGFP-*scNUP192* variants	growth analysis poly(A)$^+$ RNA export	this study
*sc*nup192Δ	BY4741	MATa, *his3Δ1, leu2Δ0, met15Δ0, ura3Δ0, scnup192::HIS3*	pRS416-P_{Nop1}-mcherry-*scNUP192*	pRS415-P_{Nop1}-eGFP-*scNUP192* variants pRS411-P_{Nop1}-*scRPL25*-mcherry	*sc*Rpl25 localization	this study
*sc*nup192Δ *sc*Nup57-GFP	BY4741 *sc*Nup57-GFP[a]	MATa, *his3Δ1, leu2Δ0, met15Δ0, ura3Δ0, scnup192::*natNT2, *scNUP57*-GFP(S65T)::*HIS3*MX6	pRS416-P_{Nop1}-mcherry-*scNUP192*	pRS415-P_{Nop1}-mcherry-*scNUP192* variants	colocalization of *sc*Nup192 variants and *sc*Nup57	this study
*sc*nic96Δ	BY4741	MATa, *his3Δ1, leu2Δ0, met15Δ0, ura3Δ0, scnic96::HIS3*	pRS416-P_{Nop1}-mcherry-*scNIC96*	pRS415-P_{Nop1}-eGFP-*scNIC96* variants	growth analysis	this study
*sc*nic96Δ *sc*Nup57-GFP	BY4741 *sc*Nup57-GFP[a]	MATa, *his3Δ1, leu2Δ0, met15Δ0, ura3Δ0, scnic96::*natNT2, *scNUP57*-GFP(S65T)::*HIS3*MX6	pRS416-P_{Nop1}-mcherry-*scNIC96*	pRS415-P_{Nop1}-mcherry-*scNIC96* variants	colocalization of *sc*Nic96 variants and *sc*Nup57 poly(A)$^+$ RNA export	this study
*sc*nup49Δ	BY4741	MATa, *his3Δ1, leu2Δ0, met15Δ0, ura3Δ0, scnup49::*natNT2	pRS416-P_{Nop1}-mcherry-*scNUP49*	pRS415-P_{Nop1}-eGFP-*scNUP49* variants	growth analysis poly(A)$^+$ RNA assay	this study
*sc*nup49Δ	BY4741	MATa, *his3Δ1, leu2Δ0, met15Δ0, ura3Δ0, scnup49::*natNT2	pRS416-P_{Nop1}-mcherry-*scNUP49*	pRS415-P_{Nop1}-eGFP-*scNUP49* variants pRS413-P_{Nop1}-*scRPL25*-mcherry	*sc*Rpl25 localization	this study
*sc*nup49Δ scNup57-GFP	BY4741 *sc*Nup57-GFP[a]	MATa, *his3Δ1, leu2Δ0, met15Δ0, ura3Δ0, scnup49::*natNT2, *scNUP57*-GFP(S65T)::*HIS3*MX6	pRS416-P_{Nop1}-mcherry-*scNUP49*	pRS415-P_{Nop1}-eGFP-*scNUP49* variants	colocalization of *sc*Nup192 variants and *sc*Nup57	this study

[a] purchased from Invitrogen

Table S9.

Crystallization and cryo protection conditions

Protein(s)	Concentration	Crystallization condition	Cryo protection condition
Nup192^{TAIL}	10 mg/ml	50 mM HEPES, pH 7.1 15 % (w/v) PEG 200 340 mM sodium chloride (optimized by microseeding)	paratone oil
Nup188^{TAIL}	10 mg/ml	100 mM HEPES, pH 6.9 16 % (w/v) PEG 3,350 200 mM ammonium citrate	35 % (w/v) PEG 3,350
*hs*Nup49$^{CCS2+3*}$•*hs*Nup57^{CCS3*} 2:2 stoichiometry	15 mg/ml	100 mM sodium citrate, pH 5.4 0.5 M sodium chloride	25 % (v/v) ethylene glycol (stepwise, 20 %, 25 %)
*hs*Nup49$^{CCS2+3*}$•*hs*Nup57^{CCS3*} 1:2 stoichiometry	20 mg/ml	100 mM sodium acetate, pH 3.8 70 mM calcium chloride	20 % (v/v) glycerol
*hs*Nup49$^{CCS2+3*}$	8 mg/ml	28 % (v/v) dioxane 10 % (v/v) glycerol	20 % (v/v) glycerol
*hs*Nup57^{CCS3*}	16 mg/ml	1.0 M sodium acetate pH 5.3 1.9 M sodium formate	paraffin oil
Nup57^{CCS3*} homo-dimer	16 mg/ml	5 % (w/v) PEG 1,000 12 % (w/v) PEG 8,000	paraffin oil
Nup82^{NTD}•Nup159^{T}•Nup145N^{APD}	30 mg/ml	100 mM lithium citrate 20 % (w/v) PEG 3,350 3 % (v/v) MPD	20 % (v/v) MPD
CNT•Nic96^{R1}•sAB-158	25 mg/ml	0.1M TRIS, pH 8.7 5.7 % (w/v) PEG 20,000 1 % (v/v) 1-propanol	25 % (v/v) ethylene glycol (stepwise, 2 % steps)

Movie S1.
Rotating *C. thermophilum* CNT•Nic96^{R1} monomer in cartoon representation. CNT•Nic96^{R1} is colored according to Figure 4. sAb-158 is removed for clarity.

Movie S2.
Rotating *C. thermophilum* CNT•Nic96^{R1} monomer in surface representation. CNT•Nic96^{R1} is colored according to Figure 4. sAb-158 is removed for clarity.

Movie S3.
Rotating Nic96^{R1} interaction with the three coiled-coil domains of the CNT. The structure is colored according to Figure 4. Nic96^{R1} is shown in surface representation and Nsp1, Nup49, and Nup57 are shown in ribbon representation. The Nup49 residues that are mutated in the EPP mutant are shown in ball-and-stick representations and colored in magenta.

Movie S4.
Rotating structure of the *C. thermophilum* CNT•Nic96^{R1} asymmetric unit dimer. The two CNT•Nic96^{R1} complexes are colored in blue (CNT) and magenta (Nic96^{R1}) and yellow (CNT) and red (Nic96^{R1}), respectively. The two sAB-158 molecules are colored in gray.

REFERENCES AND NOTES

42. E. Mossessova, C. D. Lima, Ulp1-SUMO crystal structure and genetic analysis reveal conserved interactions and a regulatory element essential for cell growth in yeast. *Mol. Cell* **5**, 865-876 (2000).
43. C. Romier *et al.*, Co-expression of protein complexes in prokaryotic and eukaryotic hosts: experimental procedures, database tracking and case studies. *Acta Crystallogr. D Biol. Crystallogr.* **62**, 1232-1242 (2006).
44. A. Hoelz, A. C. Nairn, J. Kuriyan, Crystal structure of a tetradecameric assembly of the association domain of Ca2+/calmodulin-dependent kinase II. *Mol. Cell* **11**, 1241-1251 (2003).
45. S. Doublie, Preparation of selenomethionyl proteins for phase determination. *Methods Enzymol.* **276**, 523-530 (1997).
46. M. Paduch *et al.*, Generating conformation-specific synthetic antibodies to trap proteins in selected functional states. *Methods* **60**, 3-14 (2013).
47. K. R. Miller *et al.*, T cell receptor-like recognition of tumor in vivo by synthetic antibody fragment. *PLoS One* **7**, e43746 (2012).
48. A. Koide, J. Wojcik, R. N. Gilbreth, R. J. Hoey, S. Koide, Teaching an old scaffold new tricks: monobodies constructed using alternative surfaces of the FN3 scaffold. *J. Mol. Biol.* **415**, 393-405 (2012).
49. R. B. Stockbridge, A. Koide, C. Miller, S. Koide, Proof of dual-topology architecture of Fluc F-channels with monobody blockers. *Nat. Commun.* **5**, 5120 (2014).
50. P. J. Wyatt, Multiangle light scattering: The basic tool for macromolecular characterization. *Instrum. Sci. Technol.* **25**, 1-18 (1997).
51. C. Janke *et al.*, A versatile toolbox for PCR-based tagging of yeast genes: new fluorescent proteins, more markers and promoter substitution cassettes. *Yeast* **21**, 947-962 (2004).
52. R. S. Sikorski, P. Hieter, A system of shuttle vectors and yeast host strains designed for efficient manipulation of DNA in Saccharomyces cerevisiae. *Genetics* **122**, 19-27 (1989).
53. T. Stuwe, D. H. Lin, L. N. Collins, E. Hurt, A. Hoelz, Evidence for an evolutionary relationship between the large adaptor nucleoporin Nup192 and karyopherins. *Proc. Natl. Acad. Sci. U.S.A.* **111**, 2530-2535 (2014).
54. V. Doye, R. Wepf, E. C. Hurt, A novel nuclear pore protein Nup133p with distinct roles in poly(A)+ RNA transport and nuclear pore distribution. *EMBO J.* **13**, 6062-6075 (1994).
55. O. Gadal *et al.*, Nuclear export of 60s ribosomal subunits depends on Xpo1p and requires a nuclear export sequence-containing factor, Nmd3p, that associates with the large subunit protein Rpl10p. *Mol. Cell Biol.* **21**, 3405-3415 (2001).
56. C. Gwizdek *et al.*, Ubiquitin-associated domain of Mex67 synchronizes recruitment of the mRNA export machinery with transcription. *Proc. Natl. Acad. Sci. U.S.A.* **103**, 16376-16381 (2006).
57. H. S. Seo *et al.*, Structural and functional analysis of Nup120 suggests ring formation of the Nup84 complex. *Proc. Natl. Acad. Sci. U.S.A.* **106**, 14281-14286 (2009).
58. W. Kabsch, Xds. *Acta Crystallogr. D Biol. Crystallogr.* **66**, 125-132 (2010).
59. Z. Otwinowski, W. Minor, Processing of X-ray diffraction data collected in oscillation mode. *Method Enzymol.* **276**, 307-326 (1997).
60. A. J. McCoy *et al.*, Phaser crystallographic software. *J. Appl. Crystallogr.* **40**, 658-674 (2007).
61. P. D. Adams *et al.*, PHENIX: a comprehensive Python-based system for macromolecular structure solution. *Acta Crystallogr. D Biol. Crystallogr.* **66**, 213-221 (2010).
62. P. Emsley, K. Cowtan, Coot: model-building tools for molecular graphics. *Acta Crystallogr. D Biol. Crystallogr.* **60**, 2126-2132 (2004).
63. I. W. Davis *et al.*, MolProbity: all-atom contacts and structure validation for proteins and nucleic acids. *Nucleic Acids Res.* **35**, W375-383 (2007).
64. F. Jeanmougin, J. D. Thompson, M. Gouy, D. G. Higgins, T. J. Gibson, Multiple sequence alignment with Clustal X. *Trends Biochem. Sci.* **23**, 403-405 (1998).
65. G. J. Barton, ALSCRIPT: a tool to format multiple sequence alignments. *Protein Eng.* **6**, 37-40 (1993).

66. N. A. Baker, D. Sept, S. Joseph, M. J. Holst, J. A. McCammon, Electrostatics of nanosystems: application to microtubules and the ribosome. *Proc. Natl. Acad. Sci. U.S.A.* **98**, 10037-10041 (2001).
67. T. Stuwe, L. S. von Borzyskowski, A. M. Davenport, A. Hoelz, Molecular basis for the anchoring of proto-oncoprotein Nup98 to the cytoplasmic face of the nuclear pore complex. *J. Mol. Biol.* **419**, 330-346 (2012).
68. K. R. Andersen *et al.*, Scaffold nucleoporins Nup188 and Nup192 share structural and functional properties with nuclear transport receptors. *Elife* **2**, e00745 (2013).
69. I. Melcak, A. Hoelz, G. Blobel, Structure of Nup58/45 suggests flexible nuclear pore diameter by intermolecular sliding. *Science* **315**, 1729-1732 (2007).
70. S. R. Solmaz, G. Blobel, I. Melcak, Ring cycle for dilating and constricting the nuclear pore. *Proc. Natl. Acad. Sci. U.S.A.* **110**, 5858-5863 (2013).
71. S. R. Solmaz, R. Chauhan, G. Blobel, I. Melcak, Molecular architecture of the transport channel of the nuclear pore complex. *Cell* **147**, 590-602 (2011).
72. S. Frank, A. Lustig, T. Schulthess, J. Engel, R. A. Kammerer, A distinct seven-residue trigger sequence is indispensable for proper coiled-coil formation of the human macrophage scavenger receptor oligomerization domain. *J. Biol. Chem.* **275**, 11672-11677 (2000).
73. A. Sharma, S. R. Solmaz, G. Blobel, I. Melcak, Ordered Regions of Channel Nucleoporins Nup62, Nup54 and Nup58 Form Dynamic Complexes in Solution. *J. Biol. Chem.*, pii: jbc.M115.663500 (2015).
74. A. Ulrich, J. R. Partridge, T. U. Schwartz, The stoichiometry of the nucleoporin 62 subcomplex of the nuclear pore in solution. *Mol. Biol. Cell* **25**, 1484-1492 (2014).
75. B. Bradatsch *et al.*, Structure of the pre-60S ribosomal subunit with nuclear export factor Arx1 bound at the exit tunnel. *Nat. Struct. Mol. Biol.* **19**, 1234-1241 (2012).
76. K. H. Bui, A. von Appen *et al.*, Integrated structural analysis of the human nuclear pore complex scaffold. *Cell* **155**, 1233-1243 (2013).
77. Y. Matsuura, M. Stewart, Structural basis for the assembly of a nuclear export complex. *Nature* **432**, 872-877 (2004).